

DISSERTATION

USING BAYESIAN MODEL SELECTION AND CALIBRATION TO IMPROVE
THE DAYCENT ECOSYSTEM MODEL

Submitted by

Ram B. Gurung

Graduate Degree Program in Ecology

In partial fulfillment of the requirements

For the Degree of Doctor of Philosophy

Colorado State University

Fort Collins, Colorado

Fall 2020

Doctoral Committee:

Advisor: Stephen M. Ogle

Keith Paustian
William J Parton
F Jay Breidt

Copyright by Ram B. Gurung 2020

All Rights Reserved

ABSTRACT

USING BAYESIAN MODEL SELECTION AND CALIBRATION TO IMPROVE THE DAYCENT ECOSYSTEM MODEL

Process-based biogeochemical models have been developed and used for decades to predict the outcomes of real-world ecological processes. These models are based on a theoretical understanding of relevant ecological processes and approximated using highly complex mathematical equations and hundreds of unknown parameters—requiring calibration using physical observations of the system. These models are then used to test scientific understanding, estimate pools and fluxes, make predictions for future scenarios, and to evaluate management and policy outcomes. To provide a better understanding of the ecological processes, these models need to be simple, make accurate predictions, and account for all sources of uncertainty.

The focus of this dissertation is to develop a Bayesian model analysis framework to meet the goal of developing simple and accurate models that fully address uncertainty. This framework includes variance-based global sensitivity analysis (GSA) to identify influential model parameters, a Bayesian calibration method using sampling importance resampling (SIR) to estimate the posterior distribution of unknown model parameters and hyperparameters, and a Monte Carlo analysis to estimate the posterior predictive distribution of model outputs. The framework accounts for all sources of uncertainty, including the remaining uncertainty over the fitted parameters. Additionally, Bayesian model selection is also implemented in the framework to determine the most appropriate level of complexity during model development. The framework is applied to improve the DayCent ecosystem model in agricultural applications.

The DayCent model was improved with several model developments, including NH_3 volatilization, the release of nitrogen (N) from controlled-release N fertilizers (CRNFs) and the inhibition of the biological process of nitrification and delay the transformation of NH_4^+ to NO_3^- with nitrification inhibitor (NIs). The model development incorporates key 4R management practices that mitigate NH_3 and N_2O emissions in fertilized upland agricultural soils. In addition, I recalibrated the soil organic matter submodel to improve estimation of soil organic carbon (C) sequestration potentials to a 30 cm depth for several management practices, including organic matter amendment, adoption of no-till management, and addition of synthetic N fertilizers.

The results showed that the DayCent model predictions of C sequestration and reduction in N_2O flux as well as NH_3 volatilization from several management practices were consistent with the field observations. The model result suggested that addition of organic amendments and adoption of no-till are viable management option for C sequestration, however, the addition of synthetic N fertilizer did not produce a significant level of C sequestration. For NH_3 volatilization, the model also adequately captures the reduction potential of urease inhibitor along with the incorporation of urea by mechanical means or with immediate irrigation/rainfall. The model also shows promising results in mitigating N_2O emissions with both CRNFs and NIs in comparison to field observations. The model prediction focuses on estimating greenhouse gas (GHG) mitigation potential and estimation of uncertainty arising during model prediction—enhancing DayCent as a tool for scientific understanding, regional to global assessments, policy implementation, and carbon emission trading. Overall, the model improvements enhanced the ability of the DayCent model in providing a stronger basis to support policy and management decisions associated with GHG mitigation in agricultural soils.

ACKNOWLEDGEMENTS

I would like to express my deepest appreciation to my doctoral committee, Dr. Stephen M. Ogle, Dr. Keith Paustian, Dr. William J Parton, and Dr. F. Jay Breidt, for their guidance, direction, and encouragement throughout my educational journey. The journey begins shortly after 2009, when Dr. Ogle hired me as a research associate (Statistician), and he convinced me to stay in the field of ecosystem modeling and earn a doctorate degree—my long-sought dream nurtured by my late father. I am incredibly grateful to my adviser for constantly being able to read and provide countless feedback on my research and manuscripts. He constantly challenges me to see the big picture and think outside the box throughout my study and work alike and ensure I reached my maximum potential as a researcher.

I would like to thank Dr. Stephen Del Grosso and Dr. Rodney Venterea for providing valuable datasets from GRACEnet sites. Thanks also go to Dan Reuss, Analytical Facilities Manager at EcoCore, for countless conversations about laboratory techniques on processing soil samples and sharing his different views about soils from various scientists that he had worked with over the years, and how uncertainty might be introduced during laboratory analyses. Special thanks to Steve Williams for providing support and sharing decades worth of his data collection, Dr. Yao Zhang and Dr. Melannie D. Hartman for programming DayCent, and Ty Boyack for providing technical support and maintaining the Linux cluster “rubel”.

Over the years, I had a great pleasure working with many colleagues at Natural Recourse Ecology Laboratory and want to thank Shannon Spencer, Guhan Dheenadayalan Sivakami, Ernie Marx, Amy Swan, and Kendrick Killian for their collaboration. I would also like to thank my neighbors at Dolan street who pushed me, supported me, and hyped me up to reach the end goal.

To my parents.... you are the reason I have made it here. Dad – your love of education, sacrifices, and most importantly your last word of advice is the main reason I have made it here. Mom – you gifted me with determination and provided the fire to get things done and you always supported and guided me during the good times and the bad. Additionally, I would like to thank my siblings (Rama, Hema, Beni, and Ishwari), relatives, and elders that have always supported my long journey in perusing my dream.

Lastly, I would like to thank my wonderful wife, Puja, for her assistance in helping raise, educate, and provide care for our two beautiful children, Jaan and Jay. Especially, for Jaan encouraging and ensuring by saying “you can do it” and “are you done writing your chapters?” and Jay with his sense of humor and making me always laugh by sitting next to my desk, opening his toy computer, and saying “I am working on my Ph.D.”. For these and countless other reasons, they have fully supported me and sacrificed in the pursuit of my Ph.D. and I will be forever grateful to them!

DEDICATION

To my beloved parents

Capt. Lekh Bahadur Gurung & Gausubha Gurung

It is all because of your inspiration and it will always be with me.

TABLE OF CONTENTS

ABSTRACT.....	ii
ACKNOWLEDGEMENTS.....	iv
DEDICATION.....	vi
CHAPTER 1. INTRODUCTION.....	1
1.1. Overview.....	1
1.2. Statistical Framework for Bayesian Inference.....	5
1.3. Bayesian Model Selection.....	7
1.4. Global Sensitivity Analysis.....	9
1.5. Bayesian Calibration.....	10
1.6. Model Prediction using Monte Carlo Approach.....	16
1.7. Organization of Dissertation.....	17
CHAPTER 2: MODELING AMMONIA VOLATILIZATION FROM UREA APPLICATION TO AGRICULTURAL SOILS: DAYCENT MODEL DEVELOPMENT.....	19
2.1. Summary.....	19
2.2. Introduction.....	20
2.3. Materials and Methods.....	22
2.3.1. DayCent Model.....	23
2.3.2. Experimental Sites.....	24
2.3.3. Model Development.....	25
2.3.3.1. Urea Hydrolysis.....	26
2.3.3.2. Diffusion of Gaseous NH ₃	27
2.3.3.3. Depth Effect on NH ₃ Diffusion.....	27
2.3.3.4. Urea and NH ₄ ⁺ Concentration Factor.....	28
2.3.3.5. Increase in Soil pH.....	30
2.3.3.6. Soil Buffering Capacity.....	30
2.3.4. Bayesian Calibration and Model Selection.....	31
2.4. Results.....	34
2.4.1. Bayesian Calibration.....	34
2.4.2. Bayesian Model Selection.....	35
2.4.3. Posterior Parameter Distribution and Performance Evaluation for the Final Model.....	37
2.5. Discussion.....	40
2.6. Conclusions.....	44
CHAPTER 3: MODELING NITROUS OXIDE MITIGATION POTENTIAL OF ENHANCED EFFICIENCY NITROGEN FERTILIZERS FROM AGRICULTURAL SYSTEM.....	45
3.1. Summary.....	45
3.2. Introduction.....	45
3.3. Materials and Methods.....	48
3.3.1. Data Sources.....	48
3.3.2. DayCent Model.....	49
3.3.3. Model Development.....	51
3.3.3.1. Fraction of Nitrified N Loss as N ₂ O.....	51

3.3.3.2. Controlled-Release Nitrogen Fertilizers (CRNFs).....	52
3.3.3.3. Nitrification Inhibitors (NIs).....	54
3.3.4. Bayesian Model Calibration Framework.....	55
3.3.4.1. Global Sensitivity Analysis.....	56
3.3.4.2. Sampling Importance Resampling.....	57
3.3.4.3. Data-likelihood.....	59
3.4. Results.....	60
3.4.1. Global Sensitivity Analysis.....	60
3.4.2. Posterior Estimates of Model Parameters.....	60
3.4.3. Posterior Prediction of Reduction Factor.....	64
3.5. Discussion.....	67
3.6. Conclusion.....	71
CHAPTER 4: BAYESIAN CALIBRATION OF THE DAYCENT ECOSYSTEM MODEL TO SIMULATE SOIL ORGANIC CARBON DYNAMICS AND REDUCE MODEL UNCERTAINTY.....	73
4.1. Summary.....	73
4.2. Introduction.....	74
4.3. Materials and Methods.....	79
4.3.1. DayCent Ecosystem Model.....	79
4.3.2. Experimental Sites.....	79
4.3.3. Global Sensitivity Analysis.....	83
4.3.4. Bayesian Calibration.....	85
4.3.5. Model Prediction Using Monte Carlo Approach.....	87
4.4. Results.....	88
4.4.1. Global Sensitivity Analysis.....	88
4.4.2. Posterior Estimates of Model Parameters.....	90
4.4.3. Posterior Model Predictions.....	93
4.5. Discussion.....	98
4.6. Conclusion.....	103
CHAPTER 5: CONCLUSION AND FUTURE DIRECTION.....	105
REFERENCES.....	108

CHAPTER 1. INTRODUCTION

1.1. Overview

We, as humans, have relied upon agricultural soils for a wide array of services, including food, fuel, and fiber in the past, present, and will play an important role for the coming future—providing the same services for growing populations. Agricultural soils also provide opportunities to mitigate global climate change (Paustian et al., 2016; Sanderman et al., 2017). Agricultural soils are a net source of greenhouse gases (GHGs) but hold the potential to reduce or even become a net sink for GHG emissions, through adoption of best management practices (BMPs). However, BMPs vary substantially due to soil heterogeneity, climatic conditions, and management practices (Lal, 2004a; Paustian et al., 1997; Smith et al., 2008). Furthermore, the reduction of GHGs through carbon sequestration (negative emission) and the reduction of nitrous oxide (N₂O) emissions should be accomplished without adversely affecting food production.

Soil contains a large reservoir of carbon (C) greater than terrestrial vegetation, and atmospheric CO₂ combined (IPCC, 2013). Land conversion for food production has caused a loss of 50-75% of the native soil C stocks (Lal et al., 2007; Ogle et al., 2005; Sanderman et al., 2017) and represents a potential CO₂ sink that could return about two-thirds of initial C loss (Lal, 2004b; Lal et al., 2007; Paustian et al., 1997; Smith, 2004a). Some estimates suggest the level of sequestration can offset annual anthropogenic GHG emissions of 8.9 gigatonnes C by adopting the “4 per mille” initiative (Minasny et al., 2017)—promoted by the French Ministry of Agriculture. However, this initiative has faced criticisms due to limitation based on realistic potentials for C sequestration and challenges for widescale adoption (Poulton et al., 2018; VandenBygaart, 2018; White et al., 2018), and also N requirements due to the stoichiometric

constraints driven by the coupled C and N cycling in the ecosystem (Bertrand et al., 2019). Importantly, adopting management practices that enhance organic matter input and/or reduce C losses by limiting decomposition can sequester C (Lal et al., 2007; Ogle et al., 2005; Paustian et al., 1997) but must also consider the impacts on other GHGs from soils.

Crop production is by far the single largest use of industrially fixed nitrogen, consuming about 80% of the total N production (Galloway et al., 2008; Smil, 1999; Sutton et al., 2012) of which only about half is taken up by crops, while the rest is lost to the environment (Erisman et al., 2007; Galloway and Cowling, 2002). Increasing N available through the Haber-Bosch process, developed in the early 1900s, has alleviated nitrogen limitation in cropland, increased crop yield, and improve soil fertility (Vitousek et al., 1997), but also caused some adverse effects to human health and the environment (ApSimon et al., 1987; Asman et al., 1998; Bouwman et al., 2002a; Erisman et al., 2007). Nitrogen losses from agroecosystem include gas fluxes of NH_3 , N_2O , NO_2 , NO , and N_2 as well as leaching and runoff losses of NO_3^- , and are often the major pathways other than harvest removal. Management practices that deliver added N more efficiently to crops and improve N use efficiency often suppress N losses to the environment (Smith et al., 2008). The “4R” nutrient stewardship concept of applying the right source (or product) at the right rate, right time, and the right place has been emerging as the BMPs for N in agroecosystems.

In agroecosystems, many practices have been advocated to decrease GHG emissions. However, management options often affect more than one source of GHGs, through interactions between different mechanisms, sometimes in opposite ways, so the net GHGs reduction depends on the cumulative of all GHGs (Robertson et al., 2000; Smith et al., 2008). Additionally, different mechanisms and practices often interact with soil and climatic conditions and may not

be feasible everywhere—requiring region-specific BMPs. Hence, understanding and identifying practices that maximize the mitigation potentials through direct measurement requires a complete accounting of C and N flows through the ecosystems that are continuous, spatially explicit at various scales, and thus, is not feasible as a means of implementing mitigation projects or conducting large scale assessments. Alternatively, process-based ecosystem models allow us to test hypotheses to better understand the complex interactions present in agricultural soils by incorporating controls on biogeochemical processes, integrating knowledge from laboratory and plot experiments through model development and calibration exercises (Conant et al., 2011a; Del Grosso et al., 2001; Luo et al., 2016; Smith, 2012).

Although process-based models are extensively used to understand the complexity in an ecosystem and its underlining processes, these models are also used as tools for GHG inventories and reporting emissions and for decision support systems provide forecasting. The model needs to be calibrated or parameterized using observed data, and account for all sources of uncertainty. Above all, the model needs to be accurate and as simple as possible following the principle of parsimony (Occam’s razor). However, many process-based models rely upon hundreds of model parameters for prediction and a relatively small set of empirical data to learn from and hinders parameterization. Therefore, my main objective was to develop a statistical model analysis framework that leads to data-model integration, incorporating Bayesian model selection, Bayesian calibration, and a global sensitivity analysis (GSA) (Figure 1.1).

The platform incorporates new model development (green arrows) and model calibration only of an existing model (blue arrows) (Figure 1.1). When new model development is required, the platform can be used to test multiple models with competing hypotheses or nested models with different levels of complexity, and objectively evaluates performance with Bayesian model

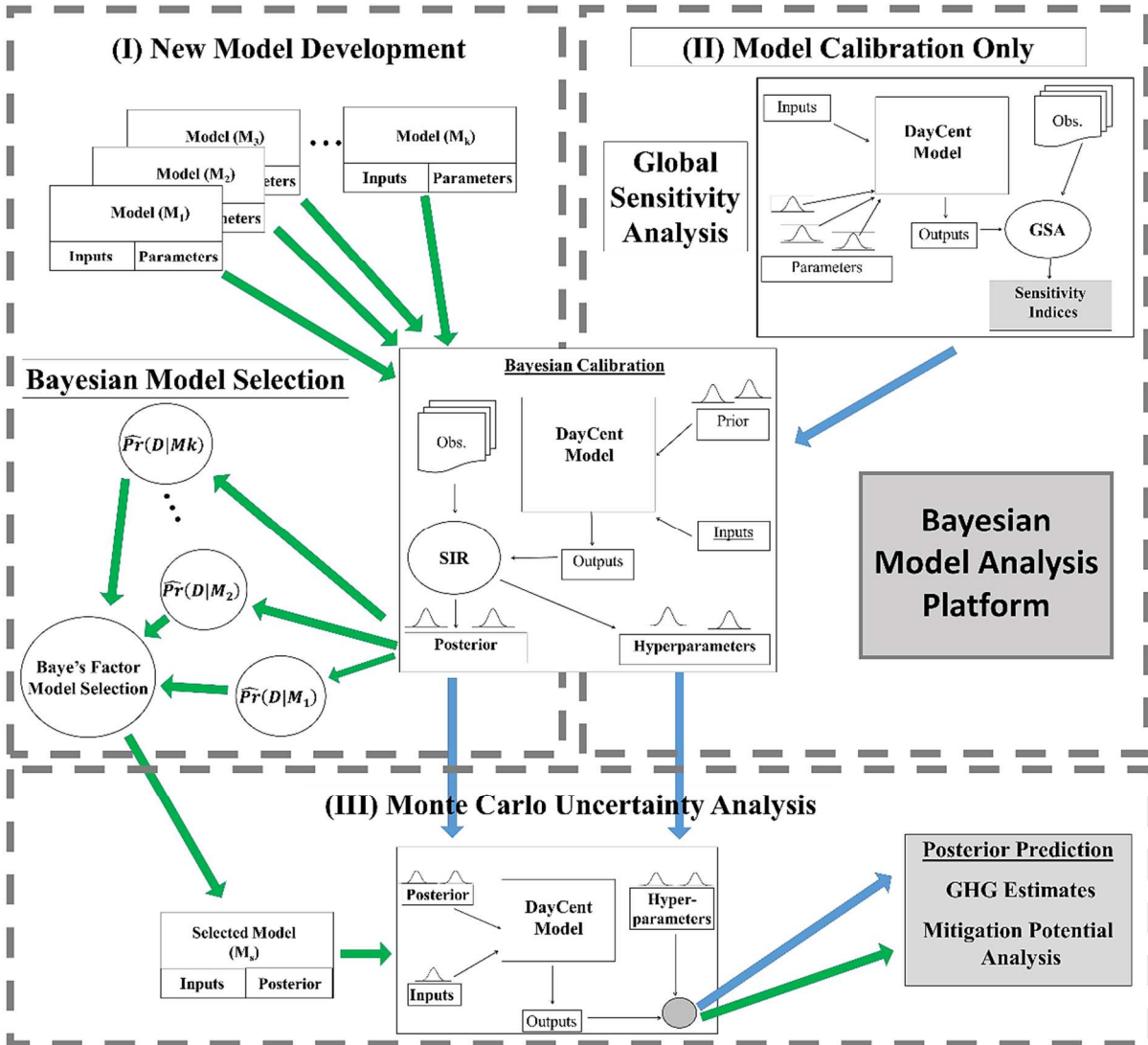


Figure 1.1. The diagram of Bayesian Model Analysis Platform for improving model predictability and quantifying model uncertainty. The diagram illustrates two scenarios for (I) New model development: competing/nested models were presented and Bayes factors are used for the purpose of Bayesian model selection (green arrow). (II) Model calibration only: where a previously developed model is further calibrated when a new dataset is available (blue arrow). Finally, the model and posterior parameters were used for (III) Monte Carlo Uncertainty Analysis to quantify model uncertainty.

selection. Specifically, variable inputs and priors were defined for each model and all the proposed models were parameterized with Bayesian calibration methods. Bayes factors were estimated by calculating integrated likelihood from the posterior. Then the final model was

selected based on the Bayes factor. The final estimates of model output and mitigation potentials were estimated using the Monte Carlo Uncertainty Analysis framework.

For the existing model, a GSA is performed to identify the most influential parameter sets using Sobols method and the non-influential parameters were set to their default values. Then, the model was parameterized using that Bayesian calibration method that provides a set of joint posterior distributions for the unknown model parameters and hyperparameters, quantifying the uncertainty in model parameters and the residual error that is not explained by the model structure, respectively. The joint posterior distribution can then be used to estimate GHG emissions and soil C stock changes with uncertainty using the Monte Carlo Uncertainty Analysis framework. The next few sections provide the underlying logic and mathematical basis for this framework.

1.2. Statistical Framework for Bayesian Inference

Let $T(x_{ij}(t))$, $O(x_{ij}(t))$, and $M(x_{ij}^*(t), \theta)$ be the true, measured, and modeled value of the ecological processes (e.g., SOC stock changes, N₂O flux) for the i^{th} site, j^{th} treatment, and year t , where $x_{ij}(t)$ represents all factors and conditions (e.g., weather, soil texture, management practices, etc.) resulting in the truth, and θ is a vector of model parameters. During the model development process, only a subset $x_{ij}^*(t)$ from $x_{ij}(t)$ are considered and used to drive the model, because, in practice, all factors and conditions are not known, and known factors may not be readily available for modeling. I denote $x_{ij}^*(t)$ as variable inputs, which may be available through the published literature or available for download from online database systems.

In situ observations or samples are collected by the investigators for further analysis using laboratory methods, as the truth is unknown. I assume that the observations are an

unbiased estimator of the truth with some level of variance, resulting in the following relationships,

$$O(x_{ij}(t)) = T(x_{ij}(t)) + \varepsilon_{ij}(t). \quad (1.1)$$

$$\varepsilon_{ij}(t) \sim N(0, \tau_{ij}^2(t)),$$

where $\varepsilon_{ij}(t)$ is normally-distributed (Gaussian) measurement error with zero mean and variance $\tau_{ij}^2(t)$.

Under conditions specified by the variable inputs and model parameter vector θ , the goal of my research is to use DayCent to predict the true values of GHG emission resulting from ecological processes (e.g., SOC stocks, N₂O flux). Assuming that DayCent output is not a perfect representation of reality, we can express the truth as an additive function of model output plus Gaussian error conditioned upon the parameter θ as follows:

$$M(x_{ij}^*(t), \theta) = T(x_{ij}(t)) + \delta(x_{ij}(t)|\theta), \quad (1.2)$$

$$\delta(x_{ij}(t)|\theta) \sim N(B_{ij}(t)|\theta, v_{ij}^2(t)|\theta),$$

where $\delta(x_{ij}(t)|\theta)$ represents model error with mean $B_{ij}(t)|\theta$, representing the model bias, and variance $v_{ij}^2(t)|\theta$. When the model is an unbiased estimator of the truth, $\delta(x_{ij}(t)|\theta)$ is a zero-mean Gaussian process (i.e. $B_{ij}(t)|\theta = 0$ for all i, j , and t); otherwise, the model has a bias due to insufficient knowledge and imperfect conceptualization of the ecosystem processes presented in the model.

Equations (1.1) and (1.2) account for three major sources of uncertainty: measurement error variance, model bias, and model error variance. Because the truth is unknown, we cannot separately identify these three sources (Kennedy and O'Hagan, 2001). However, by assuming

independence between the model error $\delta(x_{ij}(t)|\theta)$ and the measurement error ε_{ijk} , Equations (1.1) and (1.2) can be combined to allow inference accounting for all sources of uncertainty:

$$O(x_{ij}(t)) - M(x_{ij}^*(t), \theta) = \varepsilon_{ij}(t) - \delta(x_{ij}(t)|\theta) \sim N(B_{ij}(t)|\theta, \sigma_{ij}^2(t)|\theta), \quad (1.3)$$

$$\sigma_{ij}^2(t)|\theta = (v_{ij}^2(t)|\theta + \tau_{ij}^2(t)).$$

Now, combining the data across all sites i , treatment j , and year t , we have the data vectors $O(\mathbf{x})$ and $M(\mathbf{x}^*, \theta)$, each of length n (i.e., the number of observation). Applying Equation 1.3 to these vectors, we then have

$$O(\mathbf{x}) - M(\mathbf{x}^*, \theta) = \delta(\mathbf{x}|\theta), \quad (1.4)$$

$$\delta(\mathbf{x}|\theta) \sim N(B|\theta, \Sigma|\theta),$$

where I have assumed that the error vector $\delta(\mathbf{x}|\theta)$ has a multivariate normal distribution with $n \times 1$ mean vector B and $n \times n$ covariance matrix Σ given θ . In my analysis, the covariance matrix Σ represents the spatiotemporal hierarchical correlation structure in the dataset from multiple sites with repeated measures.

1.3 Bayesian Model Selection

During model development, it is necessary to make choices about the degree of precision, generality, and realism (Levins, 1966) and the appropriate level of complexity in the model (Cuddington et al., 2013). These decisions are informed by comparing different candidate models to field measurements, and Bayesian model selection provides a framework for making the necessary choices to determine the candidate model that is best for the application (Kass and Raftery, 1995; Wasserman, 2000). Many models have been developed to understand ecological systems and are often based on subject matter theories and hypotheses that vary in their underlying mechanistic explanation of the phenomenon of interest. A Bayesian model selection method provides a probabilistic framework to identify the most likely model or level of

complexity in the model supported by the measured dataset (Kass and Raftery, 1995; Wasserman, 2000). In general, using the data D , the Bayes factor provides a probabilistic scheme to compare two competing hypotheses presented in the form of mathematical models, or levels of complexity in a model, and measured by the posterior odds.

Suppose we have a total of K models, M_1, \dots, M_K under consideration and each with unknown parameter vectors, $\theta_1, \dots, \theta_K$, respectively. From Bayes' theorem, the posterior probability for the model M_k is obtained using the following equation:

$$\text{pr}(M_k|D) = \frac{\text{pr}(D|M_k)\text{pr}(M_k)}{\sum_{l=1}^K \text{pr}(D|M_l)\text{pr}(M_l)}, \quad (1.5)$$

where $\text{pr}(M_k)$ is the prior probability of the model M_k and $\text{pr}(D|M_k)$ is the integrated likelihood of the model provided by the following integrals:

$$\text{pr}(D|M_k) = \int \text{pr}(D|M_k, \theta_k)\text{pr}(\theta_k|M_k)d\theta_k. \quad (1.6)$$

where $\text{pr}(D|M_k, \theta_k)$ is the likelihood of the model M_k with parameter vector θ_k and $\text{pr}(\theta_k|M_k)$ is the prior density of θ_k for model M_k . Hence, the posterior odds can be expressed as a product of Bayes factor and prior odds for comparing model M_i versus M_j as given by the following equation:

$$B_{ij} = \frac{\text{pr}(M_i|D)}{\text{pr}(M_j|D)} = \frac{\text{pr}(D|M_i)}{\text{pr}(D|M_j)} \cdot \frac{\text{pr}(M_i)}{\text{pr}(M_j)}. \quad (1.7)$$

When $B_{ij} > 1$, the odds favor model M_i over M_j and vice versa when $B_{ij} < 1$. For example, with a Bayes factor $B_{ij} = 10$, model M_i is ten times more likely than model M_j , but if $B_{ij} = 1/10$, then model M_i is ten times less likely. A value of $B_{ij} = 1$ means both models are equally likely.

In practice, when no prior information is available about the model, the assumption of equal prior probabilities is common and the prior odds equal 1 and the posterior odds equal the Bayes factor. However, the evaluation of the Bayes factor requires calculating the integrated likelihood (Equation (1.6)), and cannot be evaluated analytically in the case of a process-based model. Alternatively, a Monte Carlo method can be applied using the harmonic mean of the posterior likelihood (Jeffreys, 1961) to estimate an integrated likelihood as follows:

$$\widehat{\text{pr}}(D|M_k) = \left\{ \frac{1}{m} \sum_{s=1}^m \text{pr}(D|M_k, \theta_k^{(s)})^{-1} \right\}^{-1}, \quad (1.8)$$

where $\text{pr}(D|M_k, \theta_k^{(s)})$ is the likelihood for model M_k and sample s in the posterior. I used the posterior likelihood from the SIR method to estimate the integrated likelihood (See Section 1.5).

1.4. Global Sensitivity Analysis

Process-based models are often over parameterized and require an unrealistically large number of simulations for Bayesian calibration. Therefore, sensitivity analysis is an important part of model development to reduce the number of parameters for conducting a Bayesian calibration analysis. Moreover, the dependency of DayCent on hundreds of unknown parameters makes the calibration process impractical. In practice, uncertainty is assigned to only a fraction of model parameters and it is assumed that other parameters are fixed without error (McAllister et al., 1994). This assumption may underrepresent uncertainty and may also introduce bias into the model output, particularly if influential parameters are set to fixed values. Thus, a global sensitivity analysis that adopts a parsimonious principle by identifying the most important or ‘sensitive’ parameters driving the model, and fixing other non-influential parameters is recommended to avoid significantly reducing estimates of model uncertainty (Saltelli et al., 2008).

The sensitivity analysis can be used to apportion the uncertainty in the model output to different sources of uncertainty in the model inputs and can be used to simplify models (Saltelli et al., 2004). Specifically, when used with the Monte Carlo framework, the parameter uncertainties are propagated through the model output to determine which parameters can be fixed without appreciably affecting the model output and the uncertainty, making the model more parsimonious (Saltelli et al., 2008), a method known as “Factor Fixing” or “Screening”.

The variance-based Sobol method (Saltelli, 2002; Sobol, 2001, 1993) is arguably one of the most robust and comprehensive global sensitivity methods (Saltelli et al., 2008). Similar to the analysis of variance, the method partitions the total variance of the model output into first-order and higher-order interaction terms and allows the estimation of the proportion of variance explained by each parameter. Unlike the local method, for example, one factor at a time (OAT) approach, this method takes into consideration the whole parameter space simultaneously in the form of a probability density function, including both main effects and interactions between parameters (Saltelli et al., 2008). The Sobol method is model-independent, works for both linear and nonlinear outputs (Sobol, 2001) and is well suited for complex and highly non-linear process-based ecosystem models, such as DayCent. (Homma and Saltelli, 1996; Saltelli, 2002).

1.5 Bayesian Model Calibration

Model parameterization is a key step to developing robust applications for estimating SOC stock changes, N₂O emissions and other model outputs. There are methods based on the optimization of parameters, such as the PEST algorithms (Necpálová et al., 2015). However, these optimization routines do not generally provide posterior distributions that could be used to quantify uncertainty in model predictions. Recent advancement in Bayesian calibration techniques has led to methods suitable for addressing uncertainty in both model parameters and

predictions. Bayesian calibration is an inverse modeling process that provides a probabilistic framework to estimate the joint posterior distribution of the unknown parameters that is consistent with the measured, model, and prior understanding. Using Bayes' theorem the posterior distribution $p(\theta|O(\mathbf{x}))$ of the parameters θ , given the measured data and model output, can be represented as a function of likelihood $L(O(\mathbf{x})|\theta)$ and the prior $p(\theta)$, where the likelihood measures the mismatch between the modeled and the measured data, and the prior is the current understanding of the distribution of model parameters based on either previous analyses or expert knowledge. In many Bayesian analyses, the posterior is known only up to a constant of proportionality and requires multidimensional integrals to calculate the normalizing constant. However, in most cases, the normalizing constant cannot be evaluated analytically (Gelman, 2014; Smith and Gelfand, 1992). Additionally, for process-based simulation models such as DayCent, model simulations are required to quantify the likelihood and an analytical solution does not exist. In this case, Monte Carlo methods provide an effective estimation by updating a sample from the prior to a sample of the posterior through the likelihood function (Rubin, 1988; Smith and Gelfand, 1992). The joint posterior distribution is defined up to a proportionality constant as follows:

$$p(\theta|O(\mathbf{x})) \propto L(O(\mathbf{x})|\theta)p(\theta). \quad (1.9)$$

In the process, the prior density $p(\theta)$ is updated to the posterior density $p(\theta|O(\mathbf{x}))$ through the data likelihood function $L(O(\mathbf{x})|\theta)$. When the data contain little information about the parameters, the posterior tends to reproduce the prior, hence nothing has been learned with the new data. However, as data become more informative, the likelihood $L(O(\mathbf{x})|\theta)$ outweighs the prior and the data dominate the posterior (Box, 1973; Gelman et al., 2014).

Many Monte Carlo methods have been developed for this purpose using the Markov Chain Monte Carlo (MCMC) approach, such as the Metropolis-Hastings (MH) algorithm (Hastings, 1970; Metropolis et al., 1953) and direct simulation such as the sampling importance resampling (SIR) algorithm (Rubin, 1988, 1987). The MH algorithm has been used in several studies for parameter estimation in process-based models (Clifford et al., 2014; Hararuk et al., 2014; Van Oijen et al., 2005; Xu et al., 2006). The MH algorithm follows a random walk through a parameter space iteratively. In each step, a new candidate vector is proposed and is accepted or rejected. This process is repeated for a large number of iterations with multiple chains to test for posterior convergence.

In contrast to MCMC, the Sampling Importance Resampling (SIR) algorithm is non-iterative and does not require a random walk through the parameter space. Instead, M random samples from the prior are obtained, and then from this, a smaller sample $m < M$ is drawn with sample probability proportional to their importance weights—resulting in an approximate sample from the joint posterior distribution. In practice, the SIR algorithm has been successfully applied in the field of fisheries to a population dynamics model for bowhead whales population (Raftery et al., 1995) and to estimate the joint posterior distribution of a 54-parameter model for age-structured yellowfin sole (McAllister and Ianelli, 1997). Being non-iterative, using the SIR algorithm, model simulations can be carried out independently and is advantageous when pairing with the inherently parallel nature of high-performance clusters and significantly reduces the waiting period compared to MCMC techniques. My approach of utilizing SIR method provides an alternative method to MCMC (e.g. Metropolis-Hastings) that lends itself inherently to parallel processing and is easily scalable—an important feature and advantage as high-performance clusters are becoming more accessible, affordable, and can be leveraged with efficiency.

The SIR algorithm (Rubin, 1987; Rubin, 1988) is a non-iterative Monte Carlo method that aims to generate a sample from the target (i.e., posterior) distribution. First, an independent random sample $\{\theta^1, \theta^2, \dots, \theta^M\}$ of size M is drawn from the prior; often, this is relatively simple. Second, model simulation is performed for each of the prior sample and likelihood values were calculated. Third, a smaller sample $\{\tilde{\theta}^1, \tilde{\theta}^2, \dots, \tilde{\theta}^m\}$ of size m ($m < M$) is drawn with or without replacement from the initial sample with probabilities, $\omega(\theta^s)$, proportional to the importance ratios or equivalently to the likelihood when the prior is also the “importance function” (Givens et al., 1995; Punt and Hilborn, 1997; Smith and Gelfand, 1992). Therefore, in the SIR algorithm, the likelihood gives the resampling weights, and parameters that produce higher goodness of fit between the measured and modeled output are more likely to be retained in the posterior.

The posterior sample generated using the SIR algorithm is a set of approximate draws from the posterior distribution, and the approximation improves as M increases (i.e. $M \rightarrow \infty$) (Gelman, 1993; Givens et al., 1995; Rubin, 1988). In practice, the choice of M should be large enough to achieve greater sampling efficiency (McAllister and Ianelli, 1997). It is also important that the prior to cover the entire support of the posterior (Gelman et al., 2014; Smith and Gelfand, 1992). When the prior is a poor approximation of the posterior, which may arise when no information is available about the distributional form of the model parameters, the algorithm becomes less efficient and results in few very large SIR weights and many small weights. In this situation, Gelman et al. (2014) suggested sampling without replacement to produce a more realistic intermediate approximation between the prior and the target densities. In the case of moderately informative importance weights, both samplings with or without replacement will produce similar results. In summary, the SIR algorithm has been proposed as one of the simplest

and most versatile Bayesian Monte Carlo methods for drawing samples from the posterior (Rubin, 1987; Rubin, 1988; Smith, 1991).

The calibration of DayCent model parameters using the SIR algorithm can be summarized as follows. First, a joint prior density function was constructed with independent uniform density functions for influential DayCent model parameters determined by the GSA. Second, from the joint prior density function, I drew a large ($M = 1,000,000$) independent random sample $\{\theta^1, \theta^2, \dots, \theta^M\}$, where each θ was a vector of DayCent parameters. The sample was drawn using Latin hypercube sampling techniques that effectively represent the parameter space by complete stratification on all parameters, which gives a more efficient representation of the parameter space (at a given sample size) than simple random sampling (Mckay et al., 1979; Owen, 1992; Stein, 1987). All other DayCent parameters were fixed to their default values. Third, the DayCent model was run for all treatments in the calibration sites for all M parameter sets $\{\theta^1, \theta^2, \dots, \theta^M\}$ and modeled estimates of the output of interest (e.g, N₂O and SOC) corresponding to each of the measurements were stored. Fourth, for each of the initial samples $\{s = 1, 2, \dots, M\}$, I evaluated the likelihood function $L(O(\mathbf{x})|\theta^s)$ assuming that the error was defined by the mismatch between the measured and modeled emissions or SOC stocks following a multivariate Gaussian distribution with a zero-mean vector and variance-covariance matrix Σ , addressing the spatiotemporal correlation of the dataset. Fifth, I calculated the standardized importance weights; $\{\omega(\theta^1), \omega(\theta^2), \dots, \omega(\theta^M)\}$ using the following formula:

$$\omega(\theta^s) = \frac{L(O(\mathbf{x})|\theta^s)}{\sum_{s=1}^M L(O(\mathbf{x})|\theta^s)}, \quad (1.10)$$

where $L(O(\mathbf{x})|\theta^s)$ is the likelihood function for the s^{th} sample. Sixth, I resampled ($m = 1000$) the parameter set $\{\tilde{\theta}^1, \tilde{\theta}^2, \dots, \tilde{\theta}^m\}$ without replacement from the initial set of parameters $\{\theta^1, \theta^2, \dots, \theta^M\}$ based on probabilities proportional to the weights $\{\omega(\theta^1), \omega(\theta^2), \dots, \omega(\theta^M)\}$.

When all steps were completed, I had m samples $\{\tilde{\theta}^1, \tilde{\theta}^2, \dots, \tilde{\theta}^m\}$ to approximate the posterior distribution. These samples were used to construct the marginal posterior densities of the model parameters using a kernel density estimator.

The likelihood updates the prior to obtain the posterior (Equation 1.9), where the likelihood is specified according to the distribution of the error or mismatch between the observed and the modeled estimates. As quality and quantity of observations increases, the observed data tends to dominate the posterior distribution and priors become less and less influential or even completely fade away in terms of their impact on the results (Box, 1973). In my analysis, I use datasets with repeated measures from multiple experiment sites and are highly correlated in both space and time. Some of this correlation may have been explained by the model simulation through the correlation in their variable inputs and model processes, but the model may not have explained all of the correlation. The correlation structure not explained by the model output, if present, should be incorporated in the variance-covariance matrix to correctly estimate uncertainty (Cressie et al., 2009; Hoeting, 2009).

Therefore, I assumed that the error in my dataset follows a multivariate Gaussian distribution with a zero mean and variance-covariance matrix Σ . Assumption of a Gaussian distribution with zero-mean is commonly made in practice because of convenience and flexibility, and more importantly, is often realistic. Therefore, in my analysis, I assume that the error between the observed and the modeled follow a multivariate normal distribution, i.e., $(O - M) \sim \text{MVN}(0, \Sigma)$, resulting in the following likelihood:

$$L(O|\theta) = (2\pi)^{-n/2} |\Sigma|^{-1/2} \exp\left\{-\frac{1}{2}(O - M)^T \Sigma^{-1} (O - M)\right\}, \quad (1.11)$$

where, n is the number of observation O and M are vectors of measured values, respectively, Σ^{-1} is the inverse of the variance-covariance matrix, T defines the transpose of a vector and $|\Sigma|$

denotes the determinant of the covariance matrix Σ . Here, for simplicity, I drop the variable input x from the notation. For computational efficiency, I used log-likelihood in all of the calculations instead of the likelihood itself, resulting in the following log-likelihood function.

$$l(O|\theta) \propto -\frac{1}{2}\log|\Sigma| - \frac{1}{2}(O - M)^T \Sigma^{-1}(O - M) \quad (1.12)$$

In theory, it is possible to conceptualize and assign hyper-parameters to the components of the variance-covariance matrix reflecting the hierarchical correlation structures presented in the dataset. However, in practice adopting a full Bayesian analysis demands a full and careful consideration of prior information regarding the hyper-parameters (Kennedy and O’Hagan, 2001). Fixing hyper-parameters with plausible estimates has been adopted in many studies (Braswell et al., 2005; Hurtt and Armstrong, 1996; Kennedy and O’Hagan, 2001; McAllister and Ianelli, 1997; Sacks et al., 2006; Van Oijen et al., 2005), but this only impacts the uncertainty through ‘second-order’ effects that can often be neglected without losing much information about the uncertainty (Kennedy and O’Hagan, 2001). Furthermore, when a prior for the variance was included, McAllister and Ianelli, (1997) found SIR became inefficient in practice, and fixing at its model value appeared to be a reasonable remedy and did not lead to bias in the posterior. In my analysis, I used the restricted maximum likelihood (REML) estimator within the linear mixed-effect (LME) framework to estimate the most plausible fixed values for the hyper-parameters (i.e. component of Σ matrix). The model included two levels of nested random effects (site and year within site) to account for the spatiotemporal dependencies in the dataset that was used to calibrate DayCent (see Pinheiro et al., 2010).

1.6. Model Prediction using Monte Carlo Approach

The final step in the Bayesian model analysis framework is to use a Monte Carlo approach to propagate uncertainty through the DayCent model application and derive prediction intervals.

The resulting prediction intervals address the uncertainty associated with model parameters, but also the unexplained error in model predictions based on the hyperparameters. The hyperparameters quantify uncertainty associated with parameters in other sub-models and also imperfect representation of processes in the DayCent model structure.

I applied the Monte Carlo approach using the sample from the joint posterior probability distribution of the parameters and hyperparameters, applying the model iteratively for many replicates (e.g., 1000). The Monte Carlo analysis can also address uncertainties in model inputs, such as weather data and edaphic characteristics. The main purpose or quantities of interest are the estimates and associated uncertainty for model output and GHG mitigation potentials of agricultural soils. The method assigns uncertainties by propagating the error in the parameters and hyper-parameters, which are influenced by uncertainties associated with model structure and the measurement error.

1.7 Organization of Dissertation

The dissertation is about the development and improvement (meaning, equation formulation, model selection, and calibration) of the DayCent process-based ecosystem model, which has an intermediate level of complexity. I focused on developing new model algorithms and making model predictions for several management practices, assessing their mitigation potentials, and quantifying uncertainty on the predictions. The dissertation is organized into five chapters, including this chapter with an introduction to the Bayesian model platform and highlighting some of the ecological and modeling challenges of our time. Chapter 2 presents a Bayesian model analysis framework and includes GSA to identify a set of most influential parameters, a sampling importance resampling (SIR) algorithm to draw a sample from the joint posterior distribution of model parameters and a Monte Carlo simulation to estimate prediction

uncertainty. The framework is then applied to the DayCent ecosystem model to reduce uncertainty on model prediction of SOC stocks of various management form various long-term experimental sites and stock differences within sites between two practice; (1) with and without farmyard manure, (2) adoption of no-till, and (3) with and without synthetic N fertilizer application. Chapter 3 detailed the development of six different models of varying complexity for NH_3 volatilization integrated into DayCent. All six models were calibrated using SIR algorithm and Bayesian model selection techniques to identify the most appropriate level of complexity supported by the measurement dataset. Three management options were evaluated to reduce NH_3 volatilization, including mechanical incorporation of urea; incorporation with irrigation/rainfall events; and use of urease inhibitor, a stabilized enhanced efficiency N fertilizer with urease inhibitors. Chapter 4 provides model development and improvement, application of GSA, and SIR algorithm to quantify reduction factors for N_2O emissions when switching from conventional N fertilizer to two enhanced efficiency nitrogen fertilizers. Model development incorporates the N release for controlled-release N fertilizer (CRNFs) and nitrification inhibitors (NIs) as a stabilized N product that inhibits the transformation of NH_4^+ to NO_3^- . Chapter 2-4 are formatted as per individual publication requirements and contain abstracts, introductions, materials and methods, discussions, and conclusions. Chapter 5, summarizes the results and finding from the previous three chapters (i.e., 2-4) and possible future directions.

CHAPTER 2: MODELING AMMONIA VOLATILIZATION FROM UREA APPLICATION TO AGRICULTURAL SOILS: DAYCENT MODEL DEVELOPMENT

2.1. Summary

Nitrogen (N) loss through ammonia (NH_3) volatilization in agricultural soils is a significant source of atmospheric NH_3 , contributing to low N use efficiency in crops, risk to human health, environmental pollution, and is an indirect source of nitrous oxide (N_2O) emissions. My objective was to develop an ammonia volatilization method within the DayCent ecosystem model that incorporates key 4R management practices that influence NH_3 volatilization associated with application of urea-based nitrogen fertilizers to agricultural soils. The NH_3 volatilization method was developed with Bayesian calibration using sampling importance resampling (SIR) methods and Bayes factors to select the level of complexity in the model that best represents NH_3 volatilization given the observed data. The final model included urea hydrolysis and the influence of urease inhibitors; short-term soil pH changes following fertilization; fertilizer incorporation into the soil (mechanically and through irrigation/precipitation); and specification of the fertilizer placement method (i.e. broadcast vs. banding and surface vs incorporated). DayCent predicts NH_3 volatilization with a root-mean-squared error (RMSE) of 158 (95% interval ranging from 133 to 192), bias of 7 (95% interval ranging from -106 to 102) $\text{g NH}_3\text{-N ha}^{-1} \text{ day}^{-1}$, and with a Bayesian R^2 value of 0.39 (95% interval ranging from 0.17 to 0.62). Furthermore, the model incorporates key management options influencing NH_3 volatilization related to placement method and fertilizer type with and without urease inhibitors that can be used to evaluate management and policy options for reducing losses of NH_3 from urea fertilization.

2.2. Introduction

Crop production is by far the single largest use of synthetic nitrogen (N) fertilizer, consuming about 80% of the total global production (Erisman et al., 2007; Galloway et al., 2008).

Approximately 10-20% of fertilizer applied to agricultural soil is estimated to be volatilized as ammonia (NH_3) to the atmosphere, and the volatilization rates vary based on management practices, particularly fertilizer types and application rates, as well as climatic conditions and edaphic characteristics (Bouwman et al., 2002a; Pan et al., 2016; Sommer et al., 2001). It is a significant pathway of N loss from cropping systems and a major source of atmospheric NH_3 , contributing to air pollution, reducing N use efficiency, and negatively impacting human health and the environment. Some of the environmental impacts include soil acidification, eutrophication of surface water, and loss of biodiversity (ApSimon et al., 1987; Asman et al., 1998; Bouwman et al., 2002a; Erisman et al., 2007; Roelle and Aneja, 2002). In addition, it is also an indirect source of nitrous oxide (N_2O) emissions due to the N cascade effect in the environment (Galloway et al., 2003). Furthermore, a molecule of N_2O is a more potent greenhouse gas relative to carbon dioxide contributing about 300 times more to the warming effect in the atmosphere than CO_2 over a 100-year time horizon (Schlesinger and Bernhardt, 2013), and N_2O is also a dominant ozone-depleting substance (Ravishankara et al., 2009).

Several physical and chemical processes are involved with NH_3 volatilization from fertilized soil (Freney et al., 1983; Misselbrook et al., 2005; Sommer et al., 2001). Following application of urea to the soil, urea is rapidly hydrolyzed by extracellular enzyme urease into plant-available NH_4^+ (Kissel et al., 1988). The process can be summarized by two subsequent reactions in Equation 2.1 and 2.2:



Both reactions consume H^+ and raise soil pH temporarily (Kissel et al., 1988; Sommer et al., 2001). With higher soil pH, the ratio of NH_3 to NH_4^+ increases and so does the potential for NH_3 volatilization (Freney et al., 1983; Sommer et al., 2001). However, the change in soil pH is also affected by the initial pH and the buffering capacity of the soil (Curtin et al., 1996).

There are several management practices that reduce NH_3 volatilization (Engel et al., 2011; Holcomb et al., 2011; Pan et al., 2016; Rochette et al., 2013a) following the 4R nutrient stewardship paradigm, i.e., right type, right rate, right placement and right timing of fertilizer applications (Bruulsema et al., 2009). For example, surface applied urea has a higher NH_3 volatilization rate compared to sub-surface banding or deep placement (Pan et al., 2016). When urea is placed deeper in the soil profile, losses are lower due to soil resistance to the upward diffusion of gaseous NH_3 and subsequent conversion of NH_3 to NH_4^+ , along with a greater retention of NH_4^+ in the soil (Freney et al., 1983; Sommer et al., 2001). Therefore, incorporating urea deeper into the soil profile through mechanical incorporation is recommended to reduce NH_3 loss (Bouwmeester et al., 1985; Rochette et al., 2013a). Alternatively, applied urea can be effectively moved deeper in the soil profile by rainfall or irrigation, depending on the timing and intensity of rainfall or irrigation after application (Black et al., 1987; Holcomb et al., 2011). The opportunity for deeper incorporation without mechanical incorporation into the soil can also be accomplished by treating urea with urease inhibitors. The inhibitors effectively delay urea hydrolysis, allowing more time for rainfall or irrigation to move urea deeper and diffuse through the soil profile (Dawar et al., 2011a; Engel et al., 2011; Pan et al., 2016; Watson et al., 1994).

Process-based models can provide a useful framework for understanding and predicting ecological responses (Del Grosso et al., 2012). These models are used to test scientific understanding, make predictions for future scenarios, and evaluate management and policy outcomes. DayCent (Parton et al., 1998) is an ecosystem model that can be used to evaluate the fate of applied N in crop production systems, but needs further development to improve the prediction of NH₃ volatilization.

My objective was to further develop the DayCent model to predict NH₃ volatilization from urea-based fertilizer applications to agricultural soils, along with modeling the influence of key management practices associated with 4R recommendations for reducing N losses from the soil. I focused on development of the model to simulate urea-based fertilizers with or without urease inhibitor and different methods of fertilizer placement on NH₃ volatilization. DayCent has been well tested for capturing the influence of different rates of N applications on crop yield and N₂O emissions (Fitton et al., 2014), and so that functionality was not further tested here. This study enhances the prediction capability of DayCent for estimating N losses from soils in support of management and policy decisions, while also providing insights into key uncertainties requiring further research.

2.3. Materials and Methods

I applied a framework with Bayesian model calibration and selection methods to determine the most appropriate level of complexity for the model (Kass and Raftery, 1995; Wasserman, 2000), and to minimize uncertainty in the parameters to the extent possible given the observed measurement data from multiple sites. There are four main parts to the model development and testing: (1) development of six levels of complexity for modeling NH₃ volatilization, (2) Bayesian calibration of the model using the sampling importance resampling (SIR) algorithm,

(3) Bayesian model ranking and selection using Bayes factors, and (4) performance evaluation via comparison of the model to measured NH_3 losses.

2.3.1. DayCent Model

DayCent (Del Grosso et al., 2001; Parton et al., 1998) is an ecosystem model of intermediate complexity and operates on a daily time step. It is designed to simulate the flow of carbon (C), and nitrogen (N) among several pools in plant-soil systems. The model simulates key ecosystem processes related to the N cycle including N uptake by plants, mineralization and immobilization, nitrification and denitrification, nitrate (NO_3) leaching, and N trace gas fluxes (N_2O , NO_x , N_2). The model simulates NH_3 volatilization from plant tissue associated with plant harvest, senescence, and grazing removal. It also models soil temperature and the flow of water through a multi-layered soil profile. DayCent simulates plant growth and water use based on green leaf area index (GLAI) as a function of green leaf weight ratio and accumulation of aboveground biomass (Zhang et al., 2020). Changes in green leaf weight ratio are dependent on heat units, and GLAI incorporates the influence of plant canopy cover on both photosynthesis and evapotranspiration (ET). Growth rates based on photosynthetic capacity are further constrained by soil water and nitrogen availability.

The previous version of the model assumes that N from urea fertilizer is immediately converted to NH_4^+ , which is evenly distributed in the 0-10 cm layer, and does not dynamically simulate N losses from NH_3 volatilization in the soil. In this work, I developed algorithms for simulating N losses that could be incorporated into DayCent and tested algorithms with varying levels of complexity to model NH_3 volatilization loss, based on the following processes and drivers of emissions: a) urea hydrolysis, b) effect of N placement on NH_3 volatilization (i.e., broadcast vs banded and surface application vs incorporation), c) effect of vertical and lateral

movement of urea with rainfall and irrigated water, d) short-term soil pH changes driven by the addition of urea, and e) effect of soil buffering capacity on soil pH change.

2.3.2. Experimental Sites

The dataset for model calibration and selection consisted of eight field locations in the United States (Table 2.1). One study included five sites from a cold and dry region in the state of Montana with measurements during late-fall, winter, and early spring (Engel et al., 2017, 2011). The other three sites included a rain-fed experiment in Minnesota (Thapa et al., 2015), an irrigated site in Colorado (Halvorson et al., 2016; Jantalia et al., 2012), and a site with warm and wet conditions in Louisiana (Tian et al., 2015). Collectively the dataset consisted of a total of 42 site-year-treatment combinations for a total of 479 individual observations of NH₃ emissions. Treatments mostly consisted of plots with applications of urea and urea treated with urease inhibitors, but some sites also included control plots with no fertilization.

Table 2.1. Experimental sites used for Bayesian model calibration and selection along with reported soil properties that were used in DayCent model simulation.

Site Locations	Lat.	Long.	Sand	Silt	Clay	pH	References
Baton Rouge, LA	30.35	-91.17	0.347	0.448	0.205	6.2	Tian et al. (2015)
Fergus County, MT	47.37	-110.08	0.284	0.362	0.354	6.3	Engel et al. (2017)
Fergus County, MT	47.37	-110.10	0.263	0.454	0.283	7.3	Engel et al. (2017)
Fort Collins, CO	40.65	-104.99	0.409	0.254	0.337	7.6	Halvorson et al. (2016) Jantalia et al. (2012)
Gallatin County, MT	45.79	-111.59	0.338	0.286	0.375	8.4	Engel et al. (2011)
Glyndon, MN	46.91	-96.61	0.088	0.587	0.325	8.4	Thapa et al. (2015)
Hill County, MT	48.53	-110.90	0.455	0.311	0.234	6.4	Engel et al. (2011)
Hill County, MT	48.84	-110.06	0.616	0.226	0.159	5.5	Engel et al. (2011)

2.3.3. Model Development

For model development, it is necessary to make choices about the degree of precision, generality, and realism (Levins, 1966) and the appropriate level of complexity in the model (Cuddington et al., 2013). I identified six processes and drivers that influence the rate of NH₃ volatilization for model development and testing (Table 2.2). These processes and drivers were chosen for the following reasons: (1) they could be accommodated within the structural framework of DayCent, (2) input variables were reported in the publication or were easily available from other sources, and (3) the processes covered both variation in management practices and environmental factors that influence NH₃ volatilization from agricultural soils.

Six candidate levels of model complexity {M₁, M₂, ..., M₆} were developed in this study (Table 2.2). M₁ is the full model that includes all the processes considered and drivers of emissions. The other candidates, M₂, M₃, M₄, M₅, and M₆, include subsets of the processes and drivers, of which M₆ is the least complex and only includes urea hydrolysis and a simple NH₃ diffusion process that depends on soil temperature and baseline soil pH.

Table 2.2. List of processes and six levels of complexity in the NH₃ volatilization model that was tested in the DayCent model framework. The process is included if the value is 1 and excluded if the value is 0.

Processes	M1	M2	M3	M4	M5	M6
Urea Hydrolysis	1	1	1	1	1	1
Diffusion of NH ₃	1	1	1	1	1	1
Depth Effect on NH ₃ Diffusion	1	1	1	0	0	0
N Concentration Factor	1	1	1	0	0	0
Increase in Soil pH	1	1	0	1	1	0
Soil Buffering Capacity	1	0	0	0	1	0

2.3.3.1. Urea Hydrolysis

The rate of urea hydrolysis is assumed to follow an enzymatic reaction represented by simple Michaelis-Menten kinetics (Cabrera et al., 1991; Dalal, 1975; Paulson and Kurtz, 1970; Pettit et al., 1976; Tabatabai, 1973), in which the reaction rate increases with urea concentration until there is saturation of the enzyme activity. When a urease inhibitor is added, the inhibitor binds with the free enzyme blocking the hydrolytic action of the urease enzyme and slows the hydrolysis process by shifting the reaction curve (Chou and Talalay, 1977). The rate of urea hydrolysis with or without the addition of a urease inhibitor is modeled using Equation 2.3:

$$UH_{\text{rate}} = \left(\frac{V_{\text{max}} \times [U]}{K_M + K_{UI} + [U]} \right) \times f_{ST} \times f_{SM}, \quad (2.3)$$

where UH_{rate} is the rate of urea hydrolysis (ppm sec^{-1}), V_{max} is the maximum urea hydrolysis rate that is achieved by the system (ppm sec^{-1}), and $[U]$ is the urea concentration (ppm). The K_M factor (ppm) is Michaelis constant representing the urea concentration at which the reaction rate is half of V_{max} , and K_{UI} (ppm) is the additional effect of urease inhibitors on the Michaelis constant ($K_{UI} = 0$ with no urease inhibitor applied). The rate of urea hydrolysis is known to increase with increasing temperature (Moyo et al., 1989; Sahrawat, 1984; Xu et al., 1993) and soil moisture (Kumar and Wagenet, 1984; Sahrawat, 1984). The influence of soil temperature, f_{ST} , and soil moisture, f_{SM} , are modeled as scalars on the rate of urea hydrolysis and range from 0 to 1.

The effect of temperature on urea hydrolysis is modeled as a sigmodal curve with increasing rates associated with increasing temperature (Equation 2.4):

$$f_{ST} = \frac{1}{1 + \beta_{ST1} \times \exp\{-\beta_{ST2} \times T_{\text{soil}}\}}, \quad (2.4)$$

where T_{soil} is the average soil temperature in °C, and the exact shape of the sigmoid curve is determined by two parameters β_{ST_1} and β_{ST_2} . Additionally, the effect of soil moisture on hydrolysis is assumed to be linear and increases with water-filled pore space (WFPS) as represented by Equation 2.5:

$$f_{\text{SM}} = \beta_{\text{SM}_1} + \beta_{\text{SM}_2} \times \text{WFPS}, \quad (2.5)$$

where β_{SM_1} and β_{SM_2} are the intercept and the slope term for the equation.

2.3.3.2. Diffusion of Gaseous NH_3

The rate of NH_3 loss to the atmosphere, volNH_3 ($\text{g NH}_3\text{-N ha}^{-1} \text{ day}^{-1}$), is controlled by the transfer coefficient K_a (day^{-1}) and the amount of NH_4^+ (g N ha^{-1}) present in the soil as follows:

$$\text{volNH}_3 = K_a \times \text{NH}_4^+. \quad (2.6)$$

Furthermore, I assumed that the transfer coefficient is affected by soil temperature, soil pH, and incorporation depth as represented in Equation 2.7:

$$K_a = \frac{K_{\text{max}}}{1 + \exp\{-(\alpha_0 + \alpha_{\text{pH}} \times \text{pH} + \alpha_{\text{ST}} * T_{\text{soil}})\}} \times f_{\text{depth}}, \quad (2.7)$$

where K_{max} (day^{-1}) is the maximum potential transfer coefficient; T_{soil} is the average soil temperature (°C); f_{depth} is the scaler effect of incorporation of urea on ammonia volatilization through mechanical operations or leaching associated with precipitation or irrigation; and α_0 , α_{pH} , and α_{ST} are model parameters.

2.3.3.3. Depth Effect on NH_3 Diffusion

I modeled the combined effect of fertilizer incorporation depth through mechanical and irrigation/precipitation using Equation 2.8, 2.9, and 2.10:

$$f_{\text{depth}_t} = \min(f_{\text{IDM}}, f_{\text{IDW}_t}) \quad (2.8)$$

$$f_{\text{IDW}_t} = \text{UF}_{\text{rem}_t} * \exp\{-\alpha_w \times I_{w_t}\} \quad (2.9)$$

$$f_{\text{IDM}} = \exp\{-\alpha_M \times \text{ID}_M\} \quad (2.10)$$

where f_{IDM} is the scaling factor for the incorporation depth ID_M (in mm) at the time of application, ID_M is the depth of mechanical incorporation (in cm), f_{IDW_t} is the scaling factor for water input, I_{w_t} is the amount of water infiltration (in mm), UF_{rem_t} is the remaining fraction of applied urea at time t , and α_M and α_w are model parameters. In the model, I assumed that only the remaining urea can be moved deeper in the soil profile via leaching. After hydrolysis of urea to NH_4^+ , the N is considered immobile based on the model structure.

2.3.3.4. Urea and NH_4^+ Concentration Factor

When urea is applied to the soil, there is a localized increase in N concentration around the granules. In addition, a higher concentration of urea is found with banded applications compared to broadcasting. The applied urea is rapidly hydrolyzed to form NH_4^+ and the remaining urea also moves away from the localized area in the soil both vertically and laterally creating a concentration profile (Dawar et al., 2011b; Singh and Nye, 1984). In addition to the incorporation depth, I represented the concentration profile as a fraction of soil volume occupied by the localized concentration in order to model the effect of both lateral and vertical movement on a daily time step using Equation 2.11:

$$\text{CFU}_t = \text{CFU}_{t-1} + \text{FRU}_t * (1 - \text{CFU}_{t-1}) * g(\text{WFPS}) * g(\text{ST}), \quad (2.11)$$

where CFU_t is concentration factor of urea or the fractional volume of soil covered by urea at t days after urea application, and FRU_t is the fraction of urea remaining after t days. At the time of

the urea application (i.e. $t = 0$), $FRU_0 = 1$ and CFU_0 is a parameter input. Furthermore, $g(WFPS)$ is the scaling factor (0-1) for relative soil water content defined by Equation 2.12 below:

$$g(WFPS) = \begin{cases} \frac{WFPS}{FC} & WFSP \leq FC \\ 1 & WFSP > FC \end{cases}, \quad (2.12)$$

where $WFPS$ and FC are the water-filled pore space and field capacity of the first three DayCent soil layers (i.e. 0-10cm). The term $g(ST)$ is the scaling factor for soil temperature and is represented by the following equation:

$$g(ST) = \begin{cases} 0 & Temp \leq 0 \\ \frac{Avg. ST}{ST^*} & 0 < Temp < ST^* \\ 1 & Temp \geq ST^* \end{cases}, \quad (2.13)$$

where ST^* is the maximum soil temperature at or above which urea is uniformly distributed across the 0-10 cm soil layer. In the field, the initial fraction of soil volume in which urea is concentrated depends on the type and mode of application. Application mode is an input to the model that is dynamically updated every time step following the fertilizer addition using Equation 2.11, 2.12, and 2.13.

Once the concentration factor for urea is calculated, I estimate the concentration factor of NH_4^+ (CFA_t) ($vol\ vol^{-1}$) by taking the weighted average of NH_4^+ already in the soil, new NH_4^+ from mineralization and deposition, and the amount of NH_4^+ added through the fertilization events. During the calculation, I assume that NH_4^+ from mineralization is uniformly distributed within the 0-10 cm soil layer. In addition, the f_{depth_t} and CFA_t are also adjusted for new NH_4^+ from mineralization using a weighted average until reaching an equilibrium state (i.e., uniformly distributed) in the absence of additional synthetic N fertilizer additions.

2.3.3.5. Increase in Soil pH

During urea hydrolysis, the reaction consumes a net of one H^+ ion for each NH_4^+ formed (Equation 3.1), which raises soil pH (Kissel et al., 1988; Rochette et al., 2013b). Furthermore, when NH_4^+ is consumed by other processes in the soil, such as plant uptake, nitrification, and ammonia volatilization, H^+ ions are released back to the soil and counter the increase in soil pH. Thus, I modeled the short-term increase in soil pH as a function of fraction of N applied as urea (UFNA), titratable acidity to pH 9 (TA9), NH_4^+ concentration, and concentration factor for ammonium (CFA) to account for the localized pH change as follows:

$$dpH = \Delta pH \times \left(1 - \exp \left\{ -\beta_{pH} \times \left(\frac{UFNA * [NH_4^+]}{TA9 \times CFA} \right) \right\} \right), \quad (2.14)$$

where dpH is the change in soil pH, ΔpH is the difference between reference pH (i.e., 9) minus initial soil pH, $[NH_4^+]$ is the ammonium concentration (ppm) per total soil and β_{pH} is a model parameter.

2.3.3.6. Soil Buffering Capacity

I modeled the soil buffering capacity based on a study by Curtin et al. (1996) derived from a diverse suite of 59 agricultural soils from Saskatchewan, Canada. The regression equations are derived from chemical analyses to titratable acidity of pH 9 as follows:

$$TA9 = 180 \times (\gamma_0 + \gamma_1 \times OC \times \Delta pH + \gamma_2 \times \text{clay} \times \Delta pH), \quad (2.15)$$

where TA9 is the titratable acidity to pH 9 (ppm), ΔpH is the difference between reference pH (i.e., 9) and initial soil pH, OC is the soil organic carbon ($g\ g^{-1}$), and clay is the fraction of clay in the soil.

2.3.4. Bayesian Calibration and Model Selection

Bayesian calibration was applied to all six levels of complexity in the model separately to estimate the joint posterior distribution of the unknown model parameters. I implemented a non-iterative Monte Carlo method of Sampling Importance Resampling (SIR) algorithm (Morris, 1987; Rubin, 1988) to generate an approximate sample from the posterior distribution, similar to the analysis in Gurung et al. (2020). I assigned independent uniform priors for each of the model parameters constrained within the minimum and the maximum values. Parameter bounds were based on information found in previously published journal articles and best approximations provided by the DayCent development team (Table 2.3). The likelihood is based on the assumption that the data collected from the same sites and years are correlated both spatially and temporally and the covariance is estimated with linear-mixed-effect (LME) model framework with two level of random effects for site and site by year, as presented in Gurung et al., (2020).

Many models have been developed to understand ecological systems and are often based on subject matter theories and hypotheses that vary in their underlying mechanistic explanation of the phenomenon of interest. A Bayesian model selection method provides a probabilistic framework to identify the most likely model or level of complexity in the model supported by the measured dataset (Kass and Raftery, 1995; Wasserman, 2000). In general, using the data D , Bayes factor provides a probabilistic scheme to compare two competing hypotheses presented in the form of mathematical models, or levels of complexity in a model, and measured by the posterior odds. When comparing M_i versus M_j , the posterior odds can be expressed as a product of Bayes factor and prior odds given by the following equation:

$$B_{ij} = \frac{\text{pr}(D|M_i)}{\text{pr}(D|M_j)} \cdot \frac{\text{pr}(M_i)}{\text{pr}(M_j)}. \quad (2.16)$$

Table 2.3. Lower and upper bounds of independent uniform prior distributions and definitions for NH₃ volatilization model parameters.

Parameters	Lower	Upper	Distribution	Definitions
CFU ₀	0.001	0.05	uniform	Fraction of soil volume covered by urea at the time of application
K _M	5	500	uniform	Michaelis constant (ppm) for urea hydrolysis
K _{UI}	50	1000	uniform	Urease inhibitor effect on Michaelis constant (ppm) for urea hydrolysis
β _{ST₁}	5	50	uniform	Soil temperature parameter for Vmax (urea hydrolysis)
β _{ST₂}	0.05	1	uniform	Soil temperature parameter for Vmax (urea hydrolysis)
β _{pH}	0	6	uniform	Parameter for pH change function (>0)
α _W	0	1.5	uniform	Precipitation + irrigation effect on ammonia volatilization rate
α _M	0	1.75	uniform	Effect of incorporation depth on ammonia volatilization rate
K _{max}	0.00001	0.1	uniform	Maximum rate of ammonia volatilization
α _{pH}	0.1	2	uniform	Parameter for the effect of soil pH on the rate of ammonia volatilization
α _{ST}	0.01	1	uniform	Effect of soil temperature on the rate of ammonia volatilization
V _{max}	0.0005	0.02	uniform	Maximum potential rate of urea hydrolysis (ppm/sec)
β _{SM₁}	0	0.75	uniform	Intercept for soil moisture effect on urea hydrolysis
β _{SM₂}	0.05	2	uniform	Slope for soil moisture effect on urea hydrolysis
γ ₀	-2	2	uniform	Intercept term for estimation of titratable acidity to pH 9
γ ₁	50	68	uniform	Effect of SOC and initial pH on estimation of titratable acidity to pH 9
γ ₂	3	5.5	uniform	Effect of clay and initial pH on estimation of titratable acidity to pH 9
ST*	5	35	uniform	Soil temperature threshold Limiting diffusion of urea in soil

When $B_{ij} > 1$, the odds favor model M_i over M_j and vice versa when $B_{ij} < 1$. For example, with a Bayes factor $B_{ij} = 10$, model M_i is ten times more likely than model M_j , but if $B_{ij} = 1/10$, then model M_i is ten times less likely. A value of $B_{ij} = 1$ means both models are

equally likely. A formal interpretation of the Bayes factor as a scale of evidence is provided in Table 2.4 with seven major categories. Similar evidence is also recommended using \log_{10} scale by (Jeffreys, 1961).

Table 2.4. Jeffreys' scale of evidence using Bayes factors for hypothesis testing associated with model selection.

Bayes factor	Interpretation
$B_{ij} < \frac{1}{100}$	Decisive evidence for M_j
$\frac{1}{100} < B_{ij} < \frac{1}{10}$	Strong evidence for M_j
$\frac{1}{10} < B_{ij} < \frac{1}{3.2}$	Substantial evidence for M_j
$\frac{1}{3.2} < B_{ij} < 3.2$	Weak evidence (1 neutrol)
$3.2 < B_{ij} < 10$	Substantial evidence for M_i
$10 < B_{ij} < 100$	Strong evidence for M_i
$B_{ij} < 100$	Decisive evidence for M_i

In practice, when no prior information is available about the model, the assumption of equal prior probabilities is common and the prior odds equal 1 and the posterior odds equal the Bayes factor. However, the evaluation of the Bayes factor requires calculating the integrated likelihood, and cannot be evaluated analytically in the case of a process-based model.

Alternatively, a Monte Carlo method can be applied using the harmonic mean of the posterior likelihood (Jeffreys, 1961) to estimate an integrated likelihood as follows:

$$\widehat{\text{pr}}(D|M_k) = \left\{ \frac{1}{m} \sum_{s=1}^m \text{pr}(D|M_k, \theta_k^{(s)})^{-1} \right\}^{-1}, \quad (2.17)$$

where $\text{pr}(D|M_k, \theta_k^{(s)})$ is the likelihood for model M_k and sample s in the posterior. I used the posterior likelihood from the SIR method to estimate the integrated likelihood. Additionally, I

calculated standard goodness-of-fit measures—root mean squared error (RMSE), model bias, and Bayesian R^2 (Galman et al., 2019) to evaluate the different levels of model complexity, using Equation 2.18, 2.19, and 2.20 respectively.

$$\text{RMSE}_s = \sqrt{\frac{1}{n} \sum_{i=1}^n (P_i^s - O_i)^2}, \quad (2.18)$$

$$\text{Bias}_s = \frac{1}{n} \sum_{i=1}^n (P_i^s - O_i)^2, \quad (2.19)$$

$$\text{Bayesian } R_s^2 = \frac{\text{Explained variance}}{\text{Explained variance} + \text{Residue Variance}}, \quad (2.20)$$

where, P_i^s and O_i are the model prediction for parameter set θ^s and observed NH_3 volatilization and n is the sample size of the dataset. The goodness-of-fit measures were calculated for both the prior and the posterior. In addition, point estimates for all three goodness-of-fit statistics were estimated based on maximum a posterior (MAP) estimate of the parameters after the calibration. The MAP estimates are the mode of the posterior parameter distribution, i.e., highest posterior density for the model parameters, and is considered the single best parameter set for the joint posterior probability distribution.

2.4. Results

2.4.1. Bayesian Calibration

All six levels of complexity in the model were calibrated using SIR algorithm with 1 million initial samples from the prior and 1,000 resampling draws without replacement to approximate the posterior. In Table 2.5, I have provided the mean and range (2.5 and 97.5 percentile) of root-mean-squared errors (RMSE), model bias (Bias), and Bayesian R^2 (Gelman et al., 2019) of model predictions from both the prior and posterior distributions.

The calibration process reduces the error in predicting NH₃ volatilization from the prior by a factor (mean RMSE of prior divide by mean RMSE of the posterior) between 1.72 and 2.15. For all six models, the SIR algorithm successfully retained parameter sets that produce lower RMSE, lower absolute bias, and higher R² values along with narrower ranges in the posterior parameter distributions compared to the prior distributions (Table 2.5).

Table 2.5. Mean and range (2.5 and 97.5 percentiles in the parenthesis) for the Root-Mean-Square Error (RMSE), Model Bias, and Bayesian R² for all six levels of model complexity from simulations with the prior and posterior parameter distributions. Point estimates for RMSE, Bias, and Bayesian R² values are also included for Maximum a Posterior Probability (MAP). Units for RMSE and Bias are in g NH₃-N ha⁻¹ day⁻¹.

		Model Complexity					
		M1	M2	M3	M4	M5	M6
Prior	RMSE	281 (183, 832)	280 (183, 834)	280 (185, 826)	355 (177, 709)	354 (178, 707)	351 (179, 707)
	Bias	46 (-632, 155)	45 (-635, 155)	48 (-620, 155)	-151 (-576, 150)	-149 (-572, 150)	-143 (-564, 150)
	R ²	0.12 (0.0, 0.52)	0.12 (0.0, 0.52)	0.12 (0.0, 0.52)	0.35 (0.0, 0.55)	0.35 (0.0, 0.54)	0.35 (0.0, 0.54)
	MAP						
Posterior	RMSE	160 (133, 193)	158 (133, 192)	163 (140, 196)	165 (149, 201)	165 (150, 198)	168 (151, 203)
	Bias	8 (-100, 103)	7 (-106, 102)	7 (-105, 105)	-39 (-122, 42)	-36 (-120, 47)	-38 (-124, 48)
	R ²	0.39 (0.2, 0.6)	0.39 (0.17, 0.6)	0.36 (0.15, 0.59)	0.35 (0.17, 0.5)	0.34 (0.15, 0.52)	0.34 (0.14, 0.5)
	MAP						
MAP	RMSE	124	110	126	144	155	151
	Bias	14	-9	-34	-9	-58	-53
	R ²	0.60	0.71	0.57	0.35	0.47	0.42

2.4.2. Bayesian Model Selection

The levels of complexity in the model are ranked as follows based on the Bayes factors: M₂ > M₁ > M₃ > M₄ > M₅ > M₆ (Table 2.6). Two out of the six models, M₁ (full model) and M₂ have relatively higher posterior model probabilities of 0.385 and 0.5, respectively. All other

models have posterior model probabilities of < 0.07 , and therefore are less likely to represent the dynamics associated with NH_3 volatilization.

Table 2.6. Pairwise Bayes Factors (B_{ij}) for model complexity, and overall posterior probabilities ($\text{pr}(M_k|D)$). Larger posterior probabilities imply that the level of model complexity is more likely to better represent NH_3 volatilization based on the measurement data.

	M1	M2	M3	M4	M5	M6
M1		0.77	5.61	17.09	23.74	59.71
M2	1.30		7.27	22.16	30.78	77.40
M3	0.18	0.14		3.05	4.23	10.64
M4	0.06	0.05	0.33		1.39	3.49
M5	0.04	0.03	0.24	0.72		2.51
M6	0.02	0.01	0.09	0.29	0.40	
$\text{pr}(M_k D)$	0.385	0.500	0.068	0.023	0.016	0.007

I found limited evidence that the two highest levels of complexity in the model (M_1 and M_2) differed in their ability to predict NH_3 volatilization. Specifically, the Bayes factor B_{21} of 1.3 provides weak evidence in favor of model complexity associated with M_2 . However, there is strong evidence that the final model should include the levels of complexity in M_1 and M_2 compared to further reducing complexity represented in M_3 with B_{13} and B_{23} values of 5.61 and 7.27, respectively, or the even simpler levels of complexity represented in M_4 , M_5 , and M_6 , with corresponding Bayes factors greater than 10. Therefore, the results suggest that the appropriate level of complexity is represented by M_1 or M_2 , with M_2 slightly favored, suggesting that the additional complexity in the model introduced by representing soil buffering capacity is not needed if I apply the law of parsimony. Therefore, the level of complexity in M_2 was adopted, and soil buffering capacity was treated as constant for all sites based on the mean value reported by Curtin et al. (1996).

2.4.3. Posterior Parameter Distributions and Performance Evaluation for the Final Model

The SIR algorithm reduces the variance of several model parameters in the final model (M_2) and produced marginal posteriors with smaller ranges and higher densities compared to the prior (Figure 2.1, Table 2.7). Out of 15 model parameters considered for calibration, some parameters (e.g., CFU_0 , K_M , α_M , and α_{pH}) showed a considerable reduction in uncertainty, while others showed moderate (e.g., K_{UI} , β_{ST_1} , β_{ST_2} , α_{ST} , V_{max} , and ST^*) or almost no change from the prior parameter distributions (e.g. β_{pH} , α_W , K_{max} , β_{SM_1} , and β_{SM_2}).

Table 2.7. Marginal posterior distributions for parameters in model M_2 for estimating NH_3 volatilization loss including the maximum a posteriori (MAP) estimates, i.e., mode, 25th and 75th percentiles in the distribution (P25 and P75), and minimum and maximum values.

Parameter	Lower	P25	median	P75	Upper	MAP
CFU_0	0.0013	0.0029	0.0057	0.0110	0.0408	0.0014
K_M	8.0000	36.0000	86.5000	193.2500	439.0000	43.0000
K_{UI}	223.8750	489.7500	682.0000	846.7500	983.0500	660.0000
β_{ST_1}	5.4198	9.7475	17.3350	31.3575	47.5903	15.1500
β_{ST_2}	0.0533	0.1020	0.3113	0.5352	0.9173	0.8666
β_{pH}	0.2390	1.8745	3.2604	4.6576	5.8562	4.8156
α_W	0.0238	0.3823	0.7916	1.1613	1.4679	0.9173
α_M	0.2102	0.5113	0.6816	0.8644	1.4615	0.7583
K_{max}	0.0129	0.0371	0.0583	0.0787	0.0983	0.0656
α_{pH}	1.1898	1.5655	1.7503	1.8859	1.9900	1.5618
α_{ST}	0.0243	0.1608	0.3592	0.5968	0.9543	0.1220
V_{max}	0.0027	0.0088	0.0134	0.0168	0.0197	0.0166
β_{SM_1}	0.0310	0.2713	0.4352	0.5919	0.7305	0.5910
β_{SM_2}	0.1121	0.6946	1.1613	1.5927	1.9513	1.6890
ST^*	5.5098	9.4500	14.4100	20.8325	32.6630	5.7400

Overall, the modeled NH_3 loss as the percentage of applied N agrees fairly well with observations in the measurement dataset (Figure 2.2), with a mean Bayesian R^2 of 0.39 and 95%

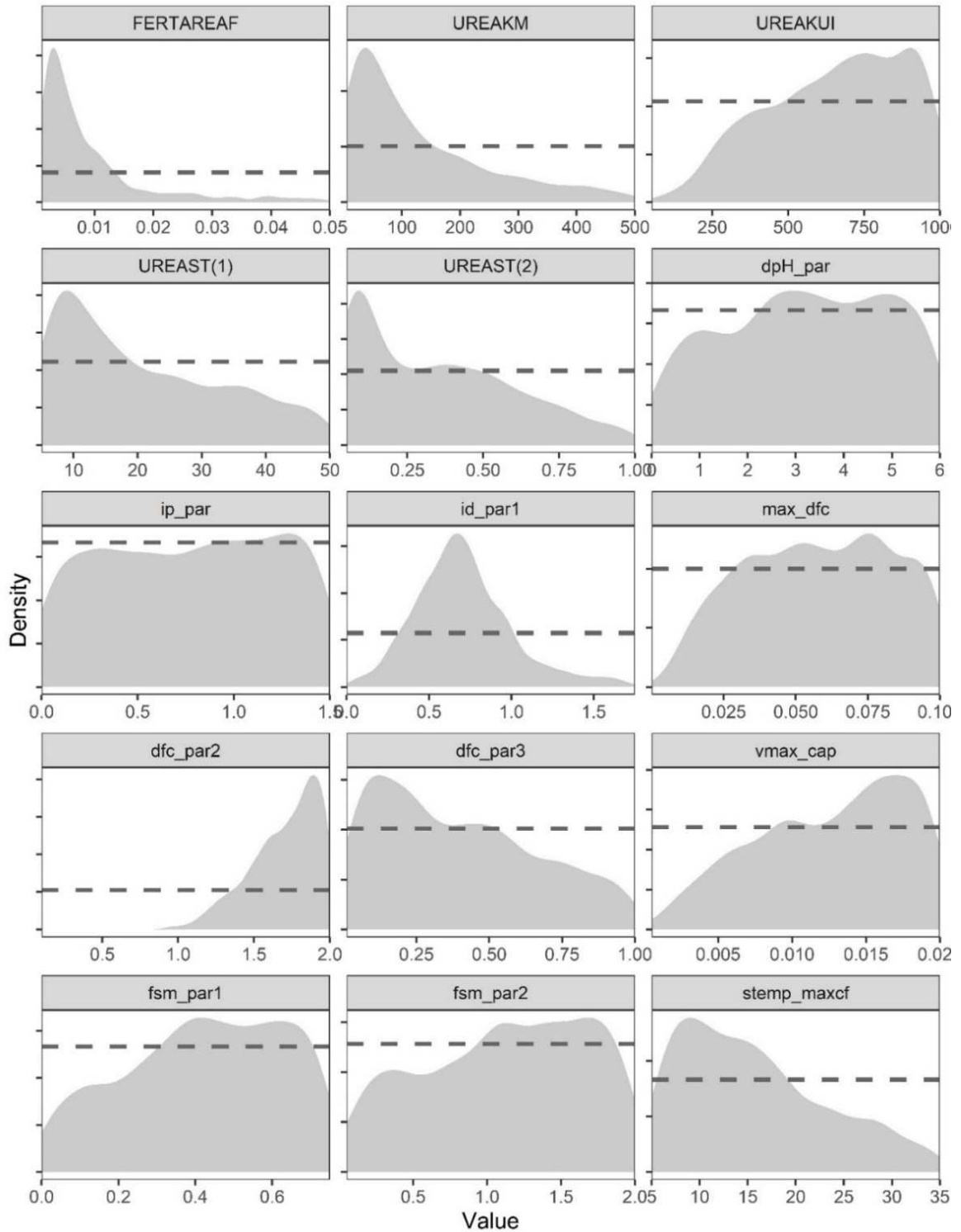


Figure 2.1. Marginal posterior density (light grey area) and priors (dark grey dashed line) for model parameters.

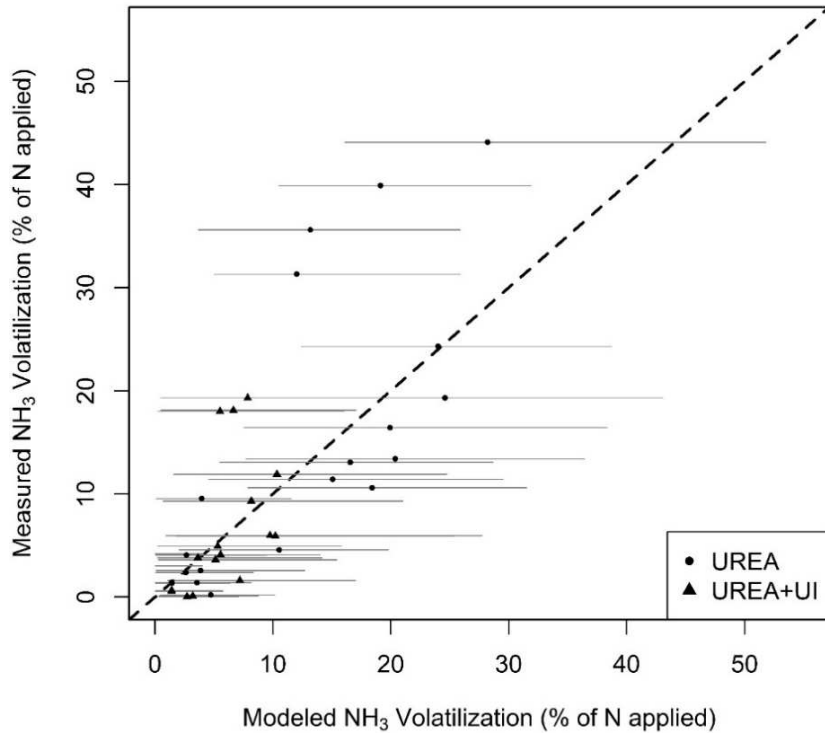


Figure 2.2. Modeled versus measured cumulative NH₃ volatilization loss as % of fertilizer N applied as urea only (circle) and urea with urease inhibitors (triangle). The error bars represent 95% posterior prediction intervals.

central credible intervals between 0.17 and 0.62. For the MAP estimates, calibration achieved a higher R² value of 0.71. The comparison between the RMSE from the prior (280, ranging from 183-834 g NH₃-N ha⁻¹ day⁻¹) and the posterior RMSE (158, ranging from 133-192 g NH₃-N ha⁻¹ day⁻¹) shows that the Bayesian calibration reduced model uncertainty by a factor of 1.8.

Additionally, the calibration is also effective in reducing the model bias from the prior of 45 (ranging from -635 to 155) to the posterior of 7 (ranging from -106 to 102) g NH₃-N ha⁻¹ day⁻¹.

The model also predicted reduction in NH₃ volatilization when urease inhibitor were applied with a median reduction factor (RF) of -54.5% similar to that of the measured RF (Figure 2.3).

Even with similar median values for both measured and the modeled data, Figure 2.3 shows that the spread of the modeled values were higher compared to the measurements. However, the model was not able to predict the outliers in the measured dataset, particularly the case where

urease inhibitors led to an increase in NH_3 volatilization or reduction exceeding >80%. (Figure 2.3). This may be an anomaly in the measurement dataset, but there was no basis for removing this data point given the information in the publication. Even though the model does capture the general patterns, the prediction intervals of the model for both percentage loss (Figure 2.2) and mitigation potentials associated with application of urease inhibitors (Figure 2.3) were large, leading to relatively low precision in model predictions.

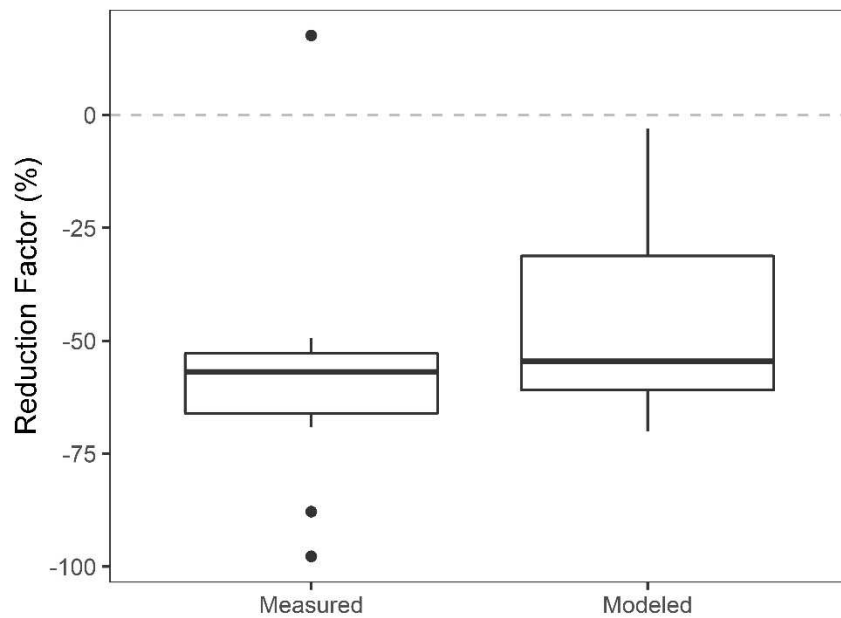


Figure 2.3. Distribution of NH_3 volatilization reduction factor (%) presented in a boxplot for the measured and the modeled datasets.

2.5. Discussion

A sub-model estimating losses of N from ammonia volatilization following urea-based fertilization has been included in the DayCent ecosystem model, accounting for key drivers and 4R management practices that can reduce volatilization from urea-based N fertilization. I used Bayes factors and followed the principle of parsimony to determine the appropriate level of complexity in the model. The final model, M_2 , includes a) urea hydrolysis, b) diffusion of

gaseous NH_3 from the soil system, c) the effect of fertilizer placement on NH_3 volatilization (i.e. broadcast vs. banding and surface vs incorporated), d) the effect of intensity and timing of irrigation and/or precipitation on NH_3 volatilization after fertilizer application, and e) the influence of short-term changes in soil pH on NH_3 volatilization. These drivers explained NH_3 volatilization slightly better than the model structure that included the dynamic effect of soil buffering capacity on pH change. Following Curtin et al. (1996), I modeled soil buffering capacity as a function of clay content, SOC concentration, and initial soil pH, with a positive relationship between clay and SOC and a negative relationship between initial soil pH and buffering capacity. These relationships suggest that there is higher buffering capacity for soils with high clay and SOC contents and a low initial soil pH. Even though soil buffering capacity is important in regulating increases in soil pH, modeling site level variability associated with buffering capacity did not contribute much to the estimation of NH_3 volatilization compared to other processes, according to the data informing the Bayesian analysis. The experimental sites in my analysis have a high mean initial soil pH of 7.2 compared to the mean soil pH of 6.35 in the underlying data that were used to develop the relationship for my model (Curtin et al., 1996). The calibration dataset, therefore, likely has soils with lower buffering capacity and may explain why the candidate model that included this process did not have a larger Bayes factor compared to the model that excluded this process. Additionally, soil buffering capacity is a secondary effect as represented in the model structure and further research could possibly improve the model in the future with a more detailed representation of buffering capacity including clay mineralogy. Regardless, more observations of NH_3 volatilization with a larger range of pH values are likely needed to adequately inform the model calibration analysis about the influence of buffering capacity.

Placement of N deeper in the soil is one of the 4R practices (Right Place) and the model simulated reductions of NH_3 emissions with mechanical incorporation. The reduction is higher with increasing depth and the result suggests a significant reduction with incorporation below 5 cm (Figure 2.4). My results are consistent with the model proposed by Rochette et al. (2013a) of negligible NH_3 emissions and maximum N retention when urea is incorporated at depths >7.5 cm. Using the posterior distribution of model parameters associated with mechanical incorporation, DayCent estimated a reduction in NH_3 emissions of 97% (65% to >99%) with an incorporation depth of 5 cm compared to a surface application. Furthermore, if N is incorporated at depths of 2.5 cm or 7.5 cm, DayCent predicted a reduction of 81% (34%, 94%) and 99% (0%, 79%) reduction, respectively (Figure 2.4).

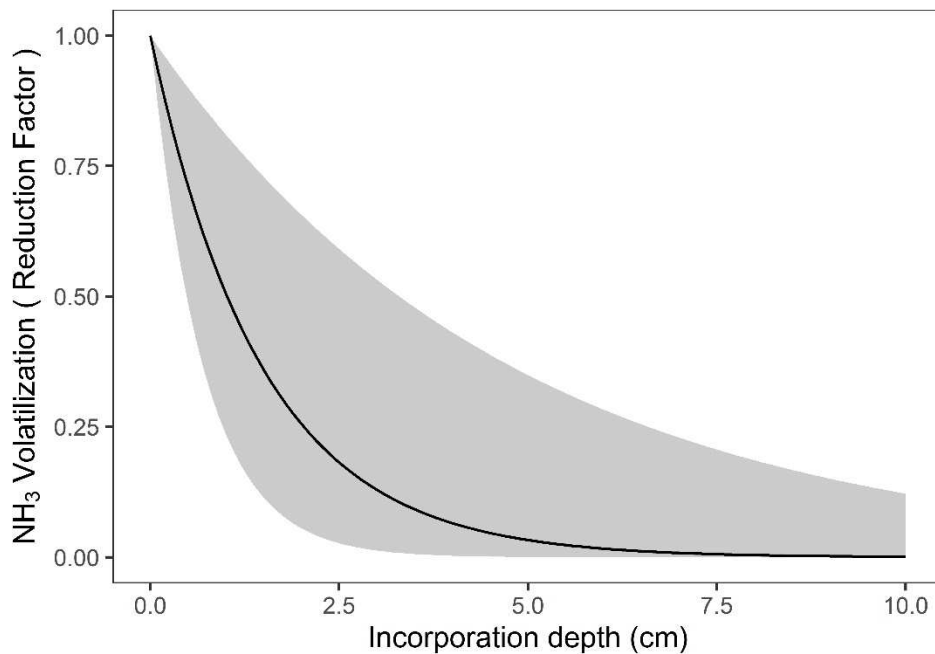


Figure 2.4. Scaling factor for NH_3 volatilization loss by depth (cm) with mechanical incorporation relative to surface-application of fertilizer.

Similar to mechanical incorporation, DayCent predicted reductions in NH_3 emissions with addition of water through irrigation and/or precipitation (Figure 2.5), consistent with the empirical model proposed by Holcomb et al., (2011). DayCent showed that, with water

infiltration of 5 to 10 mm from irrigation or precipitation on the same day of fertilization, NH_3 emissions are reduced by 98% (11%, >99%) and 99% (0%, 21%), respectively (Figure 2.5). This reduction is higher than Holcomb et al., (2011) mainly due to simulation of leaching through the profile with deeper flows from irrigation and all forms of precipitation, rather than only rainfall and irrigation inputs of water. However, uncertainties in the effect of water inputs on NH_3 volatilization are significantly higher compared to mechanical incorporation. Furthermore, I included the effect of delayed water input by adjusting reduction factors proportionally to the fraction of urea remaining. This assumption is consistent with the findings reported by Black et al. (1987) in which there was a 95% reduction when irrigation water is applied within 3 hours of urea fertilization. In contrast, delaying irrigation by 2 days reduces NH_3 volatilization by only 7% due to the rapid rate of urea hydrolysis (Black et al. 1985). When urease inhibitors are added with urea, the model extends the time for precipitation/irrigation events to reduce NH_3 volatilization through diffusion and leaching deeper in the profile.

Simulating NH_3 volatilization enhances the representation of 4R practices in DayCent because previous versions did not represent fertilizer placement or urease inhibitors. The 4R nutrient stewardship paradigm is designed to maximize crop uptake while minimizing nutrient loss to the environment (Murrell et al., 2009). With the improvements, DayCent can simulate the effect of rate, type, timing and placement of fertilizers on N retention in the soil and their influence on NH_3 volatilization from addition of ammonium (NH_4^+), nitrate (NO_3^-), and urea ($\text{CO}(\text{NH}_2)_2$), which are three primary forms of synthetic N applied to agricultural soil. Further development and/or testing is needed to represent the effect of other N fertilizers on NH_3 volatilization from agricultural soils, including slurry and/or manure, urine patches, and addition of anhydrous ammonia.

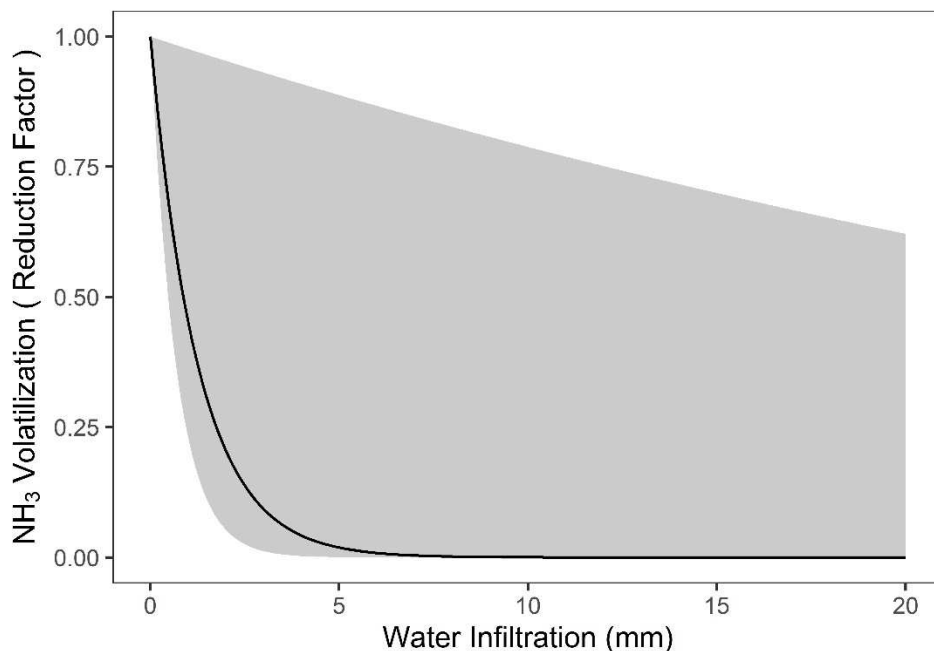


Figure 2.5. Scaling factor for NH₃ volatilization loss with leaching of fertilizer below the soil surface due to irrigation or precipitation compared to no leaching.

2.6. Conclusion

DayCent predicts NH₃ volatilization at different N rates, timing, and placement—key principles of the 4R nutrient stewardship paradigm. Furthermore, the model is able to predict the cumulative loss and mitigation potential when urea is applied with or without urease inhibitors—a key 4R recommendation (Right Type). This development enhances the ability of DayCent to evaluate best management practices for reducing environmental pollution. As more data become available, expanding both spatially and temporally, the Bayesian model selection and parameterization framework is designed to allow further testing and refinement of the model structure for NH₃ volatilization, and updating of the parameters with new information embodied in the measurement data.

CHAPTER 3: MODELING NITROUS OXIDE MITIGATION POTENTIAL OF ENHANCED EFFICIENCY NITROGEN FERTILIZERS FROM AGRICULTURAL SYSTEM

3.1. Summary

Agriculture soils are responsible for a large proportion of global nitrous oxide (N_2O) emissions—a potent greenhouse gas and ozone depleting substance. Enhanced-efficiency nitrogen (N) fertilizers (EENFs) can reduce N_2O emission from N-fertilized soils, but their effect varies considerably due to a combination of factors, including climatic conditions, edaphic characteristics and management practices. In this study, I further developed the DayCent ecosystem model to simulate two EENFs: controlled-release N fertilizers (CRNFs) and nitrification inhibitors (NIs) and evaluate their N_2O mitigation potentials. I implemented a Bayesian calibration method using the sampling importance resampling (SIR) algorithm to derive a joint posterior distribution of model parameters. The joint posterior distribution can be applied to estimate posterior predictions of N_2O reduction factors when EENFs are adopted in place of conventional N fertilizer. The resulting distribution of median reduction factors were -11.9% (-51.7% and 0.58%) for CRNFs and -26.7% (-61.8% to 3.1%) for NIs, which is compatible to the distribution of measured reduction factors in the dataset. By incorporating EENFs, the DayCent ecosystem model is able to simulate a broader suite of options to identify best management practices for reducing N_2O emissions.

3.2. Introduction

Nitrogen (N) fertilizer applied to agriculture soils accounts for a majority of anthropogenic nitrous oxide (N_2O) emissions (Bouwman et al., 2002b; Mosier and Kroeze, 2000; Reay et al., 2012) and agriculture is responsible for about 70% of global anthropogenic sources (Tian et al.,

2020). Nitrous oxide (N_2O) from soil is primarily produced by the microbial driven process of nitrification and denitrification (Firestone M.K., and Davidson, 1989), although other processes may also contribute to emissions (Butterbach-Bahl et al., 2013). N_2O emissions from agricultural soils are driven by N management practices, particularly the addition of inorganic fertilizers and manure (Mosier et al., 1998). It is an important greenhouse gas (GHG) and has approximately 298 times (100 year time horizon) the global warming potential of carbon dioxide (CO_2) on a mass basis while also contributes to the depletion of stratospheric ozone (Crutzen and Ehhalt, 1977; Ravishankara et al., 2009).

Enhanced-efficiency N fertilizers (EENFs) have shown a potential for mitigating N_2O emissions from N-fertilized agricultural soils (Akiyama et al., 2010; Eagle et al., 2017; Thapa et al., 2016), and have emerged as an important management option for mitigating N losses from agroecosystems (Halvorson et al., 2014; Sha et al., 2020; Trenkel, 2010). I studied two EENFs that can reduce N_2O emissions: (1) controlled-released N fertilizers (CRNFs) and (2) nitrification inhibitors (NIs). Best management practices can incorporate EENFs based on the 4R paradigm for nutrient stewardship (right source at right rate, right placement and right timing of fertilizer application). The rate, pattern, and duration of N release from CRNFs are predictable and controllable during preparation but may vary under field conditions (Halvorson et al., 2014; Shaviv, 2001; Timilsena et al., 2015; Trenkel, 2010). CRNFs constantly release N fertilizers into the soil, maintain low mineral N concentrations, and extend the availability for plant uptake with a release pattern more in synchrony with the crop's N requirements that minimizes environmental losses (Naz and Sulaiman, 2016; Shaviv and Mikkelsen, 1993; Trenkel, 2010). NIs stabilize N fertilizer in the form of NH_4^+ in the soil (Trenkel, 2010). Specifically, NIs inhibit the biological process of nitrification and delay the transformation of NH_4^+ to NO_3^- for a certain

period of time (four to ten weeks). Maintaining N in the form of NH_4^+ prevents gaseous loss from both nitrification and denitrification as well as leaching of NO_3^- below the rooting zone to the groundwater.

Meta-analyses have been performed to quantify the effect of EENFs on N_2O emissions compared to conventional fertilizers (Akiyama et al., 2010; Eagle et al., 2017; Han et al., 2017; Thapa et al., 2016; Wolt, 2004; Zhang et al., 2019). Significant reductions in N_2O emissions have been reported in these studies for CRNFs and NIs (Eagle et al., 2017; Thapa et al., 2016; Wolt, 2004; Zhang et al., 2019). However, the N_2O reduction from EENFs varies due to a combination of factors including type and rate of N applied, soil properties, climatic factors, and management practices. Despite meta-analysis synthesizing results from many field studies reporting N_2O reductions, the measurements are not spatially continuous resulting in data gaps for some region, making it difficult to derive empirical reduction factors from EENFs for all farms that may adopt these types of fertilizers.

In contrast to an empirical method to estimate reduction in N_2O from EENFs, I developed a process-based mechanistic approach within the DayCent ecosystem model for EENFs. The dynamic N release from CRNFs and the effectiveness of NIs on inhibiting nitrification are modeled as influenced by environmental conditions. There are several advantages of using a process-based biogeochemical model (DayCent) instead of empirical models. DayCent accounts for N_2O emissions during both nitrification and denitrification in a daily time step and accounts for factors influencing emissions patterns (N inputs, climate, soil, plant growth) at a finer time scale than most empirical methods. Furthermore, DayCent predictions of N_2O emissions have been validated and agree reasonably well with field measurements (Del Grosso et al., 2010, 2005). Previously, Del Grosso et al. (2009) implemented an algorithm to represent the impact of

NIs in DayCent with a simple approach defined by two parameters: reduction in nitrification and duration of the effect. Similar approaches have been adopted for the DNDC model in a modified version developed specifically for conditions in New Zealand (Giltrap et al., 2010). The model adopted a simplified exponential function of time to represent the degradation of NIs that did not account for impacts of soil properties. Further development of DNDC has been proposed by Li et al. (2020) for modeling the effect of NIs by incorporating soil properties, ratio of fertilizer to NIs, and soil parameters (i.e. temperature, moisture, and pH). To my knowledge, more advanced approaches have not been published for modeling CRNFs in process-based models.

The objective of this study is to develop a dynamic modeling approach for CRNFs and NIs as influenced by the soil properties and other related drivers such as weather patterns and irrigation management. I focused on the N₂O emissions from agricultural soils and reduction potentials of EENFs compared to conventional fertilizers. Furthermore, I implemented a Bayesian framework developed by Gurung et al. (2020) to calibrate the model parameters and evaluate results using field data from the Greenhouse gas Reduction through Agricultural Carbon Enhancement network of experimental sites in the United States (GRACEnet).

3.3. Materials and Methods

3.3.1. Data Sources

Most of the N₂O flux measurements used for model development were obtained from the GRACEnet research programs initiated by the USDA Agricultural Research Service and described in detail by Del Grosso et al. (2013). In brief, the dataset includes site descriptors (e.g., weather, soil class, spatial attributes), experimental design (e.g., factors manipulated, measurements performed, plot layouts), management information (e.g., planting and harvesting, fertilizer types and amounts), and N₂O-flux measurements needed for model development and

testing for agroecosystems and follows USDA-ARS GRACENet protocols (Parkin and Venterea, 2010). The experimental sites used for the Bayesian calibration of model parameters included paired plots treated with conventional N fertilizer and EENFs, and also included control plots without N fertilizer (Table 3.1). Collectively the dataset consisted of a total of 155 site-year-treatment combinations for a total of 7,503 individual observations of N₂O fluxes, 27 seasonal paired reduction factors for CRNFs, and 40 seasonal paired reduction factors for NIs.

3.3.2. DayCent Model

DayCent (Del Grosso et al., 2001; Parton et al., 1998) is a process-based ecosystem model of intermediate complexity and simulates the flow of carbon (C), and N in a plant-soil system on a daily time step. The model simulates N₂O emissions from both nitrification and denitrification (Del Grosso et al., 2000; Parton et al., 2001), where a fraction of nitrified N is emitted as N₂O, and N₂O emissions from denitrification are a function of soil NO₃⁻ concentration, water-filled pore space (WFPS), heterotrophic respiration, and soil texture. Furthermore, nitrification is calculated as a function of modeled soil NH₄⁺ concentration, WFPS, soil temperature, pH, and soil texture (Parton et al., 2001, 1996). In DayCent, nitrification increases with soil temperature, and the highest potential rates occur during the warmest month of the year. Limitations on nitrification due to moisture stress and O₂ availability for microbial activity are modeled as a function of WFPS where nitrification peaks at ~50% WFPS and decreases below and above this value. In DayCent, nitrification is also limited by pH and modeled with an exponentially decreasing curve in which there are lower nitrification rates as conditions become more acidic. In addition to N₂O emission, DayCent also simulates key ecosystem processes related to N cycle including N uptake by plants, mineralization and immobilization, NO₃⁻ leaching, and other trace gas fluxes (NO_x, NH₃, and N₂). Recent DayCent model developments include routines to

represent urea hydrolysis with or without urease inhibitors and volatilization loss of NH₃ (Gurung et al. *in review*), plant growth and water use based on green leaf area index (Zhang et al., 2020, 2018), and N₂O flux during freeze-thaw events (Del Grosso et al, *in prep*).

Table 3.1. N₂O study locations, crops, treatments, and measurement years that were used for the Bayesian model calibration. All sites except Becker, MN are part of GRACEnet network. The abbreviations for the N fertilizers are urea ammonium nitrate, UAN; ammonium nitrate, AN; a controlled-release, polymer-coated urea, ESN; a stabilized urea containing urease and nitrification inhibitors, SuperU; and a stabilized UAN solution containing urease and nitrification inhibitors, UAN+AP.

Site Locations	Lat.	Lon.	Fert-Type	Crop	Years	Reference
ARDEC, CO	40.65	-105.00	Zero-N	corn	2007-2014	Halvorson et al. (2010a)
			UAN			Halvorson et al. (2011)
			urea			Halvorson and Del Grosso (2013)
			SuperU			Halvorson and Del Grosso (2012)
			ESN			Halvorson et al. (2010b)
			UAN+AP			Halvorson et al. (2016)
Becker, MN	45.39	-93.89	Zero-N	corn	2009-2010	Maharjan et al. (2014)
			urea			
			SuperU			
			ESN			
Bowling Green, KY	36.99	-86.44	Zero-N	corn	2009-2011	Sistani et al. (2011)
			urea			
			AN			
			UAN			
			SuperU			
			ESN			
			UAN+AP			
Kimberly, ID	42.53	-114.36	Zero-N	corn	2013-2015	Dungan et al. (2017)
			Urea	barley		
			SuperU	alfalfa		

Rosemount, MN	44.75	-93.07	Zero-N urea SuperU ESN	corn	2008-2010	Venterea et al. (2011)
St. Paul, MN	44.99	-93.17	Zero-N urea SuperU ESN	corn	2011-2012 2014-2015	Maharjan & Venterea (2013) Venterea et al. (2016)

3.3.3. Model Development

DayCent model developments for this study include controlled-release N fertilizers (CRNFs) and nitrification inhibitors (NIs). Furthermore, I also developed a variable N₂O rate from nitrification as a function of WFPS primarily controlled by O₂ availability, which is discussed in the next section.

3.3.3.1. Fraction of Nitrified N Loss as N₂O

In previous versions of the DayCent model, N₂O emissions are a constant proportion of NH₄⁺ oxidized to NO₃⁻ during nitrification. To improve the model, I assumed that the rate of N₂O during nitrification is sensitive to O₂ availability (Khalil et al., 2004; Kool et al., 2011) and modeled this relationship as a function of soil WFPS using a sigmoidal curve (Figure 3.1). This allowed the model to more dynamically represent N₂O emission associated with nitrification as follows:

$$g_w = \frac{(N_2O_{adjust_max} - N_2O_{adjust_min})}{1 + \exp\left(-\left(N_2O_{adjust_Intcpt} + N_2O_{adjust_WPFS} \times avgWFPS[t]\right)\right)}, \quad (3.1)$$

$$N_2O_{adjust}[t] = N_2O_{adjust_min} + g_w \quad (3.2)$$

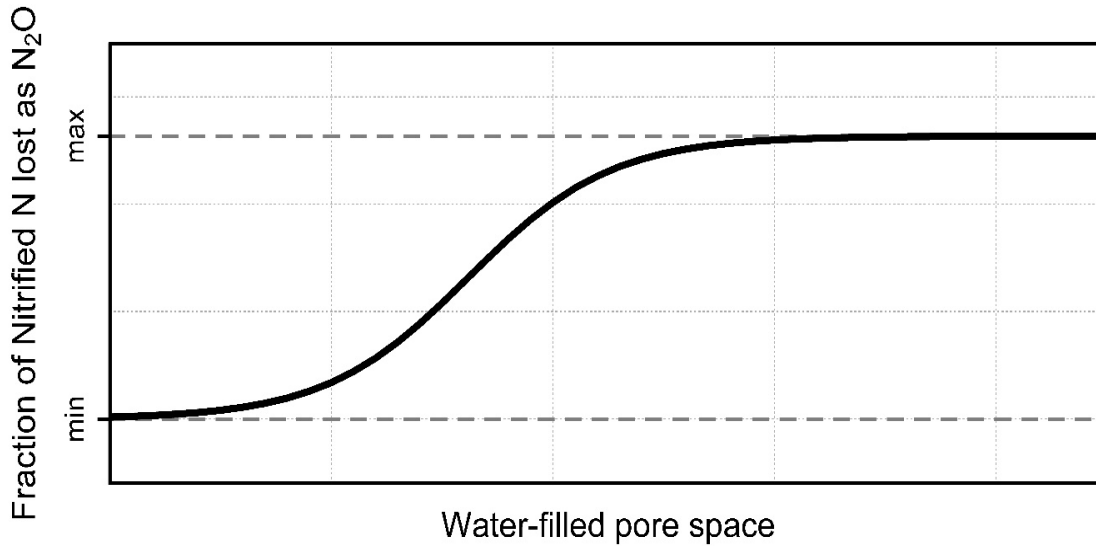


Figure 3.1. Conceptual diagram of fraction of nitrified N loss as N₂O from nitrification, which is controlled by water-filled pore space between a minimum (N₂Oadjust_min) and maximum value (N₂Oadjust_max).

where N₂Oadjust_max and N₂Oadjust_min are maximum and minimum fraction of N₂O loss during nitrification; N₂Oadjust_Intcpt and N₂Oadjust_WPFS are the intercept and the slope term of the logistic WPFS curve, avgWPFS[t] is the average WPFS of 0-10cm of DayCent soil layer and [t] represents the time index, measured in units of days. Although not directly related to the EENFs, I adopted this important control on nitrified N losses of N₂O based on recent published research with the goal of improving the model's ability to represent impacts of EENF's on N₂O emissions (i.e., including the WPFS control on nitrified N losses of N₂O improved the model's estimation of N₂O emissions overall from convention fertilizers and the reductions associated with EENFs).

3.3.3.2. Controlled-Release Nitrogen Fertilizers (CRNFs)

The cumulative release of N from CRNFs is modeled using the Gompertz equation (Equation 3.2) with a sigmoidal pattern (Figure 3.2) and controlled by soil temperature and moisture (Du et al., 2006; Trenkel, 2010). In general, the characteristics of the release pattern of CRNFs are defined by the time required for 80% of the release (T_EIGHTY or t₈₀) and the lag time

(CRFLAMBDA or λ_{CRF}) in free water at a given reference temperature (Trenkel, 2010).

Therefore, I modeled N release with the following equation:

$$N_{CRF}[t] = 100 * \left(1 - \exp \left(-\exp(\mu_{CRF} * e^{(1)} * (\lambda_{CRF} - t_{eff}[t]) + 1) \right) \right), \quad (3.3)$$

where $N_{CRF}[t]$ is the cumulative N release (%) at time t, μ_{CRF} is the maximum rate of release at the inflection point, λ_{CRF} is the lag term, and $t_{eff}[t]$ is the adjusted cumulative effective time for N release from CRNFs, which is influenced by temperature and moisture conditions. The soil temperature and moisture conditions of the field vary daily so the temperature effect is handled by adjusting the effective time (t_{eff}) of release with Q_{10} temperature coefficient and moisture conditions using the following equation:

$$t_{eff}[t] = t_{eff}[t - 1] + h2odly[t] * (Q_{10}^{CRF})^{\left(\frac{T_{soil}[t] - T_0}{10}\right)}, \quad (3.4)$$

where Q_{10}^{CRF} (i.e. CRF_QTEN) is the temperature coefficient, $T_{soil}[t]$ is the soil temperature (°C), T_0 is the reference temperature (23 °C), and $h2odly[t]$ is the delayed effect on CRNF release due to soil moisture availability. Soil water is required for the release of N from CRNFs because water dissolves the N fertilizer as the water diffuses through the polymer coating, which then releases the N to the soil at a controllable rate (Azeem et al., 2014; Du et al., 2006). The delayed effect of soil moisture availability is modeled using the maximum relative soil water content since N application. Furthermore, to satisfy the condition of 80% release at t_{80} , I defined μ_{CRF} as a function λ_{CRF} and t_{80} as follows:

$$\mu_{CRNF} = \frac{(\ln(-\ln(0.8)) - 1)}{\exp(1) * (\lambda_{CRF} - t_{80})}, \quad (3.5)$$

and consequently, the Gompertz release curve is defined by three parameters (Q_{10}^{CRF} , λ_{CRF} and t_{80}) for the reference temperature without water limitation.

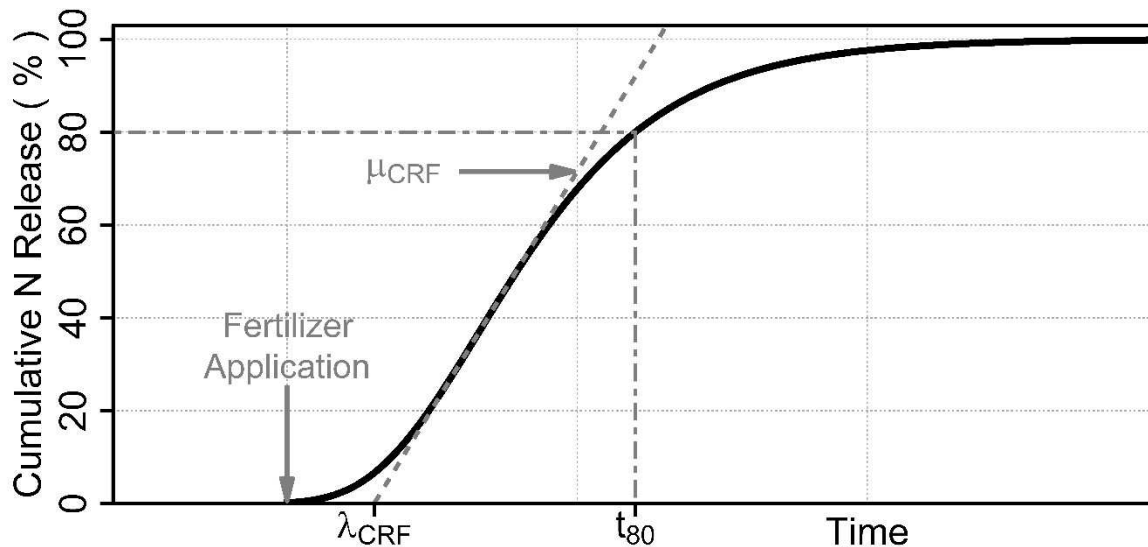


Figure 3.2. N release characteristics of the Gompertz model (solid sigmoidal line), μ_{CRF} is the maximum rate of release at the inflection point, λ_{CRF} is the lag term, and t_{80} is the numbers of days after fertilizer application date when 80% of CRNF is released to the soil.

3.3.3.3. Nitrification Inhibitors

Nitrification inhibitors delay the transformation of NH_4^+ to NO_3^- by slowing the bacterial oxidation of NH_4^+ (Trenkel, 2010), but the effect declines over time due to the decomposition of applied inhibitor by both biotic and abiotic factors (Kelliher et al., 2014; Prasad and Power, 1995; Wolt, 2000). Different soil factors can affect the effectiveness of NIs on inhibition of nitrification, of which soil temperature and soil moisture are the most significant (Prasad and Power, 1995), but leaching of NIs deeper in the soil can also limit their effectiveness because NH_4^+ tends to be more common in the topsoil (Trenkel, 2010).

In an early study, the effect of nitrification inhibitors was implemented in DayCent by reducing calculated nitrification rates by 50% for two months after the inhibitor is applied (Del Grosso et al., 2009) based on data from Bronson et al. (1992). Here I test the hypothesis that the effectiveness of NIs is dynamic and decreases over time as a function of soil temperature and soil water dynamics (Figure 3.3) (Di et al., 2014; Kelliher et al., 2014; Prasad and Power, 1995; Trenkel, 2010; Williamson et al., 1996), based on Equation 3.5 and 3.6:

$$NitRF[t] = 1 - (1 - NitRF[0]) * \min(1.0, f(CTST[t], CWF[t])), \quad (3.6)$$

$$f(CTST[t], CWF[t]) = \exp(-(FINHIB1 * CTST[t] + FINHIB2 * CWF[t] + FINHIB3)), \quad (3.7)$$

where $NitRF[0]$ (i.e., NINHIB) and $NitRF[t]$ represent the effectiveness of NIs on nitrification (0-1; unitless) at application date (maximum reduction potential) and after t days, $CTST[t]$ and $CWF[t]$ are cumulative truncated soil temperature ($^{\circ}C$) and cumulative water infiltration (cm) below the third soil layer (i.e., 10 cm) in modeled profile after t days, and FINHIB1, FINHIB2, and FINHIB3 are model parameters.

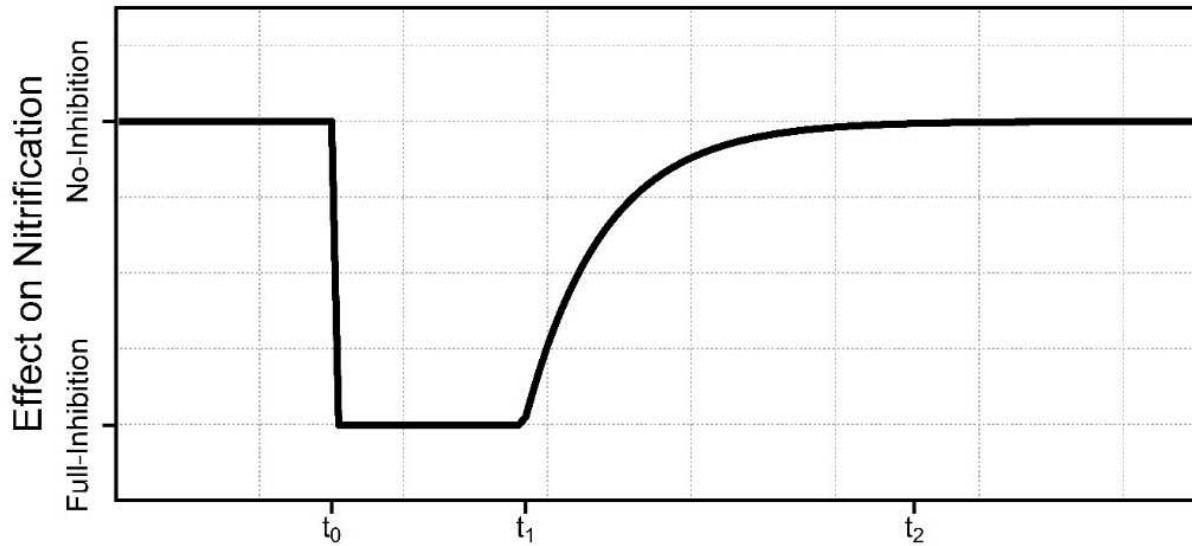


Figure 3.3. Conceptual model of the effectiveness of NIs on nitrification (y-axis) with full-inhibition (i.e. $NitRF[0]$ or maximum reduction potential) and no-inhibition (i.e., no effect or multiplier of 1), at time t_0 , t_1 , and t_2 across the x-axis based on the time of NI application, time until the NI is fully effective, and non-effective, respectively.

3.3.4. Bayesian Model Calibration Framework

The Bayesian model calibration framework incorporates a variance-based global sensitivity analysis (GSA) using Sobol method (Jansen, 1999; Saltelli, 2002; Sobol, 2001) to identify

influential model parameters associated with the prediction of N₂O emissions. Once the influential parameters are identified by GSA, the sampling importance resampling (SIR) method is applied to estimate the posterior distribution of model parameters and posterior prediction of N₂O reduction factors of EENFs.

3.3.4.1. Global Sensitivity Analysis

Variance-based GSA was performed to quantify the relative importance of parameters that have a significant influence on model output. The analysis permits us to identify a group of parameters with the most influence that can be used to make the model more parsimonious (Saltelli et al., 2008), a method known as “Factor Fixing” or “Screening.” My analysis used the Sobol method (Saltelli, 2002; Sobol, 2001) to identify influential parameters using estimated log-likelihood of model output. Similar to analysis of variance, the method partitions the total variance of the model output into first-order and higher-order interaction terms to estimate the proportion of variance explained by each parameter. The method is model independent, works for both linear and nonlinear outputs (Sobol, 2001), and is well suited for complex and highly non-linear process-based ecosystem models, such as DayCent (Gurung et al., 2020). Furthermore, this method is arguably one of the most robust and comprehensive GSA methods available (Saltelli et al., 2008).

Seventeen model parameters were considered for the GSA and can be grouped based on association with five different processes (Table 3.2). Three parameters are associated with CRNFs, four parameters with NIs, six parameters with nitrification, one parameter with denitrification, and a total of four parameters for N uptake by plants. Four parameters that control the plant N uptake are fraction of soil N available to plants (FAVAIL(1)), minimum and maximum C:N ratio of new plant growth during the seedling (i.e. with zero plant biomass), and

biomass level above which the minimum and maximum C:N ratio stays constant (BIOMAX). Out of the seventeen model parameters, eleven were introduced with the EENF model developments in this study, and the other six parameters were included because initial testing showed that these parameters, which are associated with N cycling, may have important interactions with the EENFs to influence the reduction in N₂O emissions. I assumed a uniform independent prior defined by the lower and upper bound of the distribution (Table 3.2).

3.3.4.2. Sampling Importance Resampling

The sampling importance resampling (SIR) algorithm (Rubin, 1988, 1987) is used for Bayesian calibration to generate a sample from the joint posterior distribution of model parameters. The method is described in detail by Gurung et al. (2020) and presented here in brief. The method is a non-iterative Monte Carlo method that aims to generate a sample from the target distribution. First, I draw 1,000,000 (1M) independent random samples $\{\theta^1, \theta^2, \dots, \theta^{1M}\}$ from the prior using Latin hypercube sampling (LHS) techniques. The LHS effectively subdivides the parameter space by complete stratification on all parameters and is considered more efficient for distributing the sample across the domain of the parameter space compared to simple random sampling (McKay et al., 1979; Owen, 1992; Stein, 1987). Second, for each sample θ^s , I simulated N₂O emissions and calculated importance weights $\omega(\theta^s)$. Third, I derived the posterior distribution by resampling 1,000 (1K) times without replacement $\{\tilde{\theta}^1, \tilde{\theta}^2, \dots, \tilde{\theta}^{1K}\}$ from the initial 1M samples of N₂O emissions and associated parameters sets based on probabilities proportional to the importance weights.

Table 3.2. Prior distribution and definition of seventeen parameters for global sensitivity analysis.

Parameters	Lower	Upper	Distribution	Definitions
T_EIGHTY (t_{80})	25	100	Uniform	Duration (days) for 80% release of applied CRNF at the reference temperature
CRFLAMDA (λ_{CRF})	0	30	Uniform	Lag period (days) for CRNF release
CRF_QTEN (Q_{10}^{CRF})	1	10	Uniform	Temperature coefficient for CRNF
T_EIGHTY (t_{80})	0.001	0.3	Uniform	Maximum reduction factor on nitrification rates due to nitrification inhibitors
FINHIB(1)	0	0.01	Uniform	Parameter for reduction factor curve associated with nitrification inhibitor
FINHIB(2)	0	0.08	Uniform	Parameter for reduction factor curve associated with nitrification inhibitor
FINHIB(3)	-5	0	Uniform	Parameter for reduction factor curve associated with nitrification inhibitor
MaxNitFrac	0.1	0.4	Uniform	Maximum fraction of ammonium that is converted to nitrate during nitrification
N2Oadjust_min	0.003	0.03	Uniform	Minimum proportion of nitrified N lost as N ₂ O
N2Oadjust_max ¹	0	0.07	Uniform	Maximum proportion of nitrified N lost as N ₂ O
N2Oadjust_Intcpt	5	7.5	Uniform	Intercept for logistic curve representing the proportion of nitrified N lost as N ₂ O
N2Oadjust_WFPS	15	35	Uniform	Slope for the effect of average WFPS on the logistic function representing the proportion of nitrified N lost as N ₂ O
CO2Denitr_1	0.1	1	Uniform	Coefficient for CO ₂ effect on denitrification
BIOMAX	200	800	Uniform	Biomass level above which the minimum and maximum C/N ratios of the new shoot increments are constant
PRAMN(1,1)	10	30	Uniform	Minimum C/N ratio with zero biomass
PRAMN(1,2)	20	80	Uniform	Minimum C/N ratio with biomass greater than or equal to BIOMAX
FAVAIL(1)	0.1	0.4	Uniform	Fraction of N available to plants

¹ To satisfy the theoretical requirement that parameter $N2Oadjust_max \geq N2Oadjust_min$, $N2Oadjust_max$ is set to the sum of $N2Oadjust_min$ and the distribution defined in the parameter draws.

3.3.4.3. Data-likelihood

In my analysis, I used data from multiple experimental sites with repeated measurements that are highly correlated in both space and time. Proper estimation of uncertainty requires the correlation structure to be incorporated into the variance-covariance matrix when computing the likelihood (Battese et al., 1988; Cressie et al., 2009; Hoeting, 2009). Therefore, I use the restricted maximum likelihood (REML) estimator within the linear mixed-effect (LME) model framework with two levels of nested random effects for sites (spatial) and years (time) to account for spatiotemporal correlations present in the dataset. Furthermore, I used 15-day average N₂O fluxes from field measurements and modeled values to compute the log-likelihood of the modeled emissions using the following equation:

$$l(O|\theta) \propto -\frac{1}{2} \log|\Sigma| - \frac{1}{2} (M - O)^T \Sigma^{-1} (M - O), \quad (3.8)$$

where n is the number of 15 days average N₂O flux, O and M are vectors of measured and modeled values, respectively, Σ^{-1} is the inverse of the variance-covariance matrix, T defines the transpose of a vector and $|\Sigma|$ denotes the determinant of the covariance matrix Σ .

In my analysis, I used the prior as the ‘‘importance function’’ making the importance weights proportional to the likelihood (Givens et al., 1995; Punt and Hilborn, 1997; Smith and Gelfand, 1992), and calculated the standardized importance weights;

$\{\omega(\theta^1), \omega(\theta^2), \dots, \omega(\theta^M)\}$ using the following formula:

$$\omega(\theta^s) = \frac{L(O|\theta^s)}{\sum_{s=1}^M L(O|\theta^s)}, \quad (3.9)$$

where $L(O|\theta^s)$ is the likelihood value for the s^{th} sample. As a result, the likelihood acts as the resampling weights and parameter sets producing higher goodness-of-fit are more likely to be retained in the posterior. The SIR algorithm has been proposed as one of the simplest and most

versatile Bayesian Monte Carlo methods for drawing samples from the posterior (Rubin, 1988, 1987; Smith, 1991) and is suitable for complex process-based models such as DayCent.

3.4. Results

3.4.1. Global Sensitivity Analysis

The two most sensitive parameters were both associated with nitrification and included the maximum fraction of nitrified N that is lost as N₂O (N2Oadjust_max), and the maximum fraction of NH₄⁺ that can be nitrified in a day (MaxNitFrac) (Figure 3.4). The third most sensitive parameter was the soil CO₂ concentration effect on denitrification (CO2Denitr_1), which is used as a proxy for labile C availability in DayCent. The next five most sensitive parameters are all associated with EENFs that control the release of N from CRNFs or reduction efficiency of NIs on nitrification rate. The remaining parameters were not sensitive to N₂O production based on the measurement dataset. Only the top 13 parameters in the sensitivity ranking were included in the Bayesian calibration with the SIR method, which made the analysis more parsimonious.

3.4.2. Posterior Estimates of Model Parameters

The dataset did provide sufficient information to improve the calibration of the three most sensitive parameters using the SIR method, producing marginal posteriors with smaller ranges and higher densities compared to the prior (Figure 3.5, Table 3.3). There was limited information in the measurement data to inform the other parameters and reduce the uncertainty in their prior distributions.

The posterior mean values were very similar to the maximum a posteriori (MAP) estimates for most model parameters except for one of the parameters in the reduction curve associated with nitrification inhibitors (FINHIB1), and the intercept for logistic curve representing the proportion of nitrified N lost as N₂O (N2Oadjust_Intcpt) (Table 3.3).

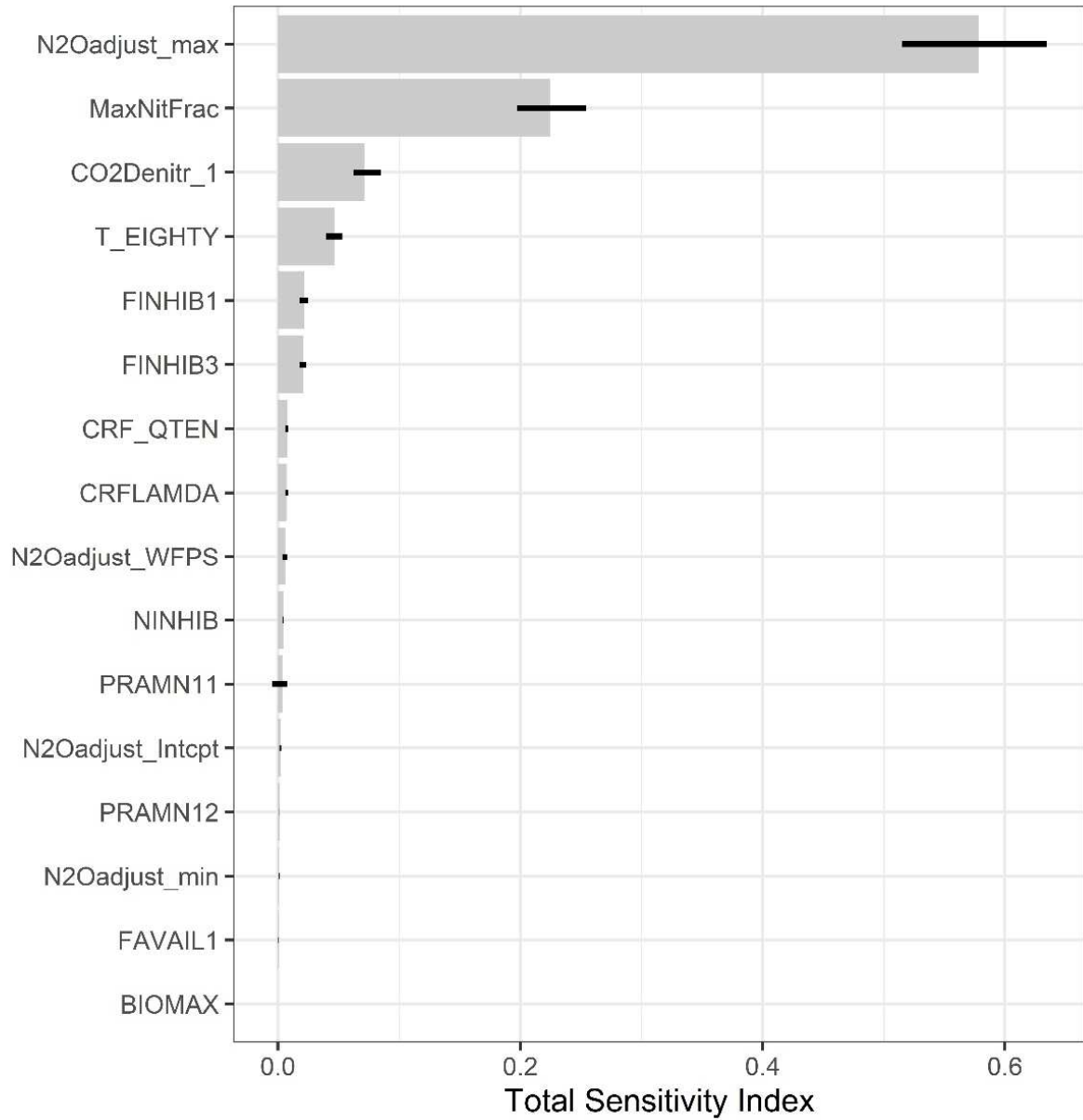


Figure 3.4. Ranked model parameters based on the total sensitivity indices with 95% bootstrap confidence interval using 100 replicates of the log-likelihood values. The parameters were ordered based on their sensitivity, with the most sensitive parameters at the top.

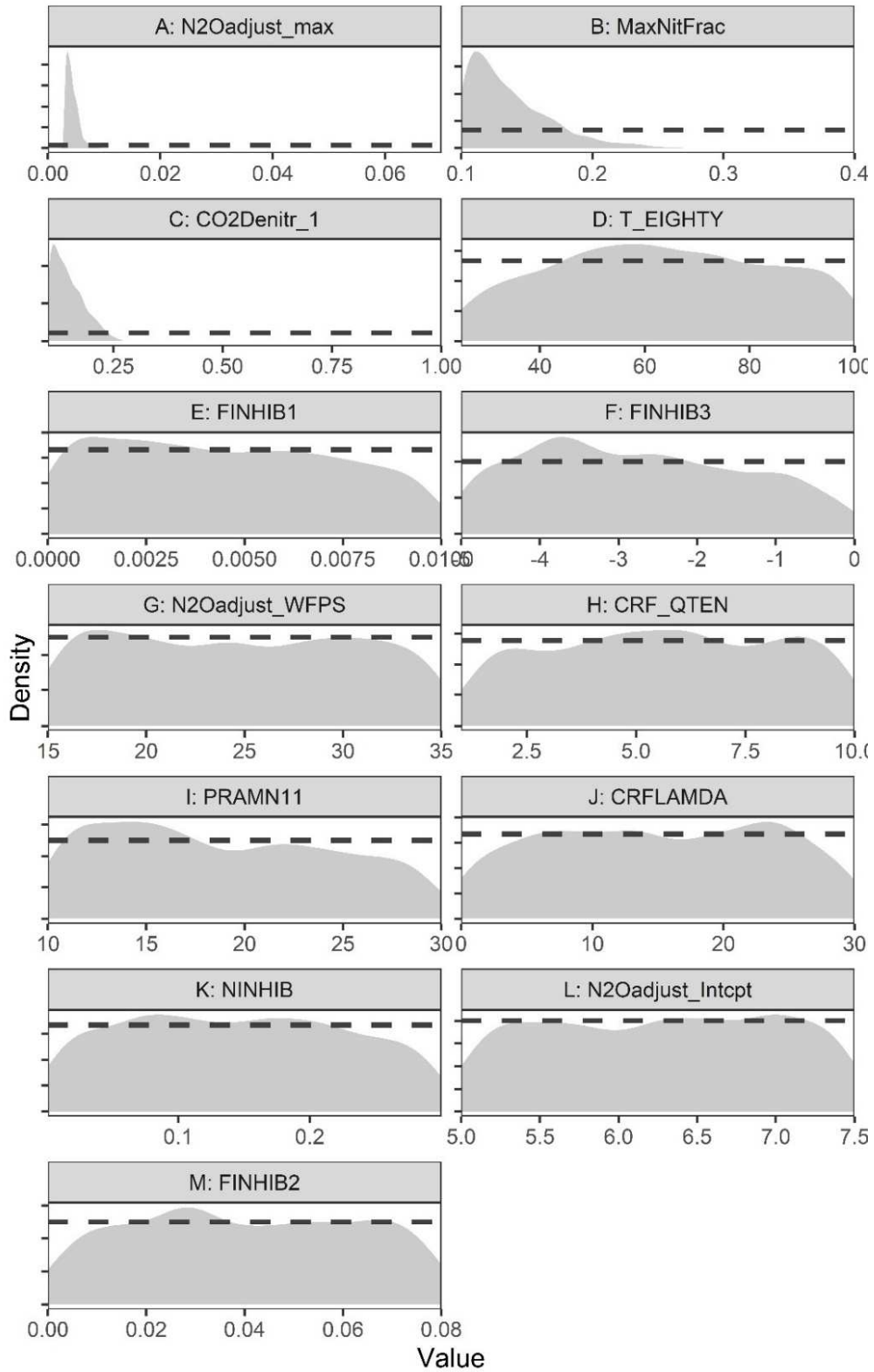


Figure 3.5. Marginal posterior density (light grey) for DayCent model parameters and uniform priors (dark grey dashed line) ranked from most sensitive to the least sensitive (A-M) according to the global sensitivity indices.

Table 3.3. Summary statistics including mean, median, and standard deviation (Std.) of the marginal posterior distribution of thirteen DayCent model parameters and three hyperparameters associated with the spatio-temporal correlation of the dataset and the maximum a posteriori (MAP) estimates.

Parameter	Mean	Median	Std.	MAP
T_EIGHTY (t_{80})	63.37	63.11	20.55	61.13
CRFLAMDA (λ_{CRF})	15.11	14.79	8.54	17.17
CRF_QTEN (Q_{10}^{CRF})	5.64	5.65	2.56	6.29
NINHIB	0.14	0.14	0.08	0.20
FINHIB1	0.0045	0.0043	0.0029	0.0001
FINHIB2	0.040	0.040	0.023	0.044
FINHIB3	-2.75	-2.84	1.37	-2.43
MaxNitFrac	0.14	0.13	0.03	0.11
N2Oadjust_max	0.0043	0.0040	0.0010	0.0043
N2Oadjust_Intcpt	6.27	6.29	0.73	5.01
N2Oadjust_WFPS	24.71	24.50	6.00	30.97
CO2Denitr_1	0.15	0.14	0.04	0.11
PRAMN11	18.82	18.08	5.76	16.02
σ_{site}^2	10.44	10.06	1.88	14.34
$\sigma_{\text{site}\times\text{year}}^2$	12.46	12.30	1.16	12.17
σ_{res}^2	175.65	177.18	6.79	155.91

The correlations between most parameters were weak (i.e., < 0.25 in absolute value) except for the three most sensitive parameters, which all have moderate negative correlations (-0.37 to -0.26). Furthermore, the uncertainty is dominated by the random effects associated with the unexplained error variance (σ_{res}^2), followed by site by year ($\sigma_{\text{site}\times\text{year}}^2$), and site (σ_{site}^2) hyperparameters. The MAP estimates (i.e., mode of the posterior distribution) are the most likely parameters given the measurement dataset, and therefore are the single best parameter set in the joint probability distribution.

3.4.3. Posterior Prediction of Reduction Factors

The mitigation potentials of EENFs were investigated by calculating the reduction factors by subtracting N₂O emissions associated with conventional N fertilizer from EENFs. I compared the distribution of reduction factors from three different estimates, (1) measured reduction factors determined by the measurement window for the crop growing season, (2) model estimates for the growing season matching the measurement window, and (3) model estimates of reduction factor for the year (Figure 3.6). The model produces very similar distributions of reduction factors for both CRNFs and NIs compared to the measurement windows for the growing season. However, the model produces lower median reduction factors for annual N₂O emissions.

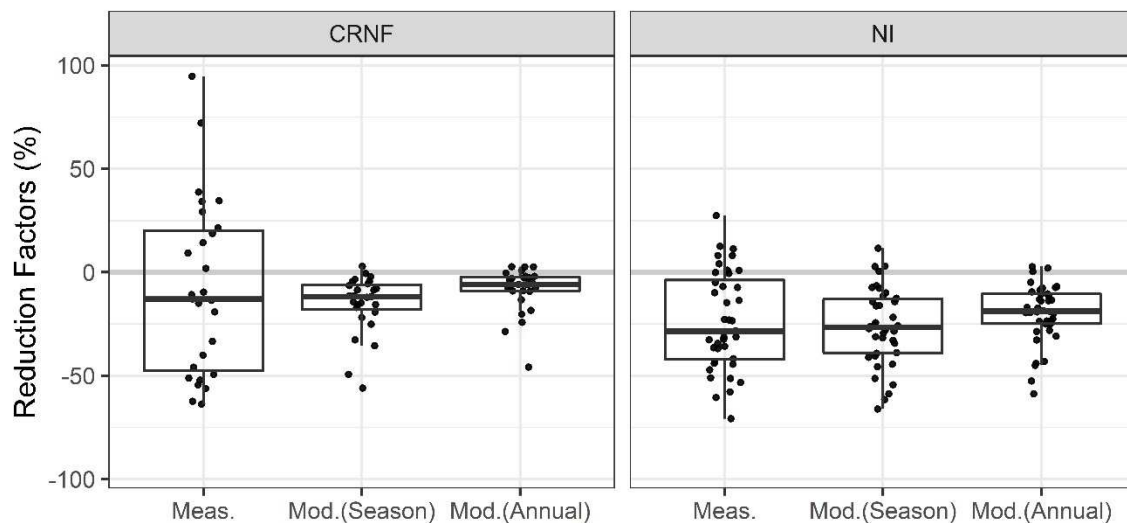


Figure 3.6. Comparison between the measured (Meas.), modeled with measurement period data (Mod. (Season)), and modeled with annual (Mod. (Annual)) N₂O Reduction Factors (%) for CRNF and NI.

The model estimates a median reduction factor of -11.9% (-51.7% and 0.58%) for CRNFs and -26.7% (-61.8% to 3.1%) for NIs, compared to the measured reduction factor for CRNFs of -13.0% (-62.8% to 80%) and -28.5% (-60.8% to 12.9%) for NIs (Note: the numbers in the parenthesis are 95% posterior prediction intervals). However, the model has more uncertainty associated with reduction factors for individual experimental treatment plots (Figure 3.7). In

addition, the model mostly estimated a reduction in N₂O emissions with EENFs compared to the control with conventional fertilizer even though a small number of the measurement had higher N₂O emissions for the EENF treatments.

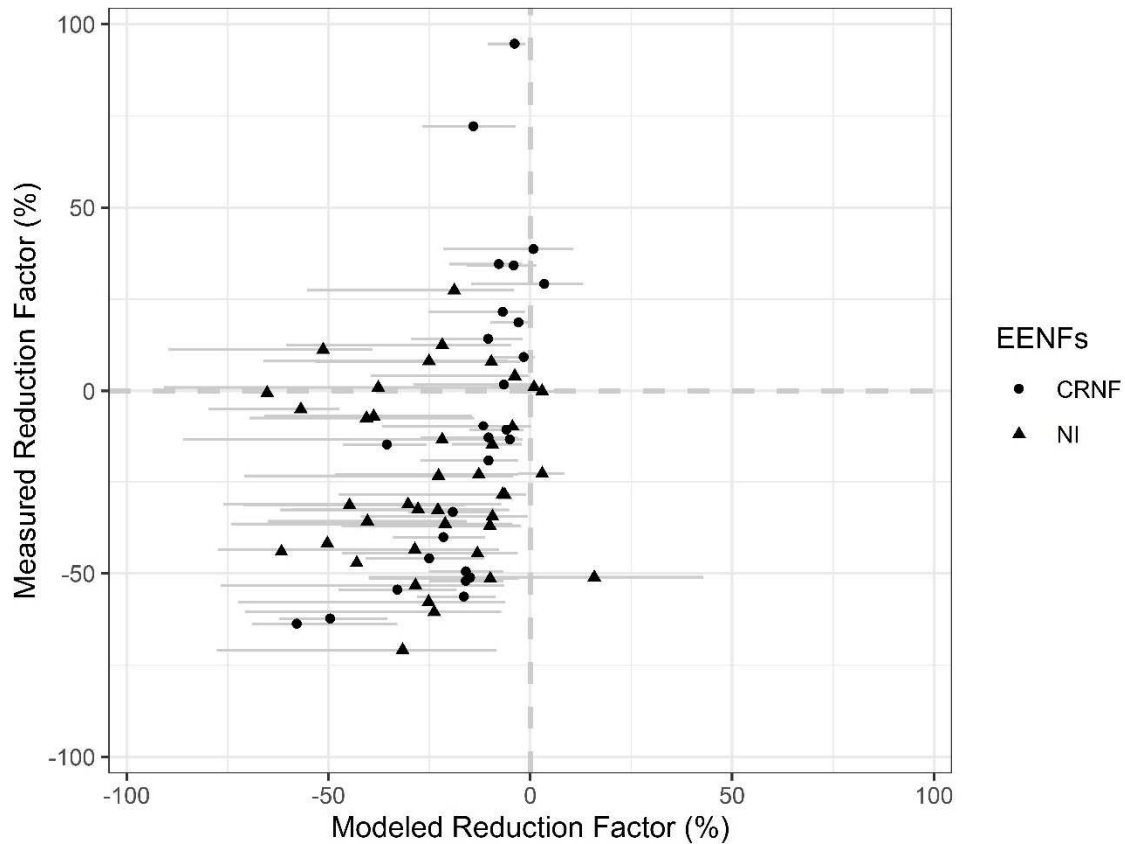


Figure 3.7. Modeled versus measured N₂O Reduction Factors (%) for CRNFs (circle) and NIs (triangle) with 95% posterior prediction intervals.

I also evaluated the time series patterns in the daily modeled emissions compared to the measurements from GRACEnet sites (Figure 3.8). The posterior estimates from DayCent and the measurements consistently showed that the EENFs initially produce significantly lower N₂O fluxes following fertilizer events and similar N₂O fluxes for the rest of the year with slightly higher N₂O fluxes later in the growing season. However, this shift in pattern to higher emissions later in the season did not offset the reductions in N₂O emissions that occurred early in the growing season for most experimental data, leading to a net reduction in N₂O emissions over the

year (Figure 3.6). Additionally, the EENFs also produce higher N₂O fluxes during the spring thaw period compared to the conventional fertilizers, but there are no measurements during this time period to evaluate the modeled pattern.

I also compared the dynamic approach for modeling NIs to the more static representation of the inhibitor effect with a constant reduction of 50% for 2 months based on Del Grosso et al., (2009). Other model improvements were retained in this comparison by setting parameter values at the MAP estimates (Table 3.3). I also made model predictions with the dynamic NIs model using the MAP parameter estimates. Both models produce similar Root-mean square error (RMSE), bias statistics, and Pearson correlation for the paired treatment differences, with at RMSE of 14.18 and 14.13 g N₂O-N ha⁻¹ day⁻¹; bias of -0.4 and 0.5 g N₂O-N ha⁻¹ day⁻¹; and Pearson correlation of 0.21 and 0.22 for dynamic NI effect and static effect models, respectively. However, the dynamic NI model generates smooth N₂O differences, whereas the constant model sometimes generated a sharp increase in N₂O at the end of the two months period, particularly at the Bowling Green site, which is an artifact of nitrogen being retained as NH₄⁺ for a set period of time rather than a gradual decline in the effectiveness of the inhibitor (Figure 3.8).

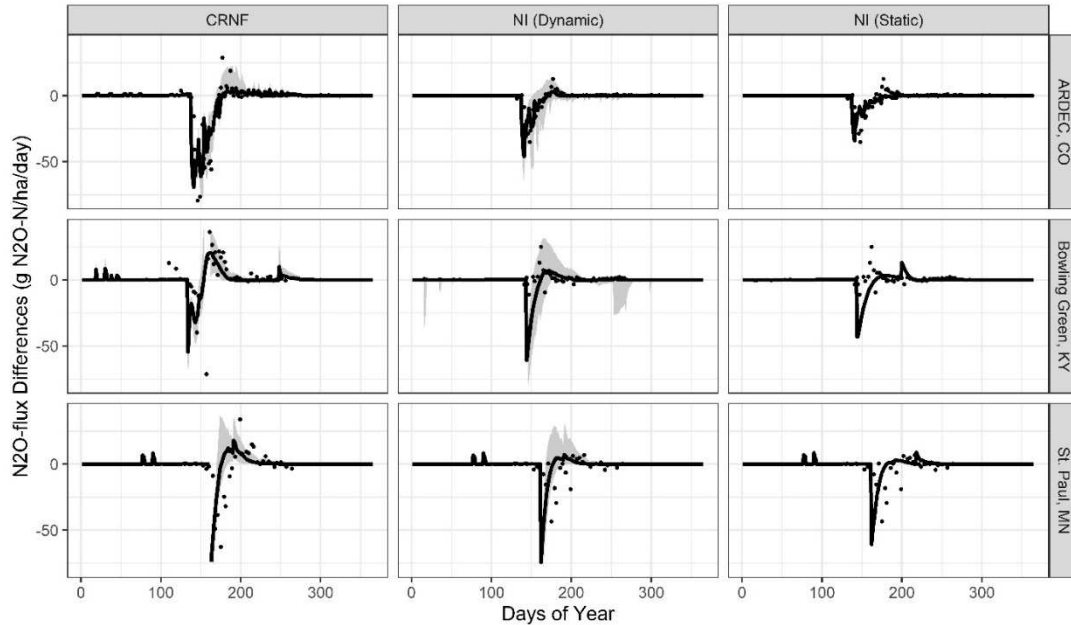


Figure 3.8. Posterior predictions (black line) and 95% central posterior prediction intervals (grey band) for the CRNF (first column), dynamic NI model (second column), and static NI routine (i.e., Del Grosso et al. 2009) (third column), and measured N₂O-flux differences (black dots) between EENFs (CRNF and NI) and conventional fertilizer for ARDEC, CO (first row); Bowling Green, KY (second row); and St. Paul, MN (third row). Values at 0 imply that there is no difference between the treatment and control, while values below 0 represent a reduction in N₂O emissions in the treatment with EENFs compared to the control, and values above 0 represent an increase in N₂O emissions in the plot with EENFs.

3.5. Discussion

Overall, DayCent was able to capture the mean effect of EENFs on N₂O reductions based on the experimental dataset. With CRNFs the model suggests a reduction of -11.9% (-51.7% and 0.58%), which is lower than reported reduction factor of -35% (-58% and -14%) by Akiyama et al. (2010) and -20% (-27% and -11%) reported by Thapa et al. (2016), but similar to reduction factor of -16% (-36% and 8%) reported by Han et al. (2017) and -5% (-18% and 7%) by Eagle et al. (2017). DayCent results also suggested that NIs are more effective in reducing N₂O compared to CRNFs (Figure 3.6) with a reduction factor of -26.7% (-61.8% to 3.1%). Higher reductions for NIs have been reported by published meta-analysis. For example, Akiyama et al., (2010) and Thapa et al., (2016) both reported reduction factors of -38% (-44% and -31%), Han et al., (2017)

reported -44% (-48% and -39%) with NI, and a reduction factor of -25% (-39% and -13%) is reported by Eagle et al., (2017). Furthermore, reduction factors reported by Eagle et al., (2017) are based on North American corn-based systems, and more comparable in terms of the level of emission reductions estimated in my model-based analysis than other meta-analyses that are based on global datasets.

I also further improved the representation of nitrification in DayCent by incorporating a dynamic estimation of nitrified-N that is emitted as N₂O rather than assuming a constant rate of N₂O emissions from nitrification (i.e., 1.2%). The dynamic rate depends on WFPS as an indicator for O₂ availability. Following Kool et al. (2011), I hypothesized that two distinct pathways lead to N₂O production during the transformation of NH₄⁺ to NO₃⁻. In an aerobic environment, oxidation of hydroxylamine (NH₂OH) during autotrophic and heterotrophic nitrification contributes to N₂O formation (nitrifier nitrification) (Sutka et al., 2003). With increasing WFPS, when the soil environment reaches sub-oxic conditions, nitrifying microorganisms reduce nitrite (NO₂⁻) to N₂O (nitrifier-denitrification) (Wrage et al., 2001).

Most N₂O emissions are released following N applications especially during the growing season, but significant N₂O fluxes have also been observed during freeze-thaw cycle (FTC) (Dusenbury et al., 2008; Pelster et al., 2019; Risk et al., 2013). Models that do not estimate N₂O emissions from FTC could underestimate global agricultural N₂O emissions by 17 to 28% (Wagner-Riddle et al., 2017). Empirical reduction factors for EENFs only capture reductions during the growing season because of a lack of measurements during other times of the year including FTC. By comparing the modeled reduction factor between the growing season and annual values, the effectiveness of EENFs was reduced by 50% for CRNFs and 35% for NIs in DayCent model simulations. The main reason for the reduced effectiveness in the model is due to

N₂O emissions during the FTC with slightly higher N₂O from EENF simulations during these events in late winter or early spring (Figure 3.8), mainly driven by higher mineral N in model simulations for the EENF plots during the spring thaw (Figure not shown). My findings raise a concern about reduction potentials that are based on empirical factors, particularly in northern latitudes where FTC is more frequent. Field research is needed to better understand the trends in mineral N content and emissions associated with EENFs for the entire annual cycle including the potential for emission pulses surrounding FTC.

The differences were not as great as I anticipated between modeling NIs with a dynamic approach incorporating environmental controls on the effectiveness of the inhibitors compared to static representation of reductions in nitrification rates (Del Grosso et al. 2009). Both models produce similar results based on the statistics, but the static representation produces an artificial pulse in N₂O at the end of the fixed two-month period. This is due to the nature of the step function in the static approach when the model simulates the 50% inhibition for two months and then switches to no inhibition. The dynamic inhibition model, in contrast, starts with the highest level of inhibition and gradually declines as the NI decays. The dynamic model is arguably more realistic with an exponential decay of NIs (Kelliher et al., 2014) and dependency on the NI concentration for inhibition effectiveness that is associated with the dynamic function (Di and Cameron, 2004).

Comprehensive research has also found a large number of chemicals having NI properties (Prasad and Power, 1995) and several products have gained popularity (Trenkel, 2010). Reduction factors for individual types of NIs have been estimated, however, most NIs are not significantly different from each other (Akiyama et al., 2010; Eagle et al., 2017; Thapa et al., 2016). Among all NIs, Dicyandiamide (DCD) is the most commonly applied NIs in experiments

including GRACENet sites, and therefore DayCent has been more fully tested for this type of inhibitor. It is noteworthy that several publications have reported that DCD is highly sensitive to temperature with decreasing half-life as temperatures increase (Di and Cameron, 2004; Kelliher et al., 2008; Prasad and Power, 1995). Additionally, DCD is also readily soluble in water and susceptible to leaching, thus lowering its efficiency (Prasad and Power, 1995; Williamson et al., 1996). Moreover, most NIs are reported as sensitive to soil temperature and soil moisture dynamics (Prasad and Power, 1995; Trenkel, 2010), hence, the method and model is likely representative of a broader suite of NIs that are available on the market.

Furthermore, EENFs applied at GRACENet sites often combine urease inhibitor N-(n-butyl) thiophosphoric triamide (NBPT) with DCD, so the independent effect of NIs from urease inhibitors was not possible to evaluate with this dataset. However, a meta-analysis performed by Akiyama et al. (2010) found that the urease inhibitors, such as NBPT, had no significant effect on N₂O emission and therefore I expect that the majority of the reductions in N₂O emissions was due to the application of NIs in these experiments. Regardless, further model testing of DayCent should be done in the future as more field research is completed for a broader suite of inhibitor types and application of NIs without urease inhibitors, as well as to re-evaluate the dynamic inhibition model compared to the static approach for simulating the NI effect.

CRNFs are mainly conventional soluble fertilizers with protective coatings or are a water-insoluble with semi-permeable or impermeable coatings of porous materials (Shaviv, 2001; Trenkel, 2010). In the presence of water, the coating protects the N and leads to a slow release to the soil in a controllable manner. First, the protective coating allows moisture to diffuse into the CRNFs products, then dissolves the N fertilizer and creates a N solution. The subsequent N release through the protective coating is also influenced by the soil temperature.

Following the best management practices (BMPs) for fertilizer, CRNFs aim to release N in synchrony with the plant demand to avoid a surplus of plant-available N in the soil and N loss to the environment through nitrification, denitrification, leaching, and volatilization (Timilsena et al., 2015; Trenkel, 2010). Many products have been studied with the properties of CRNFs, and there are a variety of release patterns (Shaviv, 2001; Timilsena et al., 2015; Trenkel, 2010).

The dataset used in the analysis focused on a controlled-release, polymer-coated urea, ESN, which has been used in most experiments at GRACEnet sites. During the manufacturing process, the desired release pattern is achieved by varying the polymer coating composition or thickness, which influences release patterns as noted above (Shaviv, 2001; Trenkel, 2010). Most ESN was applied during the corn-growing seasons at GRACEnet sites and the posterior parameter distributions are suitable for simulations with corn or crops with a similar growing period. Further testing is needed to confirm if the current model calibration is sufficiently general to represent other CRNFs. Regardless, DayCent can be easily adapted to other CRNFs with a sigmoidal release pattern given sufficient experimental data for model calibration.

The use of EENFs has been considered as a potential mitigation method to reduce N losses to the environment and also improve nutrient use efficiency in crops according the 4R nutrient management paradigm. In addition to N₂O reductions, CRNFs and NIs also can effectively reduce NO₃⁻ leaching (Eagle et al., 2017; Zhang et al., 2019), NH₃ volatilization loss (Zhang et al., 2019), nitric oxides (NO_x) (Akiyama et al., 2010) and may improve crop yields (Abalos et al., 2014; Zhang et al., 2019).

3.6. Conclusion

Adoption of EENFs as an alternative to conventional fertilizers can reduce N₂O emissions, but the reduction potentials are affected by a variety of factors, including climatic conditions,

edaphic characteristics, and management practices. Process-based models that represent the N cycle may be a viable tool to understand the effect of individual factors and their interactions and make predictions about the benefit of EENFs for individual farms to regional, continental and global scales. Moreover, Bayesian calibration using the SIR method has been applied in this study to estimate appropriate parameter values for simulation of EENFs in DayCent, as well as quantifying model uncertainty—a critical requirement for scientific understanding and policy implementation for N₂O mitigation programs associated with agricultural management. Incorporating model development for EENFs into process-based models will provide a platform to better understand the multiple aspects of N dynamics and identify best management practices with the “4R” nutrient stewardship paradigm, particularly application of right source of N.

CHAP: BAYESIAN CALIBRATION OF THE DAYCENT ECOSYSTEM MODEL TO SIMULATE SOIL ORGANIC CARBON DYNAMICS AND REDUCE MODEL UNCERTAINTY

4.1. Summary

Benefits of carbon sequestration in agricultural soils are well recognized, and process-based models have been developed to better understand sequestration potential. However, most studies ignore the uncertainty arising during model prediction—a critical requirement for scientific understanding, policy implementation and carbon emission trading. Furthermore, the dependencies created in process-based models due to many parameters and a relatively small set of empirical data hinder parameterization. I have implemented a Bayesian approach using the sampling importance resampling (SIR) method to calibrate the DayCent ecosystem model for estimating soil organic carbon (SOC) stocks, and to quantify uncertainty in model predictions. A SOC dataset compiled from 19 long-term field experiments, representing 117 combinations of management treatments, with 491 measurements of SOC, was split into independent datasets for model calibration and evaluation. The most important DayCent model parameters were identified through a global sensitivity analysis (GSA) for parameterization and SIR was used to calibrate the model and produce posterior distributions for the most sensitive parameters. On average, the Bayesian calibration reduced the model uncertainty by a factor of 6.6 relative to the uncertainty associated with the prior. The Bayesian model analysis framework will allow for ongoing updates to the model as new datasets and model structural improvements are made in future research, and overall provide a stronger basis for models to support policy and management decisions associated with GHG mitigation through C sequestration in agricultural soils.

4.2. Introduction

Soil organic carbon (SOC) is a major pool in the global carbon cycle. It contains more carbon (C) than terrestrial vegetation and atmospheric CO₂ combined (IPCC, 2013). Annually, a large portion of photosynthetically-fixed C enters the soil as plant residues and is released back to the atmosphere through the activity of the microbial decomposer community (Paustian et al., 2000). Even a small change in this exchange of C between the soil and the atmosphere may have a large impact on the global carbon cycle. Moreover, less than a percentage increase in these SOC stocks per year may represent a significant level of C sequestration and reduction in anthropogenic greenhouse gas (GHG) emissions. The rate of C sequestration varies regionally and by land-use type with high potential in managed agroecosystems (Álvaro-Fuentes et al., 2017; Sanderman et al., 2017).

Currently, about 11% (1.5 billion hectares) of the earth's land surface is in crop production (Bruinsma, 2003). Much of this land has lost 50-75% of the native C stocks from the top soil layer (Lal et al., 2007; Ogle and Paustian, 2005; Sanderman et al., 2017) during the long history of intensive cultivation (Sanderman et al., 2017) and represents a potential CO₂ sink (Lal, 2004a; Paustian et al., 1997; Smith, 2004a). Adopting management practices that enhance organic matter input and/or reduce C losses by limiting decomposition can sequester C (Lal et al., 2007; Ogle and Paustian, 2005; Paustian et al., 1997) with a potential of gaining back about two thirds of initial C loss (Lal et al., 2007). It has also recently been promoted as a policy mechanism by the French Ministry of Agriculture to meet reduction commitments through "4 per mille Initiative for Food Security and Climate" (Minasny et al., 2017). However, monitoring and verification of SOC stock changes are required to incorporate SOC sequestration into mitigation programs (Smith, 2004b), and integrating measurements with process-based modeling provides a

viable method to quantify C sequestration for monitoring purposes (Conant et al., 2011a; Luo et al., 2016; Smith et al., 2012).

Although process-based models are extensively used to predict SOC stocks, such as DayCent (Del Grosso et al., 2001; Parton et al., 1998), RothC (Jenkinson and Rayner, 1977), DNDC (Changsheng Li et al., 1992), and EPIC (Izaurralde et al., 2006), uncertainty associated with model structure and parameterization are difficult to quantify and may account for the majority of uncertainty in model predictions (Ogle et al., 2010). Advancements in Bayesian calibration techniques have led to methods suitable for addressing uncertainty in both model parameters and predictions and the techniques have been used to model SOC dynamics (e.g. Clifford et al., 2014; Hararuk et al., 2014; Van Oijen et al., 2005; Xu et al., 2006). The method provides a probabilistic framework in which the posterior distributions of the uncertain model parameters are first estimated, and then the predictive distributions of the model outputs are computed (Gelman, 2014; Smith, 1991). Using Bayes' theorem (Bayes and Price, 1763), the posterior distribution is derived from the data likelihood and the prior distribution, where the likelihood measures the goodness of fit between the modeled and the measured dataset and the prior is the current understanding of the distribution of model parameters based on either previous analyses or expert knowledge.

Monte Carlo methods have been developed for conducting Bayesian calibration using a Markov Chain Monte Carlo (MCMC) approach, such as the Metropolis-Hastings (MH) algorithm (Hastings, 1970; Metropolis et al., 1953) and direct simulation such as the sampling importance resampling (SIR) method (Rubin, 1988, 1987). The MH algorithm has been used in several studies for parameter estimation of SOC simulation models (Ahrens et al., 2014; Clifford et al., 2014; Dechow et al., 2019; Sakurai et al., 2012; Van Oijen et al., 2005; Xu et al., 2006).

The MH algorithm follows a random walk through a parameter space iteratively. In each step, a new candidate vector is proposed and is accepted or rejected. This process is repeated for a large number of iterations with multiple chains to test for posterior convergence.

In contrast to MCMC, the SIR method is non-iterative and does not require a random walk through the parameter space. Instead, a large number of samples from the prior are obtained, and then from this, a smaller sub-sample is drawn with sample probability proportional to their importance weights—resulting in an approximate sample for a joint posterior distribution. In practice, the SIR method has been successfully applied in the field of fisheries (McAllister and Ianelli, 1997; Raftery et al., 1995), but to my knowledge the SIR method has not been applied to a process-based simulation model of SOC.

In a Bayesian procedure, it is desirable to account for uncertainty in all model parameters, but more parameters can require an unrealistically large number of simulations to identify the posterior probability distribution for parameters. Process-based models often have hundreds of uncertain parameters that makes the calibration process impractical. In practice, uncertainty is assigned to only a fraction of model parameters and it is assumed that other parameters are fixed without error (McAllister et al., 1994). This assumption may underrepresent uncertainty and may also introduce bias into the model output if influential parameters are not included in the parameterization. Thus, a global sensitivity analysis (GSA) that adopts a parsimonious principle by identifying the most influential or ‘sensitive’ parameters driving variation in model results is recommended to avoid significantly reducing estimates of model uncertainty (Saltelli et al., 2008).

The objective of this study is to implement a Bayesian model analysis framework that quantifies and possibly reduces uncertainty in model predictions of SOC stocks and stock

differences in the top 0-30 cm of agricultural soils (Figure 4.1). First, a variance-based GSA using the Sobol method (Jansen, 1999; Saltelli, 2002; Sobol, 2001, 1993) is performed to identify influential model parameters associated with predicting SOC stocks (Figure 4.1A). Non-influential parameters are fixed to default values, making the model more parsimonious (Saltelli et al., 2008). Second, the sampling importance resampling (SIR) method is applied to estimate the posterior distribution of parameters (Figure 4.1B) identified as influential during the GSA. Finally, a Monte Carlo analysis is used to estimate posterior predictive distributions of SOC stocks and stock differences (Figure 4.1C) based on the parameter distributions from the Bayesian analysis. The proposed framework is applied to DayCent ecosystem model to evaluate parameter uncertainty for the soil organic matter module. During the calibration process, instead of estimating posterior distributions of model parameters for each site separately, I treated the model parameters as population-level variables and estimated only one joint posterior distribution. This enables the application of DayCent to simulate SOC beyond the experimental sites in the calibration dataset, and fully quantify uncertainty in the model predictions. DayCent has been used to simulate ecosystem responses due to land-use change and change in management practices in cropland and grassland (Cheng et al., 2014; Del Grosso et al., 2008; Ogle et al., 2010; Parton and Rasmussen, 1994) and the effect of climate change in agricultural system (Parton et al., 2007; Robertson et al., 2018). DayCent has also been used to quantify C stock changes and GHG fluxes from agricultural soils for the U.S. National Greenhouse Gas Inventory compiled by the U.S. Environmental Protection Agency and reported annually to the UN Framework Convention on Climate Change (EPA, 2019).

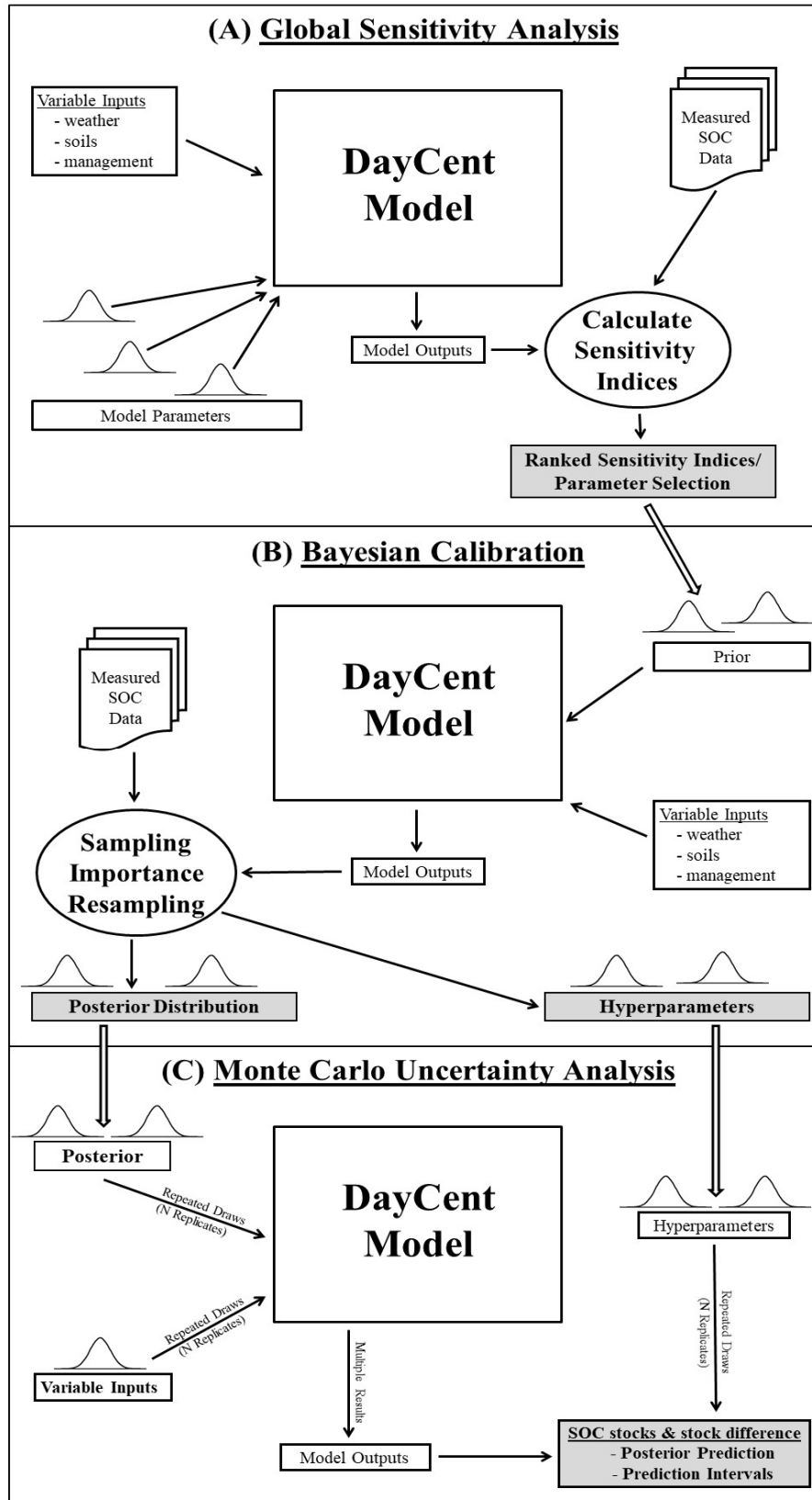


Figure 4.1. Flow Chart Diagram of the Bayesian model analysis framework

4.3. Materials and Methods

4.3.1. DayCent Ecosystem Model

DayCent (Del Grosso et al., 2001; Parton et al., 1998) is a daily time-step version of the CENTURY (Parton et al., 1987) ecosystem model with intermediate complexity and simulates the flows of carbon (C) and nitrogen (N) through plant-soil systems. DayCent includes several sub-models to simulate plant production, decomposition of litter and SOC, soil water, and temperature dynamics. The SOC sub-model consists of three (active, slow, and passive) soil C pools. The active pool has a short turnover time of months to a few years and represents soil microbes and microbial products. The slow pool includes resistant plant material and soil-stabilized microbial products with a turnover time up to a few decades. The physically and chemically stabilized SOC, which is very resistant to decomposition is the passive pool and has a turnover time on century time scales. In DayCent, carbon transfer between pools is determined by decay rates and controlled by C transfer efficiency parameters. The decay rates for all the three pools are influenced by climatic variables and the soil properties, while the tillage and/or physical disturbances only affect the decay rates for active and slow pools. Carbon transfer efficiencies are also influenced by soil texture. The site-specific variable inputs required for DayCent simulations are daily maximum and minimum temperatures, precipitation, scheduling of irrigation, site-specific soil properties, current and historic land use, management practices such as grazing, cultivation and planting schedules, organic matter inputs, fertilizer inputs and soil disturbance through tillage management.

4.3.2. Experimental Sites

A literature review was conducted to obtain data for calibration and evaluation of the model. Experimental sites were selected from published SOC studies based on the following set of

criteria: (a) the duration of the experiment must be at least 15 years or greater, (b) there must be at least two repeated measurements over the duration of the study for a given treatment, (c) SOC measurement data must be available to a depth of 30 cm or enough information for a reasonable extrapolation to 30 cm, and d) site-specific variable inputs were available for the DayCent simulations. When SOC measurements were not available to 30 cm, SOC estimates to 30 cm were calculated based on the C stocks of the nearest depth increment. In some cases, the authors of the papers were contacted to obtain additional information needed for the simulations that was not included in the publications.

The final SOC dataset for the analysis consisted of 19 long-term experimental sites with a total of 117 combinations of management treatments across all sites and 491 measured SOC stocks. The dataset was further divided into two sets for model calibration and independent evaluation. The dataset for the model calibration included 8 long-term experimental sites with a combined 56 site by treatment combinations and a total of 270 measurements (Table 4.1). The remainder of the 11 long-term experimental sites were used for model evaluation with a combined 61 site by treatment combinations and a total of 221 measurements (Table 4.2). The experimental sites have well-documented management activities including crop rotation histories, residue management, tillage practices, cover crop usage, fertilizer application rates, irrigation, and organic amendments for the duration of the experiment, and also have reported edaphic characteristics including soil texture, soil pH, and soil drainage status that are required for DayCent simulations. Additionally, hydric properties needed for model inputs were calculated using equations in Saxton et al., (1986). Daily maximum and minimum temperature and precipitation for the experimental sites in the United States were acquired from PRISM

(PRISM Climate Group, 2018), in Canada from NARR (Mesinger et al., 2006), and for rest of the sites from MsTMIP (Huntzinger et al., 2015).

For each of the experimental sites, SOC pools (state variables) were initialized with several thousand years of simulation under grassland vegetation, historical weather data, and edaphic characteristic to reach a steady-state condition. In DayCent and many ecosystem models, model initialization of SOC pools is crucial and if the state variables are not initialized within a reasonable range of steady-state conditions then there can be considerable drift in modeled SOC stocks, which may introduce significant bias into estimates of SOC stock changes (Falloon and Smith, 2000). After establishing the state variables at steady-state conditions, recent cultivation histories were simulated for the long-term experiments allowing the state variables to reach values consistent with known cultivation histories of the regions prior to the start of the experiment. These histories were based on information provided in the published literature for the experiment (Table 4.1) or from general cultivation histories that are used in the U.S. National Greenhouse Gas Inventory (EPA, 2019).

Table 4.1. SOC study locations and treatments used for the Bayesian model calibration. Treatment abbreviation are MN = mineral nitrogen additions; Omad = organic amendment; TILL = tillage change; CR = crop rotation; BF = bare fallow plots; GR = grazing intensity and n is the number of observations for the study location.

Locations	Lat.	Lon.	Sand	Silt	Clay	n	Length (years)	Trt.	References
Broadbalk Rothamsted, UK	51.8	-0.4	18	57	25	54	153	MN Omad BF	e-RA (2013) Jenkinson, (1990) Schuman et al., (1999) Manley et al., (1995)
Cheyenne Wyoming, USA	41.2	-105	68	16	16	6	21	GR	Ingram et al., (2008)
Grignon France	48.9	1.9	16	54	30	11	48	BF	Barré et al., (2010)

Mead Kansas, USA	41.2	-96	5	60	35	9	17	CR Omad	Lesoing and Doran (1997) Machado et al., (2008)
Pendleton Oregon, USA	45.4 4	-118	18	60	22	10 3	64/55	MN Omad TILL	Machado, (2011) Rasmussen and Smiley (1997) Rasmussen and Rohde, (1988)
South Charleston Ohio, USA	40	-83.5	15	65	20	9	29	Till	Dick et al. (1997)
Swift Current Saskatchewan, Canada	50.3	-108	25	49	26	60	30	Till CR	Maillard et al., (2018)
Wooster Ohio, USA	48.8	-82.0	25	60	15	18	31	CR Till	Dick et al. (1997)

Table 4.2. SOC study locations used for independent model evaluation. Treatment abbreviations are the same as in Table 4.1.

Locations	Lat.	Lon.	Sand	Silt	Clay	n	Length (years)	Trt.	References
Bad Lauchstadt Germany	51.4	11.9	11	68	21	18	96	BF Omad	Jensen et al., (1997) Smith et al., (1997) Powlson et al., (1998) Molina et al., (1997) Ludwig et al., (2007)
Dixon Springs Illinois, USA	37.4	-88.7	4	77	19	24	20	TILL	Kitur et al., (1994) Olson et al., (2010)
Hoytville Ohio, USA	41.0	-84.0	21	39	40	13	42	CR Till	Dick et al. (1997)
Lethbridge Alberta, Canada	49.7	-113	46	23	31	45	80	CR MN	Monreal and Janzen, (1993)
Lexington Kentucky, USA	38.1	-84.5	9	61	30	12	22	Till MN	Frye et al. (1997)

Mandan North Dakota, USA	46.8	-101	29	53	18	4	87	GR	Frank et al., (1995) Liebig et al., (2006)
Morrow Illinois, USA	40.1	-88.2	8	67	25	14	115	MN	Khan et al., (2007)
Park Grass Rothamsted, UK	51.5	0.5	12	66	22	19	146	MN	e-RA (2013)
Rosemount Minnesota, USA	44.7	-93.1	16	60	24	30	22	TILL MN RR	Clapp et al., (2000) Dolan et al., (2006)
Saginaw Michigan, USA	43.4	-84.1	9	44	47	21	20	CR	Christensen (1997)

4.3.3. Global Sensitivity Analysis

The first step in the Bayesian model analysis framework is to conduct a variance-based GSA to quantify the relative importance of parameters that have a significant influence on model output (Figure 4.1A). The analysis permits us to identify a group of parameters with the most influence and allows a framework to fix other less influential parameters to a reasonable value, making the model more parsimonious (Saltelli et al., 2008), a method known as “Factor Fixing” or “Screening”. My analysis used the Sobol method (Jansen, 1999; Saltelli, 2002; Sobol, 2001, 1993) to estimate the sensitivity index, which measures the influence of individual parameters or groups of parameters on the model output. Like the analysis of variance, the method partitions the total variance of the model output into first-order and higher-order interaction terms and allows the estimation of the proportion of variance explained by each parameter.

The Sobol method is model-independent, works for both linear and nonlinear outputs (Sobol, 2001) and is well suited for complex and highly non-linear process-based ecosystem models, such as DayCent. This method takes into consideration the whole parameter space simultaneously in the form of a probability density function, includes both main effect and

interactions between parameters, and is arguably one of the most robust and comprehensive global sensitivity methods (Saltelli et al., 2008). I used log-likelihood value computed from the mismatch between the measured and modeled to determine the sensitivity for the GSA.

Even though DayCent has hundreds of model parameters, here I only considered a total of 17 parameters that directly relate to SOC processes and the soil organic matter decomposition sub-routine in DayCent. For the GSA, I assigned independent uniform priors separately for each of the 17 model parameters (Table 4.3). These parameters control the decay rate of the SOC pools and C transfer efficiency. DayCent model parameters associated with other processes, such as plant production, influence the modeled SOC, but in an indirect manner through these 17 parameters.

Table 4.3. Default parameter values, prior distributions and definitions for the 17 parameters in soil organic matter decomposition sub-routine of DayCent.

Parameters	Default	Lower	Upper	Distribution	Definitions
'DEC4'	0.0025	0.001	0.005	uniform	Maximum decomposition rate of passive pool
'TEFF(1)'	14	5	30	uniform	Temperature (°C) at the inflection point for the temperature curve
'DEC5(2)'	0.12	0.07	0.25	uniform	Maximum decomposition rate of slow pool
'TEFF(2)'	0.15	0.05	0.3	uniform	Slope of line at inflection point
Till_Eff	10	5	15	uniform	Tillage Multiplier on decomposition
'PS1S3(2)'	0.032	0.02	0.06	uniform	Slope for clay effect on C transfer efficiency active to passive
'PMCO2(2)'	0.55	0.35	0.7	uniform	Fraction of C loss as CO ₂ from soil metabolic pool
'WEFF(2)'	9	6	15	uniform	Moisture effect on decomposition
'P2CO2(2)'	0.55	0.5	0.8	uniform	Fraction of C loss as CO ₂ during decomposition from slow pool
'PS1S3(1)'	0.003	0.002	0.005	uniform	Clay effect on C transfer efficiency from active to passive
'PS2S3(1)'	0.003	0.002	0.005	uniform	Clay effect on C transfer efficiency from slow to passive

'PS1CO2(2)'	0.55	0.4	0.8	uniform	Fraction C loss as CO2 from soil structural to slow pool
'P1CO2A(2)'	0.17	0.1	0.25	uniform	Sand effect on C loss as CO2 from active pool (Intercept)
'P1CO2B(2)'	0.68	0.55	0.74	uniform	Sand effect on C loss as CO2 from active pool (slow)
'WEFF(1)'	30	25	35	uniform	Moisture effect on decomposition
'PS2S3(2)'	0.009	0.006	0.013	uniform	Clay effect on C transfer efficiency slow to passive pool (Slope)
'P3CO2'	0.55	0.5	0.9	uniform	fraction of C loss as CO2 during decomposition from passive pool

4.3.4. Bayesian Calibration

The next step in the Bayesian model analysis framework is Bayesian calibration using the SIR method (Figure 4.1B). This approach to parameterization is an inverse modeling process that provides a probabilistic framework to estimate the joint posterior distribution of the uncertain model parameters that is consistent with the measured data given the model structure and prior understanding of the parameters. Using Bayes' theorem, the posterior distribution $p(\theta|O(\mathbf{x}))$ of the parameters θ , given the measured data and model output, can be represented as a function of likelihood $L(O(\mathbf{x})|\theta)$ and the prior $p(\theta)$, where the likelihood measures the mismatch between the modeled and the measured data, and the prior provides our level of understanding about the parameters. The joint posterior distribution is defined up to a proportionality constant as follows:

$$p(\theta|O(\mathbf{x})) \propto L(O(\mathbf{x})|\theta)p(\theta). \quad (2.5)$$

In the process, the prior density $p(\theta)$ is updated to the posterior density $p(\theta|O(\mathbf{x}))$ through the data likelihood function $L(O(\mathbf{x})|\theta)$. When the data contain little information about the parameters, the posterior tends to reproduce the prior, hence nothing has been learned with the new data. However, as data become more informative, the likelihood $L(O(\mathbf{x})|\theta)$ outweighs the prior and the data dominate the posterior (Box, 1973; Gelman, 2014).

The SIR method (Rubin, 1988, 1987) is a non-iterative or direct Monte Carlo method that updates the sample from the prior to generate a sample from the posterior by adopting a particle filter based on importance weights, $\omega(\theta^s)$ (Givens et al., 1995; Punt and Hilborn, 1997; Smith and Gelfand, 1992). Therefore, in the SIR method, parameters that produce higher goodness of fit between the measured and modeled SOC stocks are more likely to be retained in the posterior. The calibration of DayCent model parameters using the SIR method can be summarized as follows (Figure 4.2). First, the posterior sample generated using the SIR method is a set of approximate draws from the posterior distribution, and the approximation improves as M increases (i.e. $M \rightarrow \infty$) (Gelman, 1993; Givens et al., 1995; Rubin, 1988). In practice, the choice of M should be large enough to achieve greater sampling efficiency (McAllister and Ianelli, 1997). Therefore, I drew a large ($M = 1,000,000$) independent random sample $\{\theta^1, \theta^2, \dots, \theta^M\}$ from the prior using the Latin hypercube sampling method (McKay et al., 1979; Owen, 1992; Stein, 1987), where each θ was a vector of DayCent parameters. All other DayCent parameters were fixed to their default values. Second, the DayCent model was run for all treatments in the calibration sites for all M parameter sets $\{\theta^1, \theta^2, \dots, \theta^M\}$ and modeled SOC values corresponding to each of the measurements were stored. For each of the initial samples $\{s = 1, 2, \dots, M\}$, I evaluated the likelihood function $L(O(\mathbf{x})|\theta^s)$ assuming that the error was defined by the mismatch between the measured and modeled SOC stocks. I assumed a multivariate Gaussian distribution with a zero-mean vector and variance-covariance matrix Σ to address the spatiotemporal correlation of the dataset. I calculated the standardized importance weights; $\{\omega(\theta^1), \omega(\theta^2), \dots, \omega(\theta^M)\}$ using the following formula:

$$\omega(\theta^s) = \frac{L(O(\mathbf{x})|\theta^s)}{\sum_{s=1}^M L(O(\mathbf{x})|\theta^s)}, \quad (2.8)$$

where $L(O(\mathbf{x})|\theta^s)$ is the likelihood function for the s^{th} sample. Third, I resampled ($m = 1000$) the parameter set $\{\tilde{\theta}^1, \tilde{\theta}^2, \dots, \tilde{\theta}^m\}$ without replacement from the initial set of parameters $\{\theta^1, \theta^2, \dots, \theta^M\}$ based on probabilities proportional to their importance weights $\{\omega(\theta^1), \omega(\theta^2), \dots, \omega(\theta^M)\}$. When all steps were completed, I had m samples $\{\tilde{\theta}^1, \tilde{\theta}^2, \dots, \tilde{\theta}^m\}$ to approximate the posterior distribution. These samples were used to construct the marginal posterior densities of the model parameters with a kernel density estimator and posterior predictive distribution of SOC stocks and stocks differences.

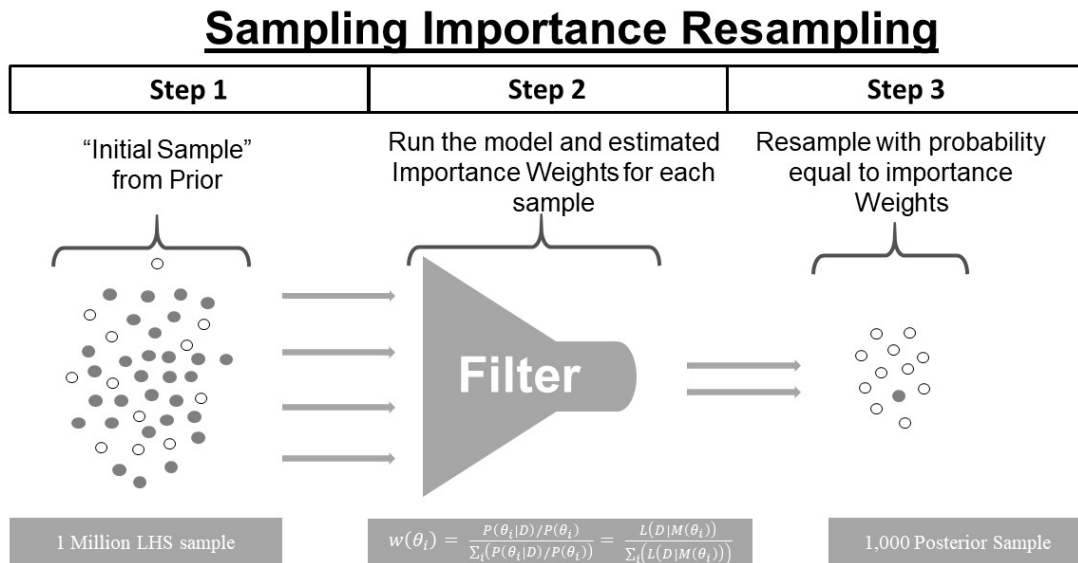


Figure 4.2. Illustration of the Sampling Importance Resampling (SIR) method. Open circles represent samples with higher and solid circles with lower importance weights.

4.3.5. Model Prediction using Monte Carlo Approach

The final step in the Bayesian model analysis framework is to use a Monte Carlo approach to propagate uncertainty through the DayCent model application and derive prediction intervals for SOC stocks and stock differences (Figure 4.1C). The resulting prediction intervals address the uncertainty associated with model parameters, but also the unexplained error in model predictions based on the hyperparameters. The hyperparameters quantify uncertainty associated

with parameters in other sub-models and also imperfect representation of processes in the DayCent model structure.

I applied the Monte Carlo approach by making joint probability draws from the parameter distributions and hyperparameters, applying the model iteratively for 1000 replicates. For external evaluation of the results, I simulated the 11 long-term experimental sites and compared the distributions of modeled to measured values. In addition, I conducted the Monte Carlo analysis with both prior and posterior distributions of the model parameters to demonstrate the reduction in uncertainty associated with the model analysis framework. The Monte Carlo analysis can also address uncertainties in model inputs, such as weather data and edaphic characteristics.

The analysis was performed using the R programming language for Linux version 3.5.0 (R Development Core Team, 2018) using the snowfall package (Knaus, 2010), sensitivity package for GSA (Iooss et al., 2020) and lhs package for Latin Hypercube sampling (Carnell, 2009). All the plots for the publication were generated using the package ggplot2 (Wickham, 2016).

4.4. Results

4.4.1. Global Sensitivity Analysis

Total sensitivity indices for each of the 17 model parameters are plotted in Figure 4.3. Parameters with total sensitivity indices $> 2.5\%$ were considered influential, which includes 9 parameters, while the remaining parameters were fixed to their default values. The threshold value of 2.5% captures the most influential parameters with goal of minimizing the overall number of parameters in the Bayesian analysis. Too many parameters could lead to an unrealistically large number of simulations to identify the posterior probability distributions for

parameters. Arguably, this threshold allows for inclusion of some parameters in the Bayesian analysis that have a relatively minor influence on the variability in modeled SOC stocks, but could be retained without creating computational limitations for the Bayesian analysis.

The three most influential parameters are related to decomposition processes, including (1) optimum decomposition rate of the passive pool (DEC4), (2) the effect of temperature on decomposition (TEFF(1)), and (3) optimum decomposition rate of the slow pool (DEC5(2)). Additionally, my analysis shows that modeled SOC stocks are also sensitive to the tillage effect on decomposition (Till_Eff) and the effect of clay on C transfer efficiency (PS1S3(2)) from active to passive pool.

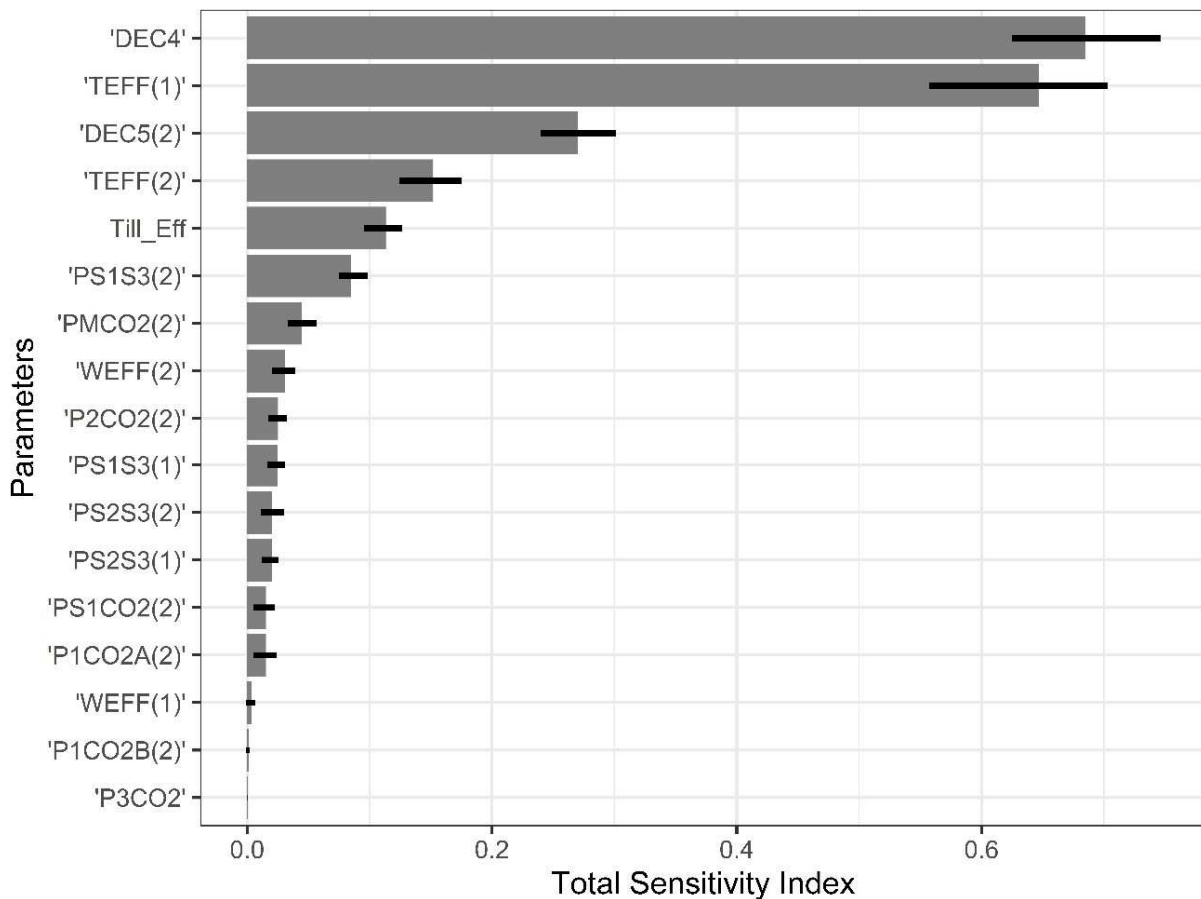


Figure 4.3. Ranked DayCent parameters based on the total sensitivity indices with 95% bootstrap confidence interval using 100 replicates.

4.4.2. Posterior Estimates of Model Parameters

The SIR method produced marginal posteriors with smaller ranges and higher densities than the priors (Figure 4.4), indicating that the measurement dataset was informative for the Bayesian calibration. Some of the parameters (e.g. TEFF(1), DEC5(2)) show a considerable reduction in uncertainty over the priors, while others shows moderate to low levels of change in the probability density of likely values from the prior distributions (e.g. PMCO2(2)).

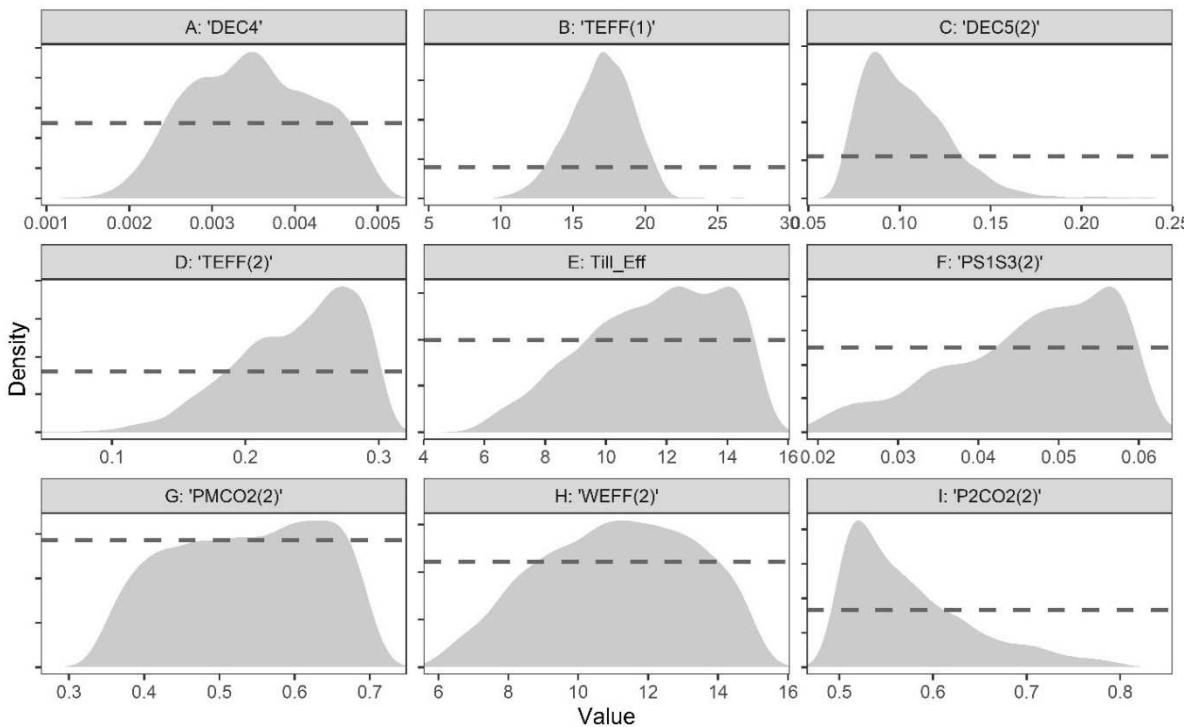


Figure 4.4. Marginal posterior density (light grey area) and uniform priors (dark grey dashed line) for DayCent parameters. The parameters are ordered according to the total sensitivity indices from highest to lowest (A-I)

The 95% posterior intervals of optimum decay rates for the slow and passive pools vary between 0.07 to 0.16 and 0.0022 to 0.0048, respectively, implying a turnover time between 6 to 14 and 200 to 500 years for the two pools. In DayCent, the optimum decay rate assumes that the temperature and the moisture are not the limiting factors for decomposition. Incorporating climatic conditions generally reduced decomposition rates due to less than optimal moisture and

temperature conditions at some point during the annual cycle, leading to longer realized turnover times for carbon in these pools.

The parameter associated with the temperature effect on decomposition, $TEFF(1)$, varies between 12 to 21 degree C and peaked around 17 degrees C, suggesting that decomposition is most sensitive to temperature changes within this range. In DayCent, the tillage parameter increases decomposition for a short period of time after soil disturbance, and the analysis found the rate is elevated by a factor of 7 to 15 times with the median value of 12. Moreover, at the site level, uncertainty is dominated by the random effects associated with the site (σ_{site}^2), followed by site by year ($\sigma_{site \times year}^2$) and unexplained error variance (σ^2) (see Table 4.4). The random effects and unexplained error variance are hyperparameters that address spatio-temporal variability in the measurements and processes that are not perfectly predicted by the model, and allow for a full estimation of model error (See Supplementary Material for more information). The uncertainty in the random effects and residual error also includes uncertainties associated with additional parameters in other sub-models (e.g., plant production), and may also be related to unknown legacy effects of past history that is not captured in model initialization, as well as limitations in the mechanistic understanding represented in the model structure.

The correlation coefficients between parameters (Figure 4.5), suggesting a few of the parameters are highly correlated. Moderate to high correlations occur among the decomposition parameters (e.g. $DEC5(2)$ and $Till_Eff$, $DEC5(2)$ and $TEFF(1)$). The correlation plot (Figure 4.5) also suggests that there is very low correlation among parameters associated with transfer efficiency of carbon ($P2CO2(2)$, $PMCO2(2)$, and $PS1S3(2)$), and between parameters associated with carbon transfer efficiency and decomposition ($DEC5(2)$, $Till_Eff$, $TEFF(1)$, $TEFF(2)$, $WEFF(2)$ and $DEC4$). Parameters with moderate to high correlations tend to complement each

other through the multiplicative equations that are used to estimate decomposition rates, which also suggests that the SOC dataset is highly informative as a whole for decomposition parameters, but not informative enough to separate the effect of these parameters individually.

Table 4.4. Summary of posterior distributions for DayCent model parameters and standard deviation for the random effects including the maximum a posteriori (MAP) estimates with the highest posterior density (i.e., best fit parameters in the joint probability distribution). Note: the MAP is the parameter value that should be used in a deterministic application of the model based on this analysis.

Parameters	Posterior quantiles					MAP
	2.5%	25%	median	75%	97.5%	
'DEC4'	0.0022	0.0029	0.0035	0.0041	0.0048	0.0043
'TEFF(1)'	12.4657	15.5257	17.0523	18.4347	20.6576	16.7717
'DEC5(2)'	0.0714	0.0856	0.0991	0.1178	0.1592	0.0866
'TEFF(2)'	0.1411	0.2077	0.2458	0.2740	0.2973	0.2781
Till_Eff	6.9301	9.9467	11.8702	13.5081	14.8353	14.0079
'PS1S3(2)'	0.0233	0.0394	0.0481	0.0551	0.0596	0.0525
'PMCO2(2)'	0.3604	0.4556	0.5383	0.6199	0.6882	0.5039
'WEFF(2)'	6.9183	9.4635	11.2136	12.8777	14.7449	9.4755
'P2CO2(2)'	0.5020	0.5221	0.5577	0.6128	0.7482	0.5162
σ_{site}^2	0.0418	0.0541	0.0619	0.0727	0.1171	0.0672
$\sigma_{year \times site}^2$	0.0054	0.0060	0.0063	0.0066	0.0074	0.0058
σ^2	0.0047	0.0048	0.0049	0.0049	0.0050	0.0047

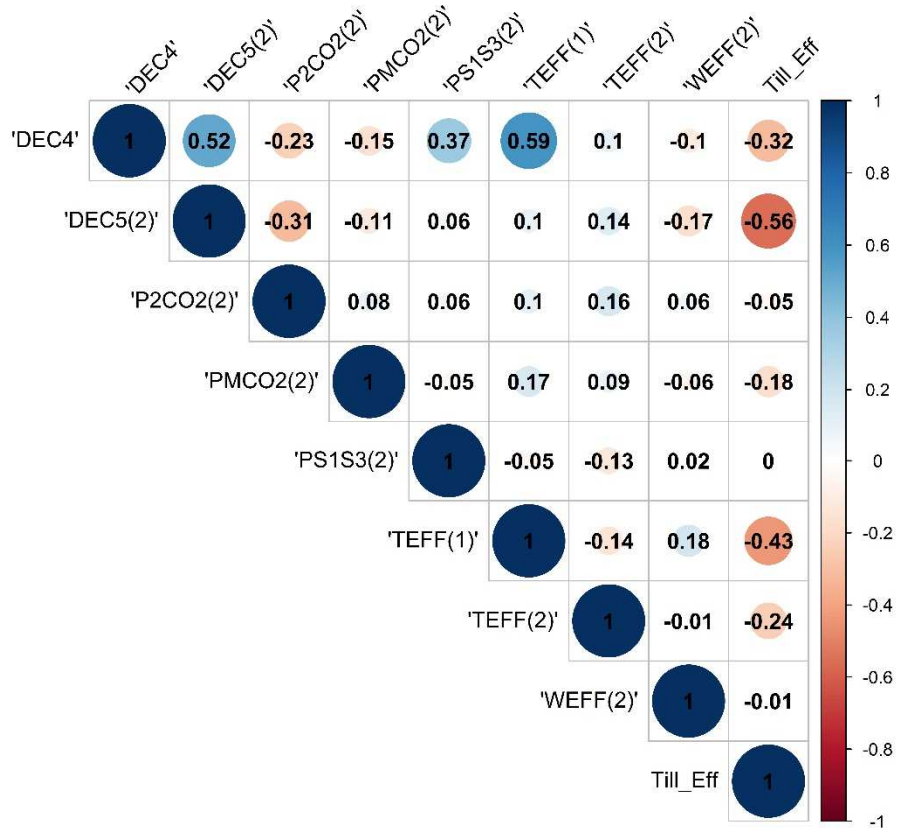


Figure 4.5. Correlation coefficients among DayCent model parameters in the posterior

4.4.3. Posterior Model Predictions

The Bayesian calibration significantly reduced the posterior prediction intervals of SOC stocks based on a comparison of model results for the prior and posterior distributions of model parameters (Figure 4.6). On average, the Bayesian calibration reduced the prediction uncertainty in the calibration datasets by a factor of 6.6, with a coefficient of variation of 211% (193% to 234%) based on the prior parameter distribution and 32% (30% to 34%) with the posterior parameter distribution. Similarly, the coefficient of variation for the posterior was 33% (30% to 39%) for the external evaluation dataset. I also compared the distribution of root-mean-squared errors (RMSE) and model bias between application of DayCent model with the prior and the posterior parameter distribution. The SIR method produced posterior parameter distributions with lower RMSE values and less bias than the prior parameter distributions (Figure 4.7).

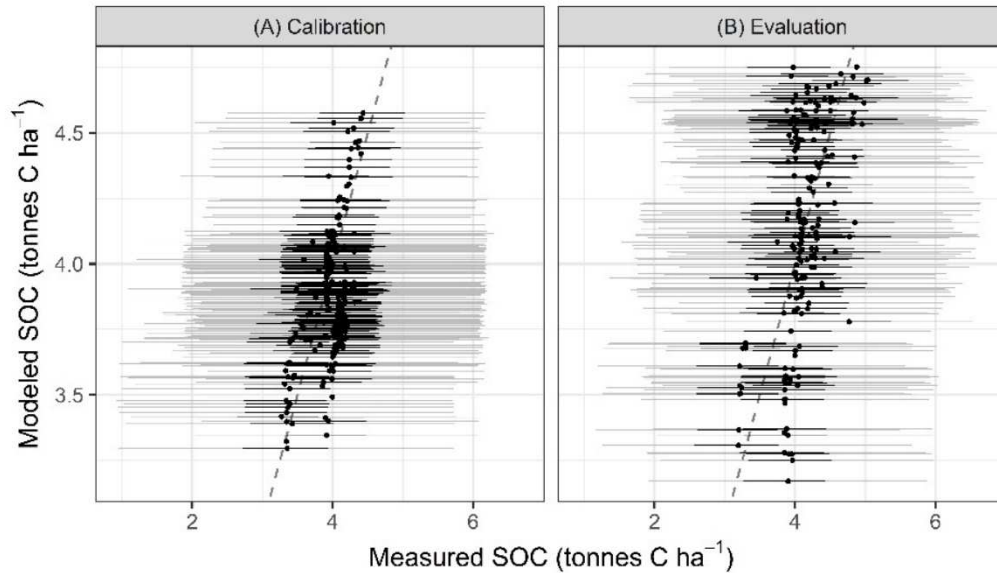


Figure 4.6. Prior prediction intervals (grey line) and posterior prediction intervals (black lines) for SOC stocks (natural log transformed) in the (A) calibration and (B) Evaluation dataset along with the posterior median SOC stocks (black dots) and the dashed (dark grey) line represent the 1:1 relationship. Prediction intervals were defined by the 95% central prediction intervals.

The predicted median value and the measured SOC values were distributed around the 1:1 line for the simulations based on the posterior parameter distribution (i.e., there would be complete agreement between the measured and modeled values if the relationship was plotted exactly on the 1:1 line in the graph), and shows a positive association between the measured and the modeled SOC stocks for both the calibration and evaluation dataset (Figure 4.8). The calibrated model was able to predict the measured low and high SOC values for both calibration and evaluation datasets. The relationship is stronger with the calibration dataset, which is expected given that the model is parameterized to these locations.

The estimates of SOC stock difference and associated prediction intervals for the calibrated DayCent model suggest that there is more agreement between measured and modeled SOC differences for organic amendment treatments in both calibration and evaluation datasets, compared to other practices (Figure 4.9). Tillage conversion from a full-till to no-till system and

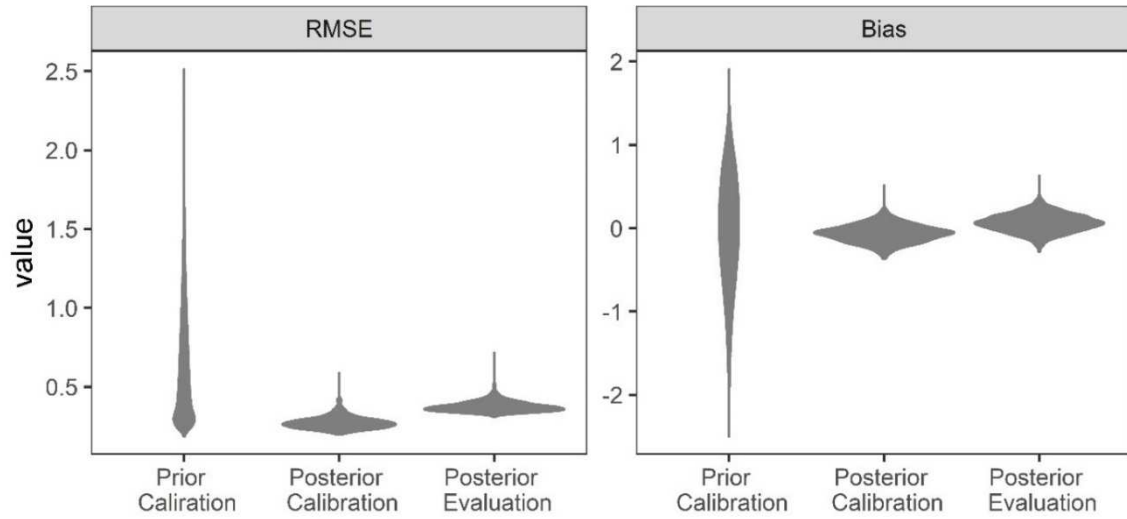


Figure 4.7. Violin plots of the distribution of root-mean square error (RMSE) and model bias for the prior and posterior model parameters in the calibration dataset and the posterior model parameters in the evaluation dataset. The units are in tonnes C ha⁻¹ (natural log transformed).

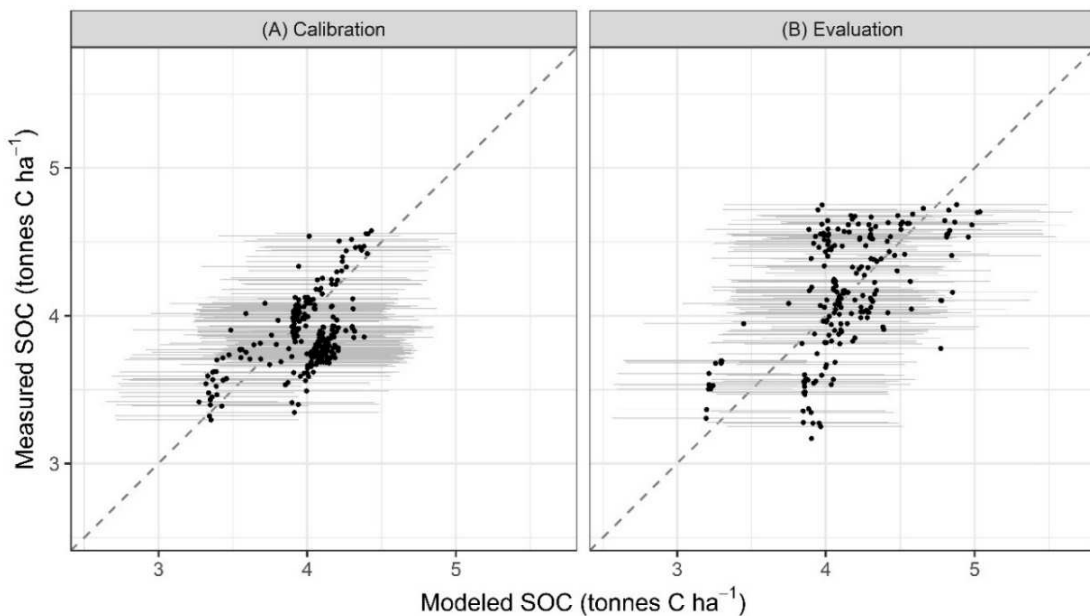


Figure 4.8. Comparison of natural-log transformed SOC stock estimates between measurements and the posterior medians (black dots) with 95% central posterior prediction interval (light grey lines) associated with the (A) calibration and (B) evaluation datasets. The diagonal dashed line represents the 1:1 line where the model predictions match the measurements.

addition of synthetic N fertilizer shows less agreement between the measured and the modeled SOC differences (Figure 4.9). Additionally, I estimated the time series of SOC stock differences after treatment change from three long-term experimental sites within the calibration sites

(Figure 4.10). The SOC stock differences between the additions of 35 metric tonnes $\text{ha}^{-1} \text{ year}^{-1}$ of fresh farmyard manure (FYM) vs. no application of FYM at the Broadbalk site were captured by the model reasonably well based on the comparison to field data (Figure 4.10A). The resulting plots show a rapid increase in SOC stocks with the FYM treatment in both modeled and measured patterns. Furthermore, posterior prediction intervals for the SOC differences includes “zero” only for the first five years (Figure 4.10A) after the start of the experiment—suggesting high confidence in the model estimates of C sequestration with FYM treatment after 5 years. The model result also suggests that the FYM treatment reaches a new equilibrium around 1950 when the slope approaches zero. SOC differences increase again in the late 1980s, which is due to higher carbon input through residue return (e-RA, 2013). Similar results were also found between treatments with or without organic amendments for both calibration and evaluation sites.

Modeled and measured trends in SOC stock differences were similar for tillage conversion from full-till to no-till at Wooster site (Figure 4.10B) and the posterior prediction intervals include “zero” until 23 years after tillage conversion. Modeled and measured patterns had similar timelines and rates of increase for other sites with tillage treatments.

The nitrogen fertilizer experiment at Pendleton site also had a similar trend with good agreement between the experimental and modeled data (Figure 4.9C). However, the mean stock differences increased slightly only after about 10 years of the experiment, and the posterior prediction intervals for the SOC stock differences always included “zero” even after 60 years of management changes. Similar trends were found for most of the experimental sites with N fertilizer treatments.

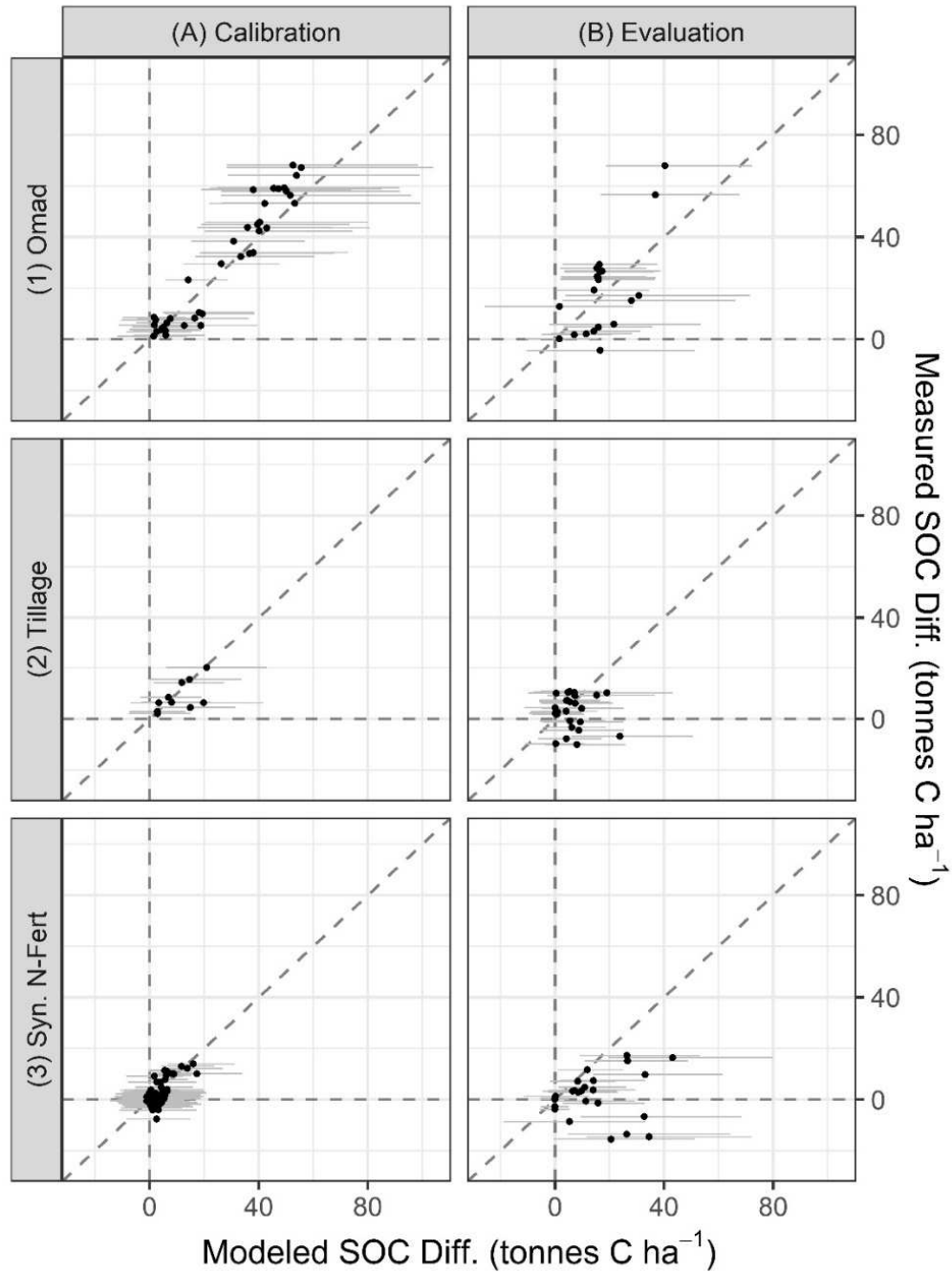


Figure 4.9. Comparison of treatment differences between the measurements and the posterior medians with 95% central posterior prediction intervals. The vertical plots include for (A) Calibration and (B) Evaluation datasets, and the horizontal plots are the management treatments, including (1) Omad: SOC differences between addition of organic amendments vs no organic amendments, (2) Tillage: SOC differences between No-Till vs Full-Till, and (3) Syn. N-Fert: SOC differences between recommended Synthetic N-fertilization rates vs Zero N controls in the rows. The diagonal dashed line represents the 1:1 line where the model predictions match the measurements.

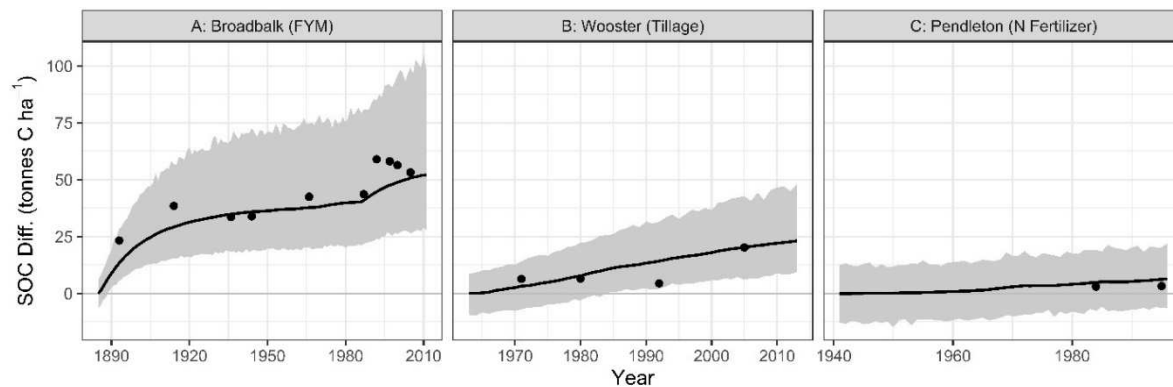


Figure 4.10. Posterior prediction (black line), 95% central posterior prediction intervals (light grey band) (uncertainty in model parameters and hyper-parameters), and measured SOC stock differences (black dots) between treatment and control for (A) Broadbalk: farmyard manure (FYM) treatment vs. no farmyard manure plots, (B) Wooster: no-till vs. full-till plots, and (C) Pendleton: 180 kg N/ha vs. control with no N fertilization.

4.5. Discussion

This study demonstrates the use of the SIR method in a Bayesian model analysis framework to calibrate the DayCent ecosystem model with repeated SOC measurements from several long-term study sites and constrained by the theoretical limits of the parameters based on prior knowledge of the model dynamics (Figure 4.1). In the calibration process, I treated the model parameters as population-level variables, meaning the resulting posterior distributions of model parameters are appropriate for application to the entire population of soils represented by these experiments. Uncertainty may arise due to unresolved processes in the model application that lead to biases in results if parameterization from one site is used to simulate ecosystem dynamics at another site (Luo and Schuur, 2020). It is possible to develop parameters that are region or site-specific to reduce uncertainty for a sub-population when applying the DayCent model. However, this may also restrict the model application to specific sites or region in the domain of interest, depending on the availability of data for parameterization. It was beyond the scope of the study to develop site or region-specific parameters, but this could be accomplished with the

methods provided in this study. The posterior distribution of model parameters from this study are suitable for application from individual sites to continental scales in which the experimental sites are located. The resulting prediction intervals fully quantify the uncertainty in model error based on posterior distribution of parameters and hyperparameters, and there is no evidence of bias from the independent evaluation of model results (Figure 4.7-4.9). Furthermore, the framework can incorporate uncertainty in model input data (Figure 4.1C), such as weather patterns and edaphic characteristics although I did not address model input uncertainty in my analysis.

Among the 17 parameters tested, decay rate of slow and passive pools, temperature effect on decay rate, soil disturbance through tillage, and soil texture have most impact on soil organic carbon dynamics in agricultural soils based on the DayCent model structure (Figure 4.3). Nécipalová et al., (2015) also found that decay rates for the slow and passive pools and temperature effect on decomposition were highly sensitive to modeled SOC at an agricultural experimental site in the Central United States near Ames, Iowa. The sensitivity analysis indicates that agricultural management has a large influence on variation in SOC dynamics based on turnover of the slow and passive pools of soil organic matter, as well as temperature, texture and cultivation modifiers to the decay rates. Temperature sensitivity of soil organic matter is highly debated (Conant et al., 2011b; Davidson and Janssens, 2006; Frey et al., 2013), and appears related to recalcitrance of soil organic matter (Bosatta and Ågren, 1999; Conant et al., 2008; Craine et al., 2010; Fierer et al., 2005) and response of the microbial community to changes in temperature (Liang et al., 2017; Schimel, 2013; Wieder et al., 2013). Texture, particularly, clays are well-known to impact soil organic matter dynamics through mineral associated organic matter that reduces decomposition rates, and this form of protection is thought to be more

important in ecosystems dominated by herbaceous vegetation, such as grasslands and annual croplands, compared to forest with woody dominated vegetation (Cotrufo et al., 2019).

I focused on predictions of C sequestration for three potential mitigation practices, addition of farmyard manure (FYM), reducing tillage disturbance, and mineral fertilization. My estimates of field-level prediction uncertainty for SOC stocks and stock differences are relatively high, but FYM provided a higher level of C sequestration and accuracy on a consistent basis based on the model predictions, and manure amendments are known to increase SOC stocks (Jiang et al., 2018; Maillard and Angers, 2014). The model also predicts increases in C stocks with adoption of no-till management in the top 30 cm of the profile. This effect does vary with deeper depths and depends on the climate and soil conditions (Ogle et al., 2019; Sun et al., 2020). Further model development in DayCent will be needed to represent the impact of tillage on SOC dynamics in the subsoil. In contrast, the results are not conclusive that the addition of synthetic N fertilizer will sequester C in soils due to high prediction uncertainty relative to expected increase in SOC. Furthermore, previous research has suggested that mineral fertilization is less effective as a C sequestration practice than other management options and may even lead to losses of SOC (Jiang et al., 2018; Khan et al., 2007; Salinas-Garcia et al., 1997).

Even though my analysis reduces the RMSE and bias in the model and is also able to reduce prediction uncertainty (Figure 4.7 and 4.8), my estimates of site-level prediction uncertainty are still relatively high, and are driven by measurement error, in addition to model structural and parameter uncertainty. There are several ways to improve upon the analysis in this study and reduce uncertainty in the future.

The first option for improving the framework is to refine data collection from experimental sites to reduce measurement uncertainty. The underlying premise of a Bayesian analysis implies that when the data are highly informative and have low measurement error, the data dominate the posterior and the choice of priors diminishes (Box, 1973). However, spatial variation in soils can lead to a large amount of sampling error in measurement data (Conant et al., 2011a). Consequently, an effective sampling protocol is needed to minimize sampling error and to detect changes in SOC (Conant and Paustian, 2002). While the experimental sites that were used in this study provide a wealth of information for SOC research and model development, the measured SOC stocks were often estimated with only a few replicates or even with a single measurement, which contributed to higher measurement error. More sites and greater replication could better constrain uncertainty in model predictions, along with a site-level sampling design that addresses local variation in SOC stocks (Conant et al., 2003; Conant and Paustian, 2002; Spencer et al., 2011; VandenBygaart, 2006). Also, the majority of long-term experiments used in my analysis were from North America and Europe. While some of these studies have been ongoing for more than 100 years, the limited spatial coverage of these data imposes limitations on the usage of the model or at least contributes to additional uncertainty when applied in other regions. The establishment of soil monitoring network sites coupled with effective sampling protocols at a national or even global scale would further improve model calibration and prediction (Smith et al., 2012). Achieving high-quality SOC datasets will address a critical gap for model calibration and evaluation, which in turn will likely improve ecosystem models and lead model applications that provide a stronger basis for policy development and management in support of soil health, food security and climate change programs.

The second option involves improving model structure in DayCent with new scientific findings or alternative models could be used in the Bayesian model analysis framework to reduce uncertainty. Traditional ecosystem-scale biogeochemical models simulate SOC with conceptually defined pools that are not measurable, which limits options for model calibration. Recent advancement in understanding of plant litter decomposition, SOM formation, and the chemical composition of stable soil C have led to development of models with more of a focus on microbial dynamics in recent years that may improve the process-based representation of soil organic matter dynamics. These models incorporate the flow of C through food webs and highlight the role of soil biota (Stockmann et al., 2013), and some of the models are embracing new paradigms emerging from the latest research on soil organic matter dynamics, such as the MEMS (Cotrufo et al., 2013; Robertson et al., 2019) and Millennial models (Abramoff et al., 2018). These models are also focus on SOC pools that are measurable that may improve model structure and reduce structural uncertainty.

In addition to refining model structure, the process of model initialization of SOC pools could be refined with less reliance on a model simulation to steady-state conditions. Studies have suggested that initialization to equilibrium conditions does not provide high precision in the initial levels of SOC for process-based model simulations (Carvalhais et al., 2008; Wutzler and Reichstein, 2007). Developing better ways to initialize the state variables will likely improve model performance and reduce uncertainty. One example of an alternative method is a Bayesian Accept-Reject method implemented by (Yeluripati et al., 2009).

The third option involves expanding the Bayesian calibration of model parameters to a broader set of processes beyond just the soil organic matter sub-model. One of the major challenges in calibrating the DayCent ecosystem model is the dependencies among the hundreds

of parameters and model outputs. By only considering the model output of SOC stocks, I were able to focus on a limited number of model parameters directly affecting the turnover times of SOC pools and C transfer efficiencies. Furthermore, a variance-based GSA was performed to identify influential parameters and set non-influential parameters to the most likely value—making the model more parsimonious. This approach does not capture the indirect effects of other parameters and processes that are represented in DayCent, such as those represented in the water and plant production sub-models. Uncertainty associated with additional model parameters in other sub-models is quantified in the hyperparameters in the form of random effects associated with site and year within site (see Supplemental Materials) and residual error. This study provides an initial set of results, however, that can be expanded in the future to incorporate other components of the model with adequate measurement datasets that address multiple outputs from the model.

Lastly, it is important to recognize that site-level prediction uncertainty is large when considering all sources of uncertainty. However, these uncertainties may be reduced when predicting SOC dynamics over larger spatial and temporal extents, for example at a regional or national scale. Specifically, the random errors associated with site level prediction may cancel out as they are aggregated across sites to larger scales, and reduce uncertainty in the estimates of SOC stocks and stock differences. For example, (Ogle et al., 2010) have shown that the uncertainty associated with SOC stock changes from 1990 to 2000 in US croplands were greater than 600% at the site scale but less than 25% during the same time period at the national scale.

4.6. Conclusions

In this study, I demonstrated a framework to reduce uncertainty in model predictions of SOC stocks and stock differences from a process-based model by combining a global sensitivity

analysis to determine influential model parameters, Bayesian calibration using the SIR method to generate approximate posterior probability distributions for DayCent model parameters, and application of a Monte Carlo approach to propagate uncertainty through the model and derive posterior prediction intervals for SOC estimates (Figure 4.1). Uncertainty in model predictions was reduced by a factor of 6.6 with application of this framework to the DayCent Ecosystem Model, relative to application of the model with the prior parameter distributions.

This framework is designed to incorporate new information in the future to further reduce uncertainty. Some key ways to reduce these uncertainties include a) improving the measurement datasets by increasing the spatial and temporal coverage of data as well as the data collection methods, b) refining the model structure or applying other models that are more accurate estimators of SOC dynamics, and c) expanding the Bayesian calibration to include other processes and associated parameters that indirectly affect soil organic matter dynamics. Finally, even though the proposed framework is applied to SOC dynamic model within DayCent, it is model independent and can be applied to any process-based model. The Bayesian model analysis framework can be used to quantify and reduce uncertainty in process-based model predictions of SOC dynamics, and ultimately support policy programs that intend to reduce GHG emissions through C sequestration in agricultural soils.

CHAPTER 5: CONCLUSION AND FUTURE DIRECTION

The research presented in this dissertation provides an insightful example of process-based model development by incorporating theoretical understanding of the mechanisms affecting model outcomes. Using Bayesian model calibration, selection, and prediction, this dissertation provides tools for ecosystem ecologists to identify an accurate model to predict the outcome and quantify uncertainty in model predictions from management practices in agroecosystems. All model developments were integrated into the DayCent ecosystem model. With the DayCent model structure including many dependencies among different mechanisms, its account for GHG mitigation potential of management practices in a robust manner.

The Bayesian model analysis framework was successful in reducing uncertainty on model parameters and estimating SOC stocks and stocks differences (Chapter 2). Analysis of model output on C sequestration potential suggests that the application of FYM provide the highest level of sequestration, the adoption of no-till also provides some C sequestration but requires a long time before there is a significant positive impact, however, the addition of synthetic N fertilizer was not a viable option. The Bayesian model selection provided refinement on the model structure for NH_3 volatilization (Chapter 3). The updated model was able to predict the cumulative loss and mitigation potential when urea is applied with or without a urease inhibitor. With additional model development to incorporate CRNFs and NIs (Chapter 3), DayCent was able to predict the distribution of reduction factors for N_2O emissions when EENFs were adopted as alternative fertilizers.

Adopting the “4R” nutrient stewardship principle of using the right source at the right rate, right timing, and the right place is recommended to identify BMPs for N fertilizers.

However, many experimental sites have only evaluated one or two factors at a time, limiting the generality of results that may be impacted by multiple factors to fully understand the environmental benefits. With the model development in my dissertation research, one can test additional “what if” scenarios to identify potential BMPs using the DayCent ecosystem model. These model improvements provide a stronger basis for models to support policy and management decisions associated with GHG mitigation through C sequestration and reductions in N₂O emissions from agricultural soils.

In agricultural soil, gain or loss of SOC and N₂O emissions are major sources of GHGs, along with the exception of methane from paddy rice cultivation. In addition, a significant amount (>60%) of applied N can be lost through NH₃ volatilization. In my dissertation, I only evaluated some of the submodels in DayCent and their associated parameters that directly affect the model output of interest. Known processes such as crop production, N uptake by plants, NO₃⁻ leaching and other trace gases also interact with the level of C sequestration and N₂O emissions. Improving other parts of the model using the Bayesian model platform would likely further enhance the ability of DayCent to more accurately predict mitigation potentials. The framework is also suitable for expanding to new model features when additional data become available.

Additionally, ecosystem models are attempting to represent high levels of complexity, leading to many challenges and are always being questioned. As a result, model improvement is an ongoing process as our understanding of ecosystems is expanded. Additionally, many competing models similar to DayCent are also operational, for example, DNDC, EPIC, and RothC. New models have also emerged, for example, MEMS and Millennial incorporating the flow of C through food webs and highlight the role of soil biota. These are examples of ecosystem models with different hypotheses and model structures for understanding the same

ecosystem processes. Ensembles can be based on Bayesian model averaging (BMA), which combines predictive distributions from several models, and may reduce uncertainty in predictions by addressing a broader representation of mechanistic understanding. This can be tested by extending the platform in future research.

Lastly, the method developed in my dissertation using Bayesian model calibration, selection, and prediction is model-independent, works for both linear and non-linear models as well as complex process-based ecosystem models. This platform allowed for further development of the DayCent ecosystem model, providing accurate results with quantification of uncertainty that can be used to support management and policy decisions associated with agricultural soils related to climate change and greenhouse gas mitigation.

REFERENCES

- Abalos, D., Jeffery, S., Sanz-Cobena, A., Guardia, G., Vallejo, A., 2014. Meta-analysis of the effect of urease and nitrification inhibitors on crop productivity and nitrogen use efficiency. *Agric. Ecosyst. Environ.* 189, 136–144. <https://doi.org/10.1016/j.agee.2014.03.036>
- Abramoff, R., Xu, X., Hartman, M., O'Brien, S., Feng, W., Davidson, E., Finzi, A., Moorhead, D., Schimel, J., Torn, M., Mayes, M.A., 2018. The Millennial model: in search of measurable pools and transformations for modeling soil carbon in the new century. *Biogeochemistry* 137, 51–71. <https://doi.org/10.1007/s10533-017-0409-7>
- Ahrens, B., Reichstein, M., Borke, W., Muhr, J., Trumbore, S.E., Wutzler, T., 2014. Bayesian calibration of a soil organic carbon model using $\delta^{14}\text{C}$ measurements of soil organic carbon and heterotrophic respiration as joint constraints. *Biogeosciences* 11, 2147–2168. <https://doi.org/10.5194/bg-11-2147-2014>
- Akiyama, H., Yan, X., Yagi, K., 2010. Evaluation of effectiveness of enhanced-efficiency fertilizers as mitigation options for N_2O and NO emissions from agricultural soils: Meta-analysis. *Glob. Chang. Biol.* 16, 1837–1846. <https://doi.org/10.1111/j.1365-2486.2009.02031.x>
- Álvaro-Fuentes, J., Arrúe, J.L., Bielsa, A., Cantero-Martínez, C., Plaza-Bonilla, D., Paustian, K., 2017. Simulating climate change and land use effects on soil nitrous oxide emissions in Mediterranean conditions using the Daycent model. *Agric. Ecosyst. Environ.* <https://doi.org/10.1016/j.agee.2016.07.017>
- ApSimon, H.M., Kruse, M., Bell, J.N.B., 1987. Ammonia emissions and their role in acid deposition. *Atmos. Environ.* 21, 1939–1946. [https://doi.org/10.1016/0004-6981\(87\)90154-5](https://doi.org/10.1016/0004-6981(87)90154-5)

- Asman, W.A.H., Sutton, M.A., Schjørring, J.K., 1998. Ammonia: Emission, atmospheric transport and deposition. *New Phytol.* 139, 27–48. <https://doi.org/10.1046/j.1469-8137.1998.00180.x>
- Azeem, B., Kushaari, K., Man, Z.B., Basit, A., Thanh, T.H., 2014. Review on materials & methods to produce controlled release coated urea fertilizer. *J. Control. Release.* <https://doi.org/10.1016/j.jconrel.2014.02.020>
- Barré, P., Eglin, T., Christensen, B.T., Ciais, P., Houot, S., Kätterer, T., Van Oort, F., Peylin, P., Poulton, P.R., Romanenkov, V., Chenu, C., 2010. Quantifying and isolating stable soil organic carbon using long-term bare fallow experiments. *Biogeosciences* 7, 3839–3850. <https://doi.org/10.5194/bg-7-3839-2010>
- Battese, G.E., Harter, R.M., Fuller, W.A., 1988. An error-components model for prediction of county crop areas using survey and satellite data. *J. Am. Stat. Assoc.* <https://doi.org/10.1080/01621459.1988.10478561>
- Bayes, M., Price, M., 1763. *JSTOR: Philosophical Transactions (1683-1775)*, Vol. 53 (1763), pp. 370-418. *Philos. Trans.*
- Bertrand, I., Viaud, V., Daufresne, T., Pellerin, S., Recous, S., 2019. Stoichiometry constraints challenge the potential of agroecological practices for the soil C storage. A review. *Agron. Sustain. Dev.* <https://doi.org/10.1007/s13593-019-0599-6>
- Black, A.S., Sherlock, R.R., Smith, N.P., 1987. Effect of timing of simulated rainfall on ammonia volatilization from urea, applied to soil of varying moisture content. *J. Soil Sci.* 38, 679–687. <https://doi.org/10.1111/j.1365-2389.1987.tb02165.x>
- Bosatta, E., Ågren, G.I., 1999. Soil organic matter quality interpreted thermodynamically. *Soil Biol. Biochem.* 31, 1889–1891. [https://doi.org/10.1016/S0038-0717\(99\)00105-4](https://doi.org/10.1016/S0038-0717(99)00105-4)

- Bouwman, A.F., Boumans, L.J.M., Batjes, N.H., 2002a. Estimation of global NH₃ volatilization loss from synthetic fertilizers and animal manure applied to arable lands and grasslands. *Global Biogeochem. Cycles* 16. <https://doi.org/10.1029/2000gb001389>
- Bouwman, A.F., Boumans, L.J.M., Batjes, N.H., 2002b. Modeling global annual N₂O and NO emissions from fertilized fields. *Global Biogeochem. Cycles* 16, 28-1-28-9. <https://doi.org/10.1029/2001gb001812>
- Bouwmeester, R.J.B., Vlek, P.L.G., Stumpe, J.M., 1985. Effect of Environmental Factors on Ammonia Volatilization from a Urea-Fertilized Soil. *Soil Sci. Soc. Am. J.* 49, 376–381. <https://doi.org/10.2136/sssaj1985.03615995004900020021x>
- Box, G.E.P., 1973. Bayesian inference in statistical analysis. Addison-Wesley Pub. Co., Reading, MA.
- Braswell, B.H., Sacks, W.J., Linder, E., Schimel, D.S., 2005. Estimating diurnal to annual ecosystem parameters by synthesis of a carbon flux model with eddy covariance net ecosystem exchange observations. *Glob. Chang. Biol.* 11, 335–355. <https://doi.org/10.1111/j.1365-2486.2005.00897.x>
- Bronson, K.F., Mosier, A.R., Bishnoi, S.R., 1992. Nitrous oxide emissions in irrigated corn as affected by nitrification inhibitors. *Soil Sci. Soc. Am. J.* 56, 161–165. <https://doi.org/10.2136/sssaj1992.03615995005600010025x>
- Bruinsma, J., 2003. *World Agriculture: Towards 2015/2030: an FAO Perspective*. Earthscan, New York, NY.
- Bruulsema, T., Lemunyon, J., Herz, B., 2009. Know your fertilizer rights. *Crop. Soils*.
- Butterbach-Bahl, K., Baggs, E.M., Dannenmann, M., Kiese, R., Zechmeister-Boltenstern, S., 2013. Nitrous oxide emissions from soils: How well do we understand the processes and

- their controls? *Philos. Trans. R. Soc. B Biol. Sci.* <https://doi.org/10.1098/rstb.2013.0122>
- Cabrera, M.L., Kissel, D.E., Bock, B.R., 1991. Urea hydrolysis in soil: Effects of urea concentration and soil pH. *Soil Biol. Biochem.* 23, 1121–1124.
[https://doi.org/10.1016/0038-0717\(91\)90023-D](https://doi.org/10.1016/0038-0717(91)90023-D)
- Carnell, R., 2009. lhs: Latin Hypercube Samples. R Package Version 0.5.
- Carvalhois, N., Reichstein, M., Seixas, J., Colltaz, G.J., Pereira, J.S., Berbigier, P., Carrara, A., Granier, A., Montagnani, L., Papale, D., Rambal, S., Sanz, M.J., Valentini, R., 2008. Implications of the carbon cycle steady state assumption for biogeochemical modeling performance and inverse parameter retrieval. *Global Biogeochem. Cycles* 22.
<https://doi.org/10.1029/2007GB003033>
- Changsheng Li, Frolking, S., Frolking, T.A., 1992. A model of nitrous oxide evolution from soil driven by rainfall events: 1. Model structure and sensitivity. *J. Geophys. Res.* 97, 9759–9776. <https://doi.org/10.1029/92jd00509>
- Cheng, K., Ogle, S.M., Parton, W.J., Pan, G., 2014. Simulating greenhouse gas mitigation potentials for Chinese Croplands using the DAYCENT ecosystem model. *Glob. Chang. Biol.* 20, 948–962. <https://doi.org/10.1111/gcb.12368>
- Chou, T.C., Talalay, P., 1977. A simple generalized equation for the analysis of multiple inhibitions of Michaelis-Menten kinetic systems. *J. Biol. Chem.* 252, 6438–6442.
- Clapp, C.E., Allmaras, R.R., Layese, M.F., Linden, D.R., Dowdy, R.H., 2000. Soil organic carbon and ¹³C abundance as related to tillage, crop residue, and nitrogen fertilization under continuous corn management in Minnesota. *Soil Tillage Res.* 55, 127–142.
[https://doi.org/10.1016/S0167-1987\(00\)00110-0](https://doi.org/10.1016/S0167-1987(00)00110-0)
- Clifford, D., Pagendam, D., Baldock, J., Cressie, N., Farquharson, R., Farrell, M., Macdonald,

- L., Murray, L., 2014. Rethinking soil carbon modelling: A stochastic approach to quantify uncertainties. *Environmetrics* 25, 265–278. <https://doi.org/10.1002/env.2271>
- Conant, R.T., Ogle, S.M., Paul, E.A., Paustian, K., 2011a. Measuring and monitoring soil organic carbon stocks in agricultural lands for climate mitigation. *Front. Ecol. Environ.* 9, 169–173. <https://doi.org/10.1890/090153>
- Conant, R.T., Paustian, K., 2002. Spatial variability of soil organic carbon in grasslands: Implications for detecting change at different scales. *Environ. Pollut.* 116, S127–S135. [https://doi.org/10.1016/S0269-7491\(01\)00265-2](https://doi.org/10.1016/S0269-7491(01)00265-2)
- Conant, R.T., Ryan, M.G., Ågren, G.I., Birge, H.E., Davidson, E.A., Eliasson, P.E., Evans, S.E., Frey, S.D., Giardina, C.P., Hopkins, F.M., Hyvönen, R., Kirschbaum, M.U.F., Lavallee, J.M., Leifeld, J., Parton, W.J., Megan Steinweg, J., Wallenstein, M.D., Martin Wetterstedt, J.Å., Bradford, M.A., 2011b. Temperature and soil organic matter decomposition rates - synthesis of current knowledge and a way forward. *Glob. Chang. Biol.* 17, 3392–3404. <https://doi.org/10.1111/j.1365-2486.2011.02496.x>
- Conant, R.T., Smith, G.R., Paustian, K., 2003. Spatial Variability of Soil Carbon in Forested and Cultivated Sites. *J. Environ. Qual.* 32, 278–286. <https://doi.org/10.2134/jeq2003.2780>
- Conant, R.T., Steinweg, J.M., Haddix, M.L., Paul, E.A., Plante, A.F., Six, J., 2008. Experimental warming shows that decomposition temperature sensitivity increases with soil organic matter recalcitrance. *Ecology* 89, 2384–2391. <https://doi.org/10.1890/08-0137.1>
- Cotrufo, M.F., Ranalli, M.G., Haddix, M.L., Six, J., Lugato, E., 2019. Soil carbon storage informed by particulate and mineral-associated organic matter. *Nat. Geosci.* 12, 989–994. <https://doi.org/10.1038/s41561-019-0484-6>
- Cotrufo, M.F., Wallenstein, M.D., Boot, C.M., Deneff, K., Paul, E., 2013. The Microbial

- Efficiency-Matrix Stabilization (MEMS) framework integrates plant litter decomposition with soil organic matter stabilization: Do labile plant inputs form stable soil organic matter? *Glob. Chang. Biol.* 19, 988–995. <https://doi.org/10.1111/gcb.12113>
- Craine, J.M., Fierer, N., McLauchlan, K.K., 2010. Widespread coupling between the rate and temperature sensitivity of organic matter decay. *Nat. Geosci.* 3, 854–857. <https://doi.org/10.1038/ngeo1009>
- Cressie, N., Calder, C.A., Clark, J.S., Ver Hoef, J.M., Wikle, C.K., 2009. Accounting for uncertainty in ecological analysis: The strengths and limitations of hierarchical statistical modeling. *Ecol. Appl.* 19, 553–570. <https://doi.org/10.1890/07-0744.1>
- Crutzen, P.J., Ehhalt, D.H., 1977. Effects of nitrogen fertilizers and combustion on the stratospheric ozone layer. *Ambio*.
- Cuddington, K., Fortin, M.J., Gerber, L.R., Hastings, A., Liebhold, A., O’connor, M., Ray, C., 2013. Process-based models are required to manage ecological systems in a changing world. *Ecosphere* 4. <https://doi.org/10.1890/ES12-00178.1>
- Curtin, D., Campbell, C.A., Messer, D., 1996. Prediction of Titratable Acidity and Soil Sensitivity to pH Change. *J. Environ. Qual.* 25, 1280–1284. <https://doi.org/10.2134/jeq1996.00472425002500060016x>
- Dalal, R.C., 1975. Urease activity in some Trinidad soils. *Soil Biol. Biochem.* 7, 5–8. [https://doi.org/10.1016/0038-0717\(75\)90022-X](https://doi.org/10.1016/0038-0717(75)90022-X)
- Davidson, E.A., Janssens, I.A., 2006. Temperature sensitivity of soil carbon decomposition and feedbacks to climate change. *Nature* 440, 165–173. <https://doi.org/10.1038/nature04514>
- Dawar, K., Zaman, M., Rowarth, J.S., Blennerhassett, J., Turnbull, M.H., 2011a. Urease inhibitor reduces N losses and improves plant-bioavailability of urea applied in fine particle and

- granular forms under field conditions. *Agric. Ecosyst. Environ.* 144, 41–50.
<https://doi.org/10.1016/j.agee.2011.08.007>
- Dawar, K., Zaman, M., Rowarth, J.S., Blennerhassett, J., Turnbull, M.H., 2011b. Urea hydrolysis and lateral and vertical movement in the soil: Effects of urease inhibitor and irrigation. *Biol. Fertil. Soils* 47, 139–146. <https://doi.org/10.1007/s00374-010-0515-3>
- Dechow, R., Franko, U., Kätterer, T., Kolbe, H., 2019. Evaluation of the RothC model as a prognostic tool for the prediction of SOC trends in response to management practices on arable land. *Geoderma* 337, 463–478. <https://doi.org/10.1016/j.geoderma.2018.10.001>
- Del Grosso, S.J., Halvorson, A.D., Parton, W.J., 2008. Testing DAYCENT Model Simulations of Corn Yields and Nitrous Oxide Emissions in Irrigated Tillage Systems in Colorado. *J. Environ. Qual.* 37, 1383–1389. <https://doi.org/10.2134/jeq2007.0292>
- Del Grosso, S.J., Mosier, A.R., Parton, W.J., Ojima, D.S., 2005. DAYCENT model analysis of past and contemporary soil N₂O and net greenhouse gas flux for major crops in the USA, in: *Soil and Tillage Research*. <https://doi.org/10.1016/j.still.2005.02.007>
- Del Grosso, S.J., Ogle, S.M., Parton, W.J., Breidt, F.J., 2010. Estimating uncertainty in N₂O emissions from U.S. cropland soils. *Global Biogeochem. Cycles*.
<https://doi.org/10.1029/2009gb003544>
- Del Grosso, S.J., Ogle, S.M., Nevison, C., Gurung R.B., Parton, W.J., Wagner-Riddle, C., Smith, W., Grant, B., Tenuta, M., Marx, E., Spencer, S., William, S., *in prep*. Previously unaccounted N₂O jeopardizes Paris Agreement.
- Del Grosso, S.J., Ojima, D.S., Parton, W.J., Stehfest, E., Heistemann, M., DeAngelo, B., Rose, S., 2009. Global scale DAYCENT model analysis of greenhouse gas emissions and mitigation strategies for cropped soils. *Glob. Planet. Change*.

<https://doi.org/10.1016/j.gloplacha.2008.12.006>

Del Grosso, S.J., Parton, W.J., Adler, P.R., Davis, S.C., Keough, C., Marx, E., 2012. Daycent model simulations for estimating soil carbon dynamics and greenhouse gas fluxes from agricultural production systems. *Manag. Agric. Greenh. Gases* 241–250.

<https://doi.org/10.1016/B978-0-12-386897-8.00014-0>

Del Grosso, S.J., Parton, W.J., Mosier, A.R., Hartman, M.D., Brenner, J., Ojima, D.S., Schimel, D.S., 2001. Simulated interaction of carbon dynamics and nitrogen trace gas fluxes using the DAYCENT model, in: Shaffer, M.J., Ma, L., Hansen, S. (Eds.), *Modeling Carbon and Nitrogen Dynamics for Soil Management*. CRC Publisher, Boca Raton, pp. 303–332.

Del Grosso, S.J., Parton, W.J., Mosier, A.R., Ojima, D.S., Kulmala, A.E., Phongpan, S., 2000. General model for N₂O and N₂ gas emissions from soils due to denitrification. *Global Biogeochem. Cycles*. <https://doi.org/10.1029/1999GB001225>

Del Grosso, S.J., White, J.W., Wilson, G., Vandenberg, B., Karlen, D.L., Follett, R.F., Johnson, J.M.F., Franzluebbers, A.J., Archer, D.W., Gollany, H.T., Liebig, M.A., Ascough, J., Reyes-Fox, M., Pellack, L., Starr, J., Barbour, N., Polumsky, R.W., Gutwein, M., James, D., 2013. Introducing the GRACEnet/REAP Data Contribution, Discovery, and Retrieval System. *J. Environ. Qual.* 42, 1274–1280. <https://doi.org/10.2134/jeq2013.03.0097>

Di, H.J., Cameron, K.C., 2004. Effects of temperature and application rate of a nitrification inhibitor, dicyandiamide (DCD), on nitrification rate and microbial biomass in a grazed pasture soil. *Aust. J. Soil Res.* <https://doi.org/10.1071/SR04050>

Di, H.J., Cameron, K.C., Podolyan, A., Robinson, A., 2014. Effect of soil moisture status and a nitrification inhibitor, dicyandiamide, on ammonia oxidizer and denitrifier growth and nitrous oxide emissions in a grassland soil. *Soil Biol. Biochem.*

<https://doi.org/10.1016/j.soilbio.2014.02.011>

Dolan, M.S., Clapp, C.E., Allmaras, R.R., Baker, J.M., Molina, J.A.E., 2006. Soil organic carbon and nitrogen in a Minnesota soil as related to tillage, residue and nitrogen management. *Soil Tillage Res.* 89, 221–231. <https://doi.org/10.1016/j.still.2005.07.015>

Du, C.W., Zhou, J.M., Shaviv, A., 2006. Release characteristics of nutrients from polymer-coated compound controlled release fertilizers. *J. Polym. Environ.*
<https://doi.org/10.1007/s10924-006-0025-4>

Dusenbury, M.P., Engel, R.E., Miller, P.R., Lemke, R.L., Wallander, R., 2008. Nitrous Oxide Emissions from a Northern Great Plains Soil as Influenced by Nitrogen Management and Cropping Systems. *J. Environ. Qual.* 37, 542–550. <https://doi.org/10.2134/jeq2006.0395>

Eagle, A.J., Olander, L.P., Locklier, K.L., Heffernan, J.B., Bernhardt, E.S., 2017. Fertilizer Management and Environmental Factors Drive N₂O and NO₃ Losses in Corn: A Meta-Analysis. *Soil Sci. Soc. Am. J.* <https://doi.org/10.2136/sssaj2016.09.0281>

Engel, R., Jones, C., Romero, C., Wallander, R., 2017. Late-Fall, Winter and Spring Broadcast Applications of Urea to No-Till Winter Wheat I. Ammonia Loss and Mitigation by NBPT. *Soil Sci. Soc. Am. J.* 81, 322–330. <https://doi.org/10.2136/sssaj2016.10.0332>

Engel, R., Jones, C., Wallander, R., 2011. Ammonia Volatilization from Urea and Mitigation by NBPT following Surface Application to Cold Soils. *Soil Sci. Soc. Am. J.* 75, 2348–2357. <https://doi.org/10.2136/sssaj2011.0229>

EPA, 2019. Inventory of U.S. Greenhouse Gas Emissions and Sinks: 1990-2017.

Erismann, J.W., Bleeker, A., Galloway, J., Sutton, M.S., 2007. Reduced nitrogen in ecology and the environment. *Environ. Pollut.* 150, 140–149.
<https://doi.org/10.1016/j.envpol.2007.06.033>

- Falloon, P.D., Smith, P., 2000. Modelling refractory soil organic matter. *Biol. Fertil. Soils*.
<https://doi.org/10.1007/s003740050019>
- Fierer, N., Craine, J.M., Mclauchlan, K., Schimel, J.P., 2005. Litter quality and the temperature sensitivity of decomposition. *Ecology* 86, 320–326. <https://doi.org/10.1890/04-1254>
- Firestone M.K., and Davidson, E.A., 1989. Microbial basis of NO and N₂O production and consumption in soil. Exchange of trace gases between terrestrial ecosystems and the atmosphere, In: M.O. Andrea and D.S. Schimel, Editors, *Exchange of Trace Gases between Terrestrial Ecosystems and the Atmosphere*,.
- Fitton, N., Datta, A., Smith, K., Williams, J.R., Hastings, A., Kuhnert, M., Topp, C.F.E., Smith, P., 2014. Assessing the sensitivity of modelled estimates of N₂O emissions and yield to input uncertainty at a UK cropland experimental site using the DailyDayCent model. *Nutr. Cycl. Agroecosystems*. <https://doi.org/10.1007/s10705-014-9622-0>
- Frank, A.B., Tanaka, D.L., Hofmann, L., Follett, R.F., 1995. Soil carbon and nitrogen of Northern Great Plains grasslands as influenced by long-term grazing. *J. Range Manag.* 48, 470–474. <https://doi.org/10.2307/4002255>
- Freney, J.R., Simpson, J.R., Denmead, O.T., 1983. Volatilization of ammonia, in: Freney, J.R., Simpson, J.R. (Eds.), *Gaseous Loss of Nitrogen from Plant-Soil Systems*. Martin Nijhoff/Dr. W. Junk, The Hague, pp. 1–32. https://doi.org/10.1007/978-94-017-1662-8_1
- Frey, S.D., Lee, J., Melillo, J.M., Six, J., 2013. The temperature response of soil microbial efficiency and its feedback to climate. *Nat. Clim. Chang.* 3, 395–398.
<https://doi.org/10.1038/nclimate1796>
- Galloway, J.N., Aber, J.D., Erisman, J.A.N.W., Sybil, P., Howarth, R.W., Cowling, E.B., Cosby, B.J., 2003. N_Cascade_BioScience. *Bioscience* 53, 341–356. <https://doi.org/10.1641/0006->

3568(2003)053[0341:tnc]2.0.co;2

Galloway, J.N., Cowling, E.B., 2002. Reactive nitrogen and the world: 200 Years of change.

Ambio 31, 64–71. <https://doi.org/10.1579/0044-7447-31.2.64>

Galloway, J.N., Townsend, A.R., Erisman, J.W., Bekunda, M., Cai, Z., Freney, J.R., Martinelli,

L.A., Seitzinger, S.P., Sutton, M.A., 2008. Transformation of the nitrogen cycle: Recent trends, questions, and potential solutions. *Science* (80-.). 320, 889–892.

<https://doi.org/10.1126/science.1136674>

Gelman, A., 2014. Bayesian data analysis , Third edit. ed, BDA3., YBP Print DDA. CRC Press,

Boca Raton.

Gelman, A., 1993. Iterative and non-iterative simulation algorithms. *Comput. Sci. Stat.* 433–433.

<https://doi.org/10.1.1.63.7666>

Gelman, A., Goodrich, B., Gabry, J., Vehtari, A., 2019. R-squared for Bayesian Regression

Models. *Am. Stat.* <https://doi.org/10.1080/00031305.2018.1549100>

Giltrap, D.L., Singh, J., Sagar, S., Zaman, M., 2010. A preliminary study to model the effects of

a nitrification inhibitor on nitrous oxide emissions from urine-amended pasture. *Agric.*

Ecosyst. Environ. <https://doi.org/10.1016/j.agee.2009.08.007>

Givens, G.H., Zeh, J.E., Raftery, A.E., 1995. Assessment of the Bering-Chukchi-Beaufort Seas

stock of bowhead whales using the BALEEN II model in a Bayesian synthesis framework.

Forty-fifth Rep. *Int. Whal. Comm.* 45, 345–364.

Gurung, R.B., Ogle, S.M., Breidt, F.J., Williams, S.A., Parton, W.J., 2020. Bayesian calibration

of the DayCent ecosystem model to simulate soil organic carbon dynamics and reduce model uncertainty. *Geoderma* 376, 114529.

<https://doi.org/https://doi.org/10.1016/j.geoderma.2020.114529>

- Gurung, R.B., Ogle, S.M., Breidt, F.J., Williams, S.A., Zhang, Y., Del Grosso, S.J., Parton, W.J., Paustian, K., *in review*. Modeling Ammonia Volatilization from Urea Application to Agricultural Soils in the DayCent Model
- Halvorson, A.D., Del Grosso, S.J., Stewart, C.E., 2016. Manure and Inorganic Nitrogen Affect Trace Gas Emissions under Semi-Arid Irrigated Corn. *J. Environ. Qual.* 45, 906–914. <https://doi.org/10.2134/jeq2015.08.0426>
- Halvorson, A.D., Snyder, C.S., Blaylock, A.D., Del Grosso, S.J., 2014. Enhanced-efficiency nitrogen fertilizers: Potential role in nitrous oxide emission mitigation. *Agron. J.* 106, 715–722. <https://doi.org/10.2134/agronj2013.0081>
- Han, Z., Walter, M.T., Drinkwater, L.E., 2017. N₂O emissions from grain cropping systems: a meta-analysis of the impacts of fertilizer-based and ecologically-based nutrient management strategies. *Nutr. Cycl. Agroecosystems*. <https://doi.org/10.1007/s10705-017-9836-z>
- Hararuk, O., Xia, J., Luo, Y., 2014. Evaluation and improvement of a global land model against soil carbon data using a Bayesian Markov chain Monte Carlo method. *J. Geophys. Res. Biogeosciences* 119, 403–417. <https://doi.org/10.1002/2013JG002535>
- Hastings, W.K., 1970. Monte carlo sampling methods using Markov chains and their applications. *Biometrika* 57, 97–109. <https://doi.org/10.1093/biomet/57.1.97>
- Hoeting, J.A., 2009. The importance of accounting for spatial and temporal correlation in analyses of ecological data. *Ecol. Appl.* 19, 574–577. <https://doi.org/10.1890/08-0836.1>
- Holcomb, J.C., Sullivan, D.M., Horneck, D.A., Clough, G.H., 2011. Effect of Irrigation Rate on Ammonia Volatilization. *Soil Sci. Soc. Am. J.* 75, 2341–2347. <https://doi.org/10.2136/sssaj2010.0446>
- Homma, T., Saltelli, A., 1996. Importance measures in global sensitivity analysis of nonlinear

- models. *Reliab. Eng. Syst. Saf.* [https://doi.org/10.1016/0951-8320\(96\)00002-6](https://doi.org/10.1016/0951-8320(96)00002-6)
- Huntzinger, D.N., Schwalm, C.R., Wei, Y., Cook, R.B., Michalak, A.M., Schaefer, K., Jacobson, A.R., Arain, M.A., Ciais, P., Fisher, J.B., Hayes, D.J., Huang, M., Huang, S., Ito, A., Jain, A.K., Lei, H., Lu, C., Maignan, F., Mao, J., Parazoo, N., Peng, C., Peng, S., Poulter, B., Zhu, Q., 2015. NACP MsTMIP: Global 0.5-deg Terrestrial Biosphere Model Outputs (version 1) in Standard Format. Data set. Available on-line [<http://daac.ornl.gov>] from Oak Ridge National Laboratory Distributed Active Archive Center, Oak Ridge, Tennessee, USA. <https://doi.org/10.3334/ORNLDAAC/1225>
- Hurt, G.C., Armstrong, R.A., 1996. A pelagic ecosystem model calibrated with BATS data. *Deep. Res. Part II Top. Stud. Oceanogr.* 43, 653–683. [https://doi.org/10.1016/0967-0645\(96\)00007-0](https://doi.org/10.1016/0967-0645(96)00007-0)
- Ingram, L.J., Stahl, P.D., Schuman, G.E., Buyer, J.S., Vance, G.F., Ganjegunte, G.K., Welker, J.M., Derner, J.D., 2008. Grazing Impacts on Soil Carbon and Microbial Communities in a Mixed-Grass Ecosystem. *Soil Sci. Soc. Am. J.* 72, 939–948. <https://doi.org/10.2136/sssaj2007.0038>
- Iooss, B., Da Veiga, S., Janon, A., Pujol, G., Broto, B., Boumhaout, K., Delage, T., Amri, R. El, Fruth, J., Gilquin, L., Guillaume, J., Gratiot, L. Le, Lemaitre, P., Marrel, A., Meynaoui, A., Nelson, B.L., Monari, F., Oomen, R., Rakovec, O., Ramos, B., Roustant, O., Song, E., Staum, J., Sueur, R., Touati, T., Weber, F., 2020. sensitivity: Global Sensitivity Analysis of Model Outputs.
- IPCC, 2013. Working Group I Contribution to the IPCC Fifth Assessment Report, Climate Change 2013: The Physical Science Basis. *Ipcc.*
- Izaurrealde, R.C., Williams, J.R., McGill, W.B., Rosenberg, N.J., Jakas, M.C.Q., 2006.

- Simulating soil C dynamics with EPIC: Model description and testing against long-term data. *Ecol. Modell.* 192, 362–384. <https://doi.org/10.1016/j.ecolmodel.2005.07.010>
- Jansen, M.J.W., 1999. Analysis of variance designs for model output. *Comput. Phys. Commun.* 117, 35–43. [https://doi.org/10.1016/S0010-4655\(98\)00154-4](https://doi.org/10.1016/S0010-4655(98)00154-4)
- Jantalia, C.P., Halvorson, A.D., Follett, R.F., Alves, B.J.R., Polidoro, J.C., Urquiaga, S., 2012. Nitrogen source effects on ammonia volatilization as measured with semi-static chambers. *Agron. J.* 104, 1595–1603. <https://doi.org/10.2134/agronj2012.0210>
- Jeffreys, H., 1961. *Theory of probability* (3rd ed.) oxford university press, Mr0187257.
- Jenkinson, D.S., 1990. The turnover of organic carbon and nitrogen in soil. *Philos. Trans. - R. Soc. London, B* 329, 361–368. <https://doi.org/10.1098/rstb.1990.0177>
- Jenkinson, D.S., Rayner, J.H., 1977. The turnover of soil organic matter in some of the rothamsted classical experiments. *Soil Sci.* 123, 298–305. <https://doi.org/10.1097/00010694-197705000-00005>
- Jensen, L.S., Mueller, T., Nielsen, N.E., Hansen, S., Crocker, G.J., Grace, P.R., Klír, J., Körschens, M., Poulton, P.R., 1997. Simulating trends in soil organic carbon in long-term experiments using the soil-plant-atmosphere model DAISY. *Geoderma* 81, 5–28. [https://doi.org/10.1016/S0016-7061\(97\)88181-5](https://doi.org/10.1016/S0016-7061(97)88181-5)
- Jiang, G., Zhang, W., Xu, M., Kuzyakov, Y., Zhang, X., Wang, J., Di, J., Murphy, D. V., 2018. Manure and Mineral Fertilizer Effects on Crop Yield and Soil Carbon Sequestration: A Meta-Analysis and Modeling Across China. *Global Biogeochem. Cycles* 32, 1659–1672. <https://doi.org/10.1029/2018GB005960>
- Kass, R.E., Raftery, A.E., 1995. Bayes factors. *J. Am. Stat. Assoc.* 90, 773–795. <https://doi.org/10.1080/01621459.1995.10476572>

- Kelliher, F.M., Clough, T.J., Clark, H., Rys, G., Sedcole, J.R., 2008. The temperature dependence of dicyandiamide (DCD) degradation in soils: A data synthesis. *Soil Biol. Biochem.* <https://doi.org/10.1016/j.soilbio.2008.03.013>
- Kelliher, F.M., van Koten, C., Kear, M.J., Sprosen, M.S., Ledgard, S.F., de Klein, C.A.M., Letica, S.A., Luo, J., Rys, G., 2014. Effect of temperature on dicyandiamide (DCD) longevity in pastoral soils under field conditions. *Agric. Ecosyst. Environ.* <https://doi.org/10.1016/j.agee.2014.01.026>
- Kennedy, M.C., O'Hagan, A., 2001. Bayesian calibration of computer models. *J. R. Stat. Soc. Ser. B Stat. Methodol.* 63, 425–464. <https://doi.org/10.1111/1467-9868.00294>
- Khalil, K., Mary, B., Renault, P., 2004. Nitrous oxide production by nitrification and denitrification in soil aggregates as affected by O₂ concentration. *Soil Biol. Biochem.* <https://doi.org/10.1016/j.soilbio.2004.01.004>
- Khan, S.A., Mulvaney, R.L., Ellsworth, T.R., Boast, C.W., 2007. The Myth of Nitrogen Fertilization for Soil Carbon Sequestration. *J. Environ. Qual.* 36, 1821–1832. <https://doi.org/10.2134/jeq2007.0099>
- Kissel, D.E., Cabrera, M.L., Ferguson, R.B., 1988. Reactions of Ammonia and Urea Hydrolysis Products with Soil. *Soil Sci. Soc. Am. J.* 52, 1793–1796. <https://doi.org/10.2136/sssaj1988.03615995005200060050x>
- Kitur, B.K., Olson, K.R., Ebelhar, S.A., Bullock, D.G., 1994. Tillage effects on growth and yields of corn on Grantsburg soil. *J. Soil Water Conserv.* 49, 266–271.
- Knaus, J., 2010. snowfall: Easier cluster computing (based on snow). R Packag. version.
- Kool, D.M., Dolfing, J., Wrage, N., Van Groenigen, J.W., 2011. Nitrifier denitrification as a distinct and significant source of nitrous oxide from soil. *Soil Biol. Biochem.*

<https://doi.org/10.1016/j.soilbio.2010.09.030>

Kumar, V., Wagenet, R.J., 1984. Urease activity and kinetics of urea transformation in soils. *Soil Sci.* 137, 263–269. <https://doi.org/10.1097/00010694-198404000-00008>

Lal, R., 2004a. Soil carbon sequestration to mitigate climate change. *Geoderma* 123, 1–22. <https://doi.org/10.1016/j.geoderma.2004.01.032>

Lal, R., 2004b. Soil carbon sequestration impacts on global climate change and food security. *Science (80-.)*. 304, 1623–1627. <https://doi.org/10.1126/science.1097396>

Lal, R., Follett, R.F., Stewart, B.A., Kimble, J.M., 2007. Soil carbon sequestration to mitigate climate change and advance food security. *Soil Sci.* 172, 943–956. <https://doi.org/10.1097/ss.0b013e31815cc498>

Levins, R., 1966. The strategy of model building in population biology. *Am. Nat.* <https://doi.org/10.2307/27836590>

Li, Y., Shah, S.H.H., Wang, J., 2020. Modelling of nitrification inhibitor and its effects on emissions of nitrous oxide (N₂O) in the UK. *Sci. Total Environ.* <https://doi.org/10.1016/j.scitotenv.2019.136156>

Liang, C., Schimel, J.P., Jastrow, J.D., 2017. The importance of anabolism in microbial control over soil carbon storage. *Nat. Microbiol.* <https://doi.org/10.1038/nmicrobiol.2017.105>

Liebig, M.A., Gross, J.R., Kronberg, S.L., Hanson, J.D., Frank, A.B., Phillips, R.L., 2006. Soil response to long-term grazing in the northern Great Plains of North America. *Agric. Ecosyst. Environ.* 115, 270–276. <https://doi.org/10.1016/j.agee.2005.12.015>

Ludwig, B., Schulz, E., Rethemeyer, J., Merbach, I., Flessa, H., 2007. Predictive modelling of C dynamics in the long-term fertilization experiment at Bad Lauchstädt with the Rothamsted Carbon Model. *Eur. J. Soil Sci.* 58, 1155–1163. <https://doi.org/10.1111/j.1365->

2389.2007.00907.x

- Luo, Y., Ahlström, A., Allison, S.D., Batjes, N.H., Brovkin, V., Carvalhais, N., Chappell, A., Ciais, P., Davidson, E.A., Finzi, A., Georgiou, K., Guenet, B., Hararuk, O., Harden, J.W., He, Y., Hopkins, F., Jiang, L., Koven, C., Jackson, R.B., Jones, C.D., Lara, M.J., Liang, J., McGuire, A.D., Parton, W., Peng, C., Randerson, J.T., Salazar, A., Sierra, C.A., Smith, M.J., Tian, H., Todd-Brown, K.E.O., Torn, M., Van Groenigen, K.J., Wang, Y.P., West, T.O., Wei, Y., Wieder, W.R., Xia, J., Xu, Xia, Xu, Xiaofeng, Zhou, T., 2016. Toward more realistic projections of soil carbon dynamics by Earth system models. *Global Biogeochem. Cycles* 30, 40–56. <https://doi.org/10.1002/2015GB005239>
- Luo, Y., Schuur, E.A.G., 2020. Model parameterization to represent processes at unresolved scales and changing properties of evolving systems. *Glob. Chang. Biol.* <https://doi.org/10.1111/gcb.14939>
- Machado, S., 2011. Soil organic carbon dynamics in the pendleton long-term experiments: Implications for biofuel production in pacific Northwest. *Agron. J.* 103, 253–260. <https://doi.org/10.2134/agronj2010.0205s>
- Machado, S., Petrie, S., Rhinhardt, K., Ramig, R.E., 2008. Tillage effects on water use and grain yield of winter wheat and green pea in rotation. *Agron. J.* 100, 154–162. <https://doi.org/10.2134/agronj2006.0218>
- Maillard, É., Angers, D.A., 2014. Animal manure application and soil organic carbon stocks: A meta-analysis. *Glob. Chang. Biol.* 20, 666–679. <https://doi.org/10.1111/gcb.12438>
- Maillard, É., McConkey, B.G., St. Luce, M., Angers, D.A., Fan, J., 2018. Crop rotation, tillage system, and precipitation regime effects on soil carbon stocks over 1 to 30 years in Saskatchewan, Canada. *Soil Tillage Res.* 177, 97–104.

<https://doi.org/10.1016/j.still.2017.12.001>

Manley, J.T., Schuman, G.E., Reeder, J.D., Hart, R.H., 1995. Rangeland soil carbon and nitrogen responses to grazing. *J. Soil Water Conserv.* 50, 294–298.

McAllister, M.K., Ianelli, J.N., 1997. Bayesian stock assessment using catch-age data and the sampling - Importance resampling algorithm. *Can. J. Fish. Aquat. Sci.* 54, 284–300.

<https://doi.org/10.1139/cjfas-54-2-284>

McAllister, M.K., Pikitch, E.K., Punt, A.E., Hilborn, R., 1994. A Bayesian approach to stock assessment and harvest decisions using the sampling/importance resampling algorithm.

Can. J. Fish. Aquat. Sci. 51, 2673–2687. <https://doi.org/10.1139/f94-267>

McKay, M.D., Beckman, R.J., Conover, W.J., 1979. A Comparison of Three Methods for Selecting Values of Input Variables in the Analysis of Output from a Computer Code.

Technometrics 21, 239. <https://doi.org/10.2307/1268522>

Mesinger, F., DiMego, G., Kalnay, E., Mitchell, K., Shafran, P.C., Ebisuzaki, W., Jović, D., Woollen, J., Rogers, E., Berbery, E.H., Ek, M.B., Fan, Y., Grumbine, R., Higgins, W., Li, H., Lin, Y., Manikin, G., Parrish, D., Shi, W., 2006. North American regional reanalysis.

Bull. Am. Meteorol. Soc. 87, 343–360. <https://doi.org/10.1175/BAMS-87-3-343>

Metropolis, N., Rosenbluth, A.W., Rosenbluth, M.N., Teller, A.H., Teller, E., 1953. Equation of state calculations by fast computing machines. *J. Chem. Phys.* 21, 1087–1092.

<https://doi.org/10.1063/1.1699114>

Minasny, B., Malone, B.P., McBratney, A.B., Angers, D.A., Arrouays, D., Chambers, A., Chaplot, V., Chen, Z.S., Cheng, K., Das, B.S., Field, D.J., Gimona, A., Hedley, C.B., Hong, S.Y., Mandal, B., Marchant, B.P., Martin, M., McConkey, B.G., Mulder, V.L., O'Rourke, S., Richer-de-Forges, A.C., Odeh, I., Padarian, J., Paustian, K., Pan, G., Poggio, L., Savin,

- I., Stolbovoy, V., Stockmann, U., Sulaeman, Y., Tsui, C.C., Vågen, T.G., van Wesemael, B., Winowiecki, L., 2017. Soil carbon 4 per mille. *Geoderma* 292, 59–86.
<https://doi.org/10.1016/j.geoderma.2017.01.002>
- Misselbrook, T.H., Misselbrook, T.H., Sutton, M.A., Scholefield, D., 2005. A simple process-based model for estimating ammonia emissions from agricultural land after fertilizer applications. *Soil Use Manag.* 20, 365–372. <https://doi.org/10.1079/sum2004280>
- Molina, J.A.E., Crocker, G.J., Grace, P.R., Klír, J., Körschens, M., Poulton, P.R., Richter, D.D., 1997. Simulating trends in soil organic carbon in long-term experiments using the NCSOIL and NCSWAP models. *Geoderma* 81, 91–107. [https://doi.org/10.1016/S0016-7061\(97\)00083-9](https://doi.org/10.1016/S0016-7061(97)00083-9)
- Monreal, C.M., Janzen, H.H., 1993. Soil organic-carbon dynamics after 80 years of cropping a dark brown Chernozem. *Can. J. Soil Sci.* 73, 133–136. <https://doi.org/10.4141/cjss93-014>
- Morris, C.N., 1987. The Calculation of Posterior Distributions by Data Augmentation: Comment: Simulation in Hierarchical Models. *J. Am. Stat. Assoc.* 82, 542.
<https://doi.org/10.2307/2289459>
- Mosier, A., Kroeze, C., 2000. Potential impact on the global atmospheric N₂O budget of the increased nitrogen input required to meet future global food demands. *Chemosph. - Glob. Chang. Sci.* [https://doi.org/10.1016/S1465-9972\(00\)00039-8](https://doi.org/10.1016/S1465-9972(00)00039-8)
- Mosier, A.R., Duxbury, J.M., Freney, J.R., Heinemeyer, O., Minami, K., 1998. Assessing and mitigating N₂O emissions from agricultural soils. *Clim. Change.*
<https://doi.org/10.1023/A:1005386614431>
- Moyo, C.C., Kissel, D.E., Cabrera, M.L., 1989. Temperature effects on soil urease activity. *Soil Biol. Biochem.* 21, 935–938. [https://doi.org/10.1016/0038-0717\(89\)90083-7](https://doi.org/10.1016/0038-0717(89)90083-7)

- Murrell, T.S., Lafond, G.P., Vyn, T.J., 2009. Know Your Fertilizer Rights: Right Place. *Crop. Soils* 42, 4.
- Naz, M.Y., Sulaiman, S.A., 2016. Slow release coating remedy for nitrogen loss from conventional urea: A review. *J. Control. Release*.
<https://doi.org/10.1016/j.jconrel.2016.01.037>
- Necpálová, M., Anex, R.P., Fienen, M.N., Del Grosso, S.J., Castellano, M.J., Sawyer, J.E., Iqbal, J., Pantoja, J.L., Barker, D.W., 2015. Understanding the DayCent model: Calibration, sensitivity, and identifiability through inverse modeling. *Environ. Model. Softw.* 66, 110–130. <https://doi.org/10.1016/j.envsoft.2014.12.011>
- Ogle, S.M., Alsaker, C., Baldock, J., Bernoux, M., Breidt, F.J., McConkey, B., Regina, K., Vazquez-Amabile, G.G., 2019. Climate and Soil Characteristics Determine Where No-Till Management Can Store Carbon in Soils and Mitigate Greenhouse Gas Emissions. *Sci. Rep.* 9. <https://doi.org/10.1038/s41598-019-47861-7>
- Ogle, S.M., Breidt, F.J., Paustian, K., 2005. Agricultural management impacts on soil organic carbon storage under moist and dry climatic conditions of temperate and tropical regions. *Biogeochemistry* 72, 87–121. <https://doi.org/10.1007/s10533-004-0360-2>
- Ogle, S.M., Jay Breidt, F., Easter, M., Williams, S., Killian, K., Paustian, K., 2010. Scale and uncertainty in modeled soil organic carbon stock changes for US croplands using a process-based model. *Glob. Chang. Biol.* 16, 810–822. <https://doi.org/10.1111/j.1365-2486.2009.01951.x>
- Ogle, S.M., Paustian, K., 2005. Soil organic carbon as an indicator of environmental quality at the national scale: Inventory monitoring methods and policy relevance. *Can. J. Soil Sci.* 85, 531–540. <https://doi.org/10.4141/s04-087>

- Olson, K.R., Ebelhar, S.A., Lang, J.M., 2010. Cover crop effects on crop yields and soil organic carbon content. *Soil Sci.* 175, 89–98. <https://doi.org/10.1097/SS.0b013e3181cf7959>
- Owen, A.B., 1992. A Central-Limit-Theorem for Latin Hypercube Sampling. *J. R. Stat. Soc. Ser. B-Methodological* 54, 541–551.
- Pan, B., Lam, S.K., Mosier, A., Luo, Y., Chen, D., 2016. Ammonia volatilization from synthetic fertilizers and its mitigation strategies: A global synthesis. *Agric. Ecosyst. Environ.* 232, 283–289. <https://doi.org/10.1016/j.agee.2016.08.019>
- Parkin, T.B., Venterea, R.T., 2010. USDA-ARS GRACEnet project protocols, chapter 3. Chamber-based trace gas flux measurements. *Sampl. Protoc.* Beltsville, MD p 1–39.
- Parton, W.J., Hartman, M., Ojima, D., Schimel, D., 1998. DAYCENT and its land surface submodel: Description and testing. *Glob. Planet. Change* 19, 35–48. [https://doi.org/10.1016/S0921-8181\(98\)00040-X](https://doi.org/10.1016/S0921-8181(98)00040-X)
- Parton, W.J., Holland, E.A., Del Grosso, S.J., Hartman, M.D., Martin, R.E., Mosier, A.R., Ojima, D.S., Schimel, D.S., 2001. Generalized model for NO_x and N₂O emissions from soils. *J. Geophys. Res.* 106, 17403–17419. <https://doi.org/10.1029/2001JD900101>
- Parton, W.J., Morgan, J.A., Wang, G., Del Grosso, S., 2007. Projected ecosystem impact of the Prairie Heating and CO₂ Enrichment experiment. *New Phytol.* 174, 823–834. <https://doi.org/10.1111/j.1469-8137.2007.02052.x>
- Parton, W.J., Mosier, A.R., Ojima, D.S., Valentine, D.W., Schime, D.S., Weier, K., Kulmala, A.E., 1996. Generalized model for N₂ and N₂O production from nitrification and denitrification. *Global Biogeochem. Cycles.* <https://doi.org/10.1029/96GB01455>
- Parton, W.J., Rasmussen, P.E., 1994. Long-Term Effects of Crop Management in Wheat-Fallow: II. CENTURY Model Simulations. *Soil Sci. Soc. Am. J.* 58, 530–536.

<https://doi.org/10.2136/sssaj1994.03615995005800020040x>

Parton, W.J., Schimel, D.S., Cole, C. V., Ojima, D.S., 1987. Analysis of Factors Controlling Soil Organic Matter Levels in Great Plains Grasslands. *Soil Sci. Soc. Am. J.* 51, 1173–1179.

<https://doi.org/10.2136/sssaj1987.03615995005100050015x>

Paulson, K.N., Kurtz, L.T., 1970. Michaelis Constant of Soil Urease. *Soil Sci. Soc. Am. J.* 34, 70–72. <https://doi.org/10.2136/sssaj1970.03615995003400010021x>

Paustian, K., Andrén, O., Janzen, H.H., Lal, R., Smith, P., Tian, G., Tiessen, H., Van Noordwijk, M., Woomer, P.L., 1997. Agricultural soils as a sink to mitigate CO₂ emissions. *Soil Use Manag.* 13, 230–244. <https://doi.org/10.1111/j.1475-2743.1997.tb00594.x>

Paustian, K., Lehmann, J., Ogle, S., Reay, D., Robertson, G.P., Smith, P., 2016. Climate-smart soils. *Nature* 532, 49–57. <https://doi.org/10.1038/nature17174>

Paustian, K., Six, J., Elliott, E.T., Hunt, H.W., 2000. Management options for reducing CO₂ emissions from agricultural soils. *Biogeochemistry* 48, 147–163.

<https://doi.org/10.1023/A:1006271331703>

Pelster, D.E., Chantigny, M.H., Rochette, P., Bertrand, N., Angers, D.A., Zebarth, B.J., Goyer, C., 2019. Rates and intensity of freeze–thaw cycles affect nitrous oxide and carbon dioxide emissions from agricultural soils. *Can. J. Soil Sci.* 99, 472–484. <https://doi.org/10.1139/cjss-2019-0058>

Pettit, N.M., Smith, A.R.J., Freedman, R.B., Burns, R.G., 1976. Soil urease: Activity, stability and kinetic properties. *Soil Biol. Biochem.* 8, 479–484. [https://doi.org/10.1016/0038-0717\(76\)90089-4](https://doi.org/10.1016/0038-0717(76)90089-4)

Poulton, P., Johnston, J., Macdonald, A., White, R., Powlson, D., 2018. Major limitations to achieving “4 per 1000” increases in soil organic carbon stock in temperate regions:

- Evidence from long-term experiments at Rothamsted Research, United Kingdom. *Glob. Chang. Biol.* <https://doi.org/10.1111/gcb.14066>
- Powlson, D.S., Smith, P., Coleman, K., Smith, J.U., Glendining, M.J., Körschens, M., Franko, U., 1998. A European network of long-term sites for studies on soil organic matter. *Soil Tillage Res.* 47, 263–274. [https://doi.org/10.1016/S0167-1987\(98\)00115-9](https://doi.org/10.1016/S0167-1987(98)00115-9)
- Prasad, R., Power, J.F., 1995. Nitrification Inhibitors for Agriculture, Health, and the Environment, in: *Advances in Agronomy*. [https://doi.org/10.1016/S0065-2113\(08\)60901-3](https://doi.org/10.1016/S0065-2113(08)60901-3)
- Punt, A.E., Hilborn, R., 1997. Fisheries stock assessment and decision analysis: The Bayesian approach. *Rev. Fish Biol. Fish.* 7, 35–63. <https://doi.org/10.1023/A:1018419207494>
- R Development Core Team, 2018. A Language and Environment for Statistical Computing. *R Found. Stat. Comput.*
- Raftery, A.E., Givens, G.H., Zeh, J.E., 1995. Inference from a deterministic population dynamics model for bowhead whales. *J. Am. Stat. Assoc.* 90, 402–416. <https://doi.org/10.1080/01621459.1995.10476529>
- Rasmussen, P.E., Rohde, C.R., 1988. Long-term Tillage and Nitrogen Fertilization Effects on Organic Nitrogen and Carbon in a Semiarid Soil. *Soil Sci. Soc. Am. J.* <https://doi.org/10.2136/sssaj1988.03615995005200040041x>
- Ravishankara, A.R., Daniel, J.S., Portmann, R.W., 2009. Nitrous oxide (N₂O): The dominant ozone-depleting substance emitted in the 21st century. *Science* (80-.). 326, 123–125. <https://doi.org/10.1126/science.1176985>
- Reay, D.S., Davidson, E.A., Smith, K.A., Smith, P., Melillo, J.M., Dentener, F., Crutzen, P.J., 2012. Global agriculture and nitrous oxide emissions. *Nat. Clim. Chang.* 2, 410–416. <https://doi.org/10.1038/nclimate1458>

- Risk, N., Snider, D., Wagner-Riddle, C., 2013. Mechanisms leading to enhanced soil nitrous oxide fluxes induced by freeze-thaw cycles. *Can. J. Soil Sci.*
<https://doi.org/10.4141/CJSS2012-071>
- Robertson, A.D., Paustian, K., Ogle, S., Wallenstein, M.D., Lugato, E., Francesca Cotrufo, M., 2019. Unifying soil organic matter formation and persistence frameworks: The MEMS model. *Biogeosciences* 16, 1225–1248. <https://doi.org/10.5194/bg-16-1225-2019>
- Robertson, A.D., Zhang, Y., Sherrod, L.A., Rosenzweig, S.T., Ma, L., Ahuja, L., Schipanski, M.E., 2018. Climate Change Impacts on Yields and Soil Carbon in Row Crop Dryland Agriculture. *J. Environ. Qual.* 47, 684–694. <https://doi.org/10.2134/jeq2017.08.0309>
- Robertson, G.P., Paul, E.A., Harwood, R.R., 2000. Greenhouse gases in intensive agriculture: Contributions of individual gases to the radiative forcing of the atmosphere. *Science* (80-.).
<https://doi.org/10.1126/science.289.5486.1922>
- Rochette, P., Angers, D.A., Chantigny, M.H., Gasser, M.-O., MacDonald, J.D., Pelster, D.E., Bertrand, N., 2013a. Ammonia Volatilization and Nitrogen Retention: How Deep to Incorporate Urea? *J. Environ. Qual.* 42, 1635–1642.
<https://doi.org/10.2134/jeq2013.05.0192>
- Rochette, P., Angers, D.A., Chantigny, M.H., Gasser, M.O., MacDonald, J.D., Pelster, D.E., Bertrand, N., 2013b. NH₃ volatilization, soil NH₄⁺ concentration and soil pH following subsurface banding of urea at increasing rates. *Can. J. Soil Sci.* 93, 261–268.
<https://doi.org/10.4141/CJSS2012-095>
- Roelle, P.A., Aneja, V.P., 2002. Characterization of ammonia emissions from soils in the upper coastal plain, North Carolina. *Atmos. Environ.* 36, 1087–1097.
[https://doi.org/10.1016/S1352-2310\(01\)00355-7](https://doi.org/10.1016/S1352-2310(01)00355-7)

- Rubin, D.B., 1988. Using the SIR Algorithm to Simulate Posterior Distributions, in: Bernardo, J.M., Degroot, M.H., Lindley, D. V, Smith, A.F.M. (Eds.), Bayesian Statistics. Oxford University Press, Cambridge, Massachusetts, pp. 395–402.
- Rubin, D.B., 1987. The Calculation of Posterior Distributions by Data Augmentation: Comment: A Noniterative Sampling/Importance Resampling Alternative to the Data Augmentation Algorithm for Creating a Few Imputations When Fractions of Missing Information Are Modest: The SIR. *J. Am. Stat. Assoc.* 82, 543. <https://doi.org/10.2307/2289460>
- Sacks, W.J., Schimel, D.S., Monson, R.K., Braswell, B.H., 2006. Model-data synthesis of diurnal and seasonal CO₂ fluxes at Niwot Ridge, Colorado. *Glob. Chang. Biol.* 12, 240–259. <https://doi.org/10.1111/j.1365-2486.2005.01059.x>
- Sahrawat, K.L., 1984. Effects of temperature and moisture on urease activity in semi-arid tropical soils. *Plant Soil* 78, 401–408. <https://doi.org/10.1007/BF02450373>
- Sakurai, G., Jomura, M., Yonemura, S., Iizumi, T., Shirato, Y., Yokozawa, M., 2012. Inversely estimating temperature sensitivity of soil carbon decomposition by assimilating a turnover model and long-term field data. *Soil Biol. Biochem.* 46, 191–199. <https://doi.org/10.1016/j.soilbio.2011.11.005>
- Salinas-Garcia, J.R., Hons, F.M., Matocha, J.E., 1997. Long-Term Effects of Tillage and Fertilization on Soil Organic Matter Dynamics. *Soil Sci. Soc. Am. J.* 61, 152–159. <https://doi.org/10.2136/sssaj1997.03615995006100010023x>
- Saltelli, A., 2002. Sensitivity analysis for importance assessment. *Risk Anal.* 22, 579–590. <https://doi.org/10.1111/0272-4332.00040>
- Saltelli, A., Ratto, M., Andres, T., Campolongo, F., Cariboni, J., Gatelli, D., Saisana, M., Tarantola, S., 2008. Global Sensitivity Analysis. The Primer, *Global Sensitivity Analysis*.

The Primer. John Wiley & Sons, Ltd, Chichester, UK.

<https://doi.org/10.1002/9780470725184>

Saltelli, A., Tarantola, S., Campolongo, F., Ratto, M., 2004. Sensitivity analysis in practice: a guide to assessing scientific models. Wiley Online Library.

Sanderman, J., Hengl, T., Fiske, G.J., 2017. Soil carbon debt of 12,000 years of human land use. Proc. Natl. Acad. Sci. U. S. A. 114, 9575–9580. <https://doi.org/10.1073/pnas.1706103114>

Saxton, K.E., Rawls, W.J., Romberger, J.S., Papendick, R.I., 1986. Estimating Generalized Soil-water Characteristics from Texture. Soil Sci. Soc. Am. J. 50, 1031–1036.
<https://doi.org/10.2136/sssaj1986.03615995005000040039x>

Schimel, J., 2013. Soil carbon: Microbes and global carbon. Nat. Clim. Chang.
<https://doi.org/10.1038/nclimate2015>

Schlesinger, W.H., Bernhardt, E.S., 2013. Biogeochemistry: An Analysis of Global Change, Third Edition, Biogeochemistry: An Analysis of Global Change, Third Edition.
<https://doi.org/10.1016/C2010-0-66291-2>

Schuman, G.E., Reeder, J.D., Manley, J.T., Hart, R.H., Manley, W.A., 1999. Impact of Grazing Management on the Carbon and Nitrogen Balance of a Mixed-Grass Rangeland. Ecol. Appl. 9, 65. <https://doi.org/10.2307/2641168>

Sha, Z., Ma, X., Wang, J., Lv, T., Li, Q., Misselbrook, T., Liu, X., 2020. Effect of N stabilizers on fertilizer-N fate in the soil-crop system: A meta-analysis. Agric. Ecosyst. Environ.
<https://doi.org/10.1016/j.agee.2019.106763>

Shaviv, A., 2001. Advances in controlled-release fertilizers. Adv. Agron.
[https://doi.org/10.1016/s0065-2113\(01\)71011-5](https://doi.org/10.1016/s0065-2113(01)71011-5)

Shaviv, A., Mikkelsen, R.L., 1993. Controlled-release fertilizers to increase efficiency of nutrient

use and minimize environmental degradation - A review. *Fertil. Res.*

<https://doi.org/10.1007/BF00750215>

Singh, R., Nye, P.H., 1984. Diffusion of urea, ammonium and soil alkalinity from surface applied urea. *J. Soil Sci.* 35, 529–538. <https://doi.org/10.1111/j.1365-2389.1984.tb00610.x>

Smil, V., 1999. Nitrogen in crop production: An account of global flows. *Global Biogeochem. Cycles* 13, 647–662. <https://doi.org/10.1029/1999GB900015>

Smith, A.F.M., 1991. Bayesian computational methods. *Philos. Trans. R. Soc. London. Ser. A Phys. Eng. Sci.* 337, 369–386. <https://doi.org/10.1098/rsta.1991.0130>

Smith, A.F.M., Gelfand, A.E., 1992. Bayesian Statistics without Tears: A Sampling-Resampling Perspective. *Am. Stat.* 46, 84. <https://doi.org/10.2307/2684170>

Smith, P., 2012. Soils and climate change. *Curr. Opin. Environ. Sustain.* 4, 539–544. <https://doi.org/10.1016/j.cosust.2012.06.005>

Smith, P., 2004a. Carbon sequestration in croplands: The potential in Europe and the global context. *Eur. J. Agron.* 20, 229–236. <https://doi.org/10.1016/j.eja.2003.08.002>

Smith, P., 2004b. Monitoring and verification of soil carbon changes under Article 3.4 of the Kyoto Protocol. *Soil Use Manag.* 20, 264–270. <https://doi.org/10.1079/sum2004239>

Smith, P., Davies, C.A., Ogle, S., Zanchi, G., Bellarby, J., Bird, N., Boddey, R.M., McNamara, N.P., Powlson, D., Cowie, A., van Noordwijk, M., Davis, S.C., Richter, D.D.B., Kryzanowski, L., van Wijk, M.T., Stuart, J., Kirton, A., Eggar, D., Newton-Cross, G., Adhya, T.K., Braimoh, A.K., 2012. Towards an integrated global framework to assess the impacts of land use and management change on soil carbon: Current capability and future vision. *Glob. Chang. Biol.* 18, 2089–2101. <https://doi.org/10.1111/j.1365-2486.2012.02689.x>

- Smith, P., Martino, D., Cai, Z., Gwary, D., Janzen, H., Kumar, P., McCarl, B., Ogle, S., O'Mara, F., Rice, C., Scholes, B., Sirotenko, O., Howden, M., McAllister, T., Pan, G., Romanenkov, V., Schneider, U., Towprayoon, S., Wattenbach, M., Smith, J., 2008. Greenhouse gas mitigation in agriculture. *Philos. Trans. R. Soc. B Biol. Sci.*
<https://doi.org/10.1098/rstb.2007.2184>
- Smith, P., Smith, J.U., Powlson, D.S., McGill, W.B., Arah, J.R.M., Chertov, O.G., Coleman, K., Franko, U., Frolking, S., Jenkinson, D.S., Jensen, L.S., Kelly, R.H., Klein-Gunnewiek, H., Komarov, A.S., Li, C., Molina, J.A.E., Mueller, T., Parton, W.J., Thornley, J.H.M., Whitmore, A.P., 1997. A comparison of the performance of nine soil organic matter models using datasets from seven long-term experiments. *Geoderma* 81, 153–225.
[https://doi.org/10.1016/S0016-7061\(97\)00087-6](https://doi.org/10.1016/S0016-7061(97)00087-6)
- Sobol, I.M., 2001. Global sensitivity indices for nonlinear mathematical models and their Monte Carlo estimates. *Math. Comput. Simul.* 55, 271–280. [https://doi.org/10.1016/S0378-4754\(00\)00270-6](https://doi.org/10.1016/S0378-4754(00)00270-6)
- Sobol, I.M., 1993. Sensitivity estimates for nonlinear mathematical models. *Math Model. Comput. Exp.* 1, 407–414.
- Sommer, S.G., Schjoerring, J.K., Denmead, O.T., 2001. Ammonia Emission from Mineral Fertilizers and Fertilized Crops. *Adv. Agron.* 82, 557–622. [https://doi.org/10.1016/s0065-2113\(03\)82008-4](https://doi.org/10.1016/s0065-2113(03)82008-4)
- Spencer, S., Ogle, S.M., Breidt, F.J., Goebel, J.J., Paustian, K., 2011. Designing a national soil carbon monitoring network to support climate change policy: a case example for US agricultural lands. *Greenh. Gas Meas. Manag.* 1, 167–178.
<https://doi.org/10.1080/20430779.2011.637696>

- Stein, M., 1987. Large Sample Properties of Simulations Using Latin Hypercube Sampling. *Technometrics* 29, 143. <https://doi.org/10.2307/1269769>
- Stockmann, U., Adams, M.A., Crawford, J.W., Field, D.J., Henakaarchchi, N., Jenkins, M., Minasny, B., McBratney, A.B., Courcelles, V. de R. de, Singh, K., Wheeler, I., Abbott, L., Angers, D.A., Baldock, J., Bird, M., Brookes, P.C., Chenu, C., Jastrow, J.D., Lal, R., Lehmann, J., O'Donnell, A.G., Parton, W.J., Whitehead, D., Zimmermann, M., 2013. The knowns, known unknowns and unknowns of sequestration of soil organic carbon. *Agric. Ecosyst. Environ.* 164, 80–99. <https://doi.org/10.1016/j.agee.2012.10.001>
- Sun, W., Canadell, J.G., Yu, Lijun, Yu, Lingfei, Zhang, W., Smith, P., Fischer, T., Huang, Y., 2020. Climate drives global soil carbon sequestration and crop yield changes under conservation agriculture. *Glob. Chang. Biol.* 26, 3325–3335. <https://doi.org/10.1111/gcb.15001>
- Sutka, R.L., Ostrom, N.E., Ostrom, P.H., Gandhi, H., Breznak, J.A., 2003. Nitrogen isotopomer site preference of N₂O produced by *Nitrosomonas europaea* and *Methylococcus capsulatus* bath. *Rapid Commun. Mass Spectrom.* <https://doi.org/10.1002/rcm.968>
- Sutton, M.A., Reis, S., Billen, G., Cellier, P., Erisman, J.W., Mosier, A.R., Nemitz, E., Sprent, J., Van Grinsven, H., Voss, M., Beier, C., Skiba, U., 2012. Preface: “Nitrogen & global change.” *Biogeosciences* 9, 1691–1693. <https://doi.org/10.5194/bg-9-1691-2012>
- Tabatabai, M.A., 1973. Michaelis Constants of Urease in Soils and Soil Fractions. *Soil Sci. Soc. Am. J.* 37, 707–710. <https://doi.org/10.2136/sssaj1973.03615995003700050024x>
- Thapa, R., Chatterjee, A., Awale, R., McGranahan, D.A., Daigh, A., 2016. Effect of Enhanced Efficiency Fertilizers on Nitrous Oxide Emissions and Crop Yields: A Meta-analysis. *Soil Sci. Soc. Am. J.* 80, 1121–1134. <https://doi.org/10.2136/sssaj2016.06.0179>

- Thapa, R., Chatterjee, A., Johnson, J.M.F., Awale, R., 2015. Stabilized nitrogen fertilizers and application rate influence nitrogen losses under rainfed spring wheat. *Agron. J.* 107, 1885–1894. <https://doi.org/10.2134/agronj15.0081>
- Tian, H., Xu, R., Canadell, J.G., Thompson, R.L., Winiwarter, W., Suntharalingam, P., Davidson, E.A., Ciais, P., Jackson, R.B., Janssens-Maenhout, G., Prather, M.J., Regnier, P., Pan, N., Pan, S., Peters, G.P., Shi, H., Tubiello, F.N., Zaehle, S., Zhou, F., Arneth, A., Battaglia, G., Berthet, S., Bopp, L., Bouwman, A.F., Buitenhuis, E.T., Chang, J., Chipperfield, M.P., Dangal, S.R.S., Dlugokencky, E., Elkins, J.W., Eyre, B.D., Fu, B., Hall, B., Ito, A., Joos, F., Krummel, P.B., Landolfi, A., Laruelle, G.G., Lauerwald, R., Li, W., Lienert, S., Maavara, T., MacLeod, M., Millet, D.B., Olin, S., Patra, P.K., Prinn, R.G., Raymond, P.A., Ruiz, D.J., van der Werf, G.R., Vuichard, N., Wang, J., Weiss, R.F., Wells, K.C., Wilson, C., Yang, J., Yao, Y., 2020. A comprehensive quantification of global nitrous oxide sources and sinks. *Nature*.
- Tian, Z., Wang, J.J., Liu, S., Zhang, Z., Dodla, S.K., Myers, G., 2015. Application effects of coated urea and urease and nitrification inhibitors on ammonia and greenhouse gas emissions from a subtropical cotton field of the Mississippi delta region. *Sci. Total Environ.* 533, 329–338. <https://doi.org/10.1016/j.scitotenv.2015.06.147>
- Timilsena, Y.P., Adhikari, R., Casey, P., Muster, T., Gill, H., Adhikari, B., 2015. Enhanced efficiency fertilisers: A review of formulation and nutrient release patterns. *J. Sci. Food Agric.* <https://doi.org/10.1002/jsfa.6812>
- Trenkel, M.E., 2010. Slow- and Controlled-Release and Stabilized Fertilizers: An Option for Enhancing Nutrient Use Efficiency in Agriculture, Second. ed. International Fertilizer Industry Association (IFA), Paris, France.

- Van Oijen, M., Rougier, J., Smith, R., 2005. Bayesian calibration of process-based forest models: Bridging the gap between models and data. *Tree Physiol.* 25, 915–927.
<https://doi.org/10.1093/treephys/25.7.915>
- VandenBygaart, A.J., 2018. Comments on soil carbon 4 per mille by Minasny et al. 2017. *Geoderma* 309, 113–114. <https://doi.org/10.1016/j.geoderma.2017.05.024>
- VandenBygaart, A.J., 2006. Monitoring soil organic carbon stock changes in agricultural landscapes: Issues and a proposed approach. *Can. J. Soil Sci.* 86, 451–463.
<https://doi.org/10.4141/S05-105>
- Vitousek, P.M., Aber, J.D., Howarth, R.W., Likens, G.E., Matson, P.A., Schindler, D.W., Schlesinger, W.H., Tilman, D.G., 1997. Technical Report: Human Alteration of the Global Nitrogen Cycle: Sources and Consequences. *Ecol. Appl.* 7, 737.
<https://doi.org/10.2307/2269431>
- Wagner-Riddle, C., Congreves, K.A., Abalos, D., Berg, A.A., Brown, S.E., Ambadan, J.T., Gao, X., Tenuta, M., 2017. Globally important nitrous oxide emissions from croplands induced by freeze-thaw cycles. *Nat. Geosci.* 10, 279–283. <https://doi.org/10.1038/ngeo2907>
- Wasserman, L., 2000. Bayesian model selection and model averaging. *J. Math. Psychol.* 44, 92–107. <https://doi.org/10.1006/jmps.1999.1278>
- Watson, C.J., Miller, H., Poland, P., Kilpatrick, D.J., Allen, M.D.B., Garrett, M.K., Christianson, C.B., 1994. Soil properties and the ability of the urease inhibitor N-(n-BUTYL) thiophosphoric triamide (nBTPT) to reduce ammonia volatilization from surface-applied urea. *Soil Biol. Biochem.* 26, 1165–1171. [https://doi.org/10.1016/0038-0717\(94\)90139-2](https://doi.org/10.1016/0038-0717(94)90139-2)
- White, R.E., Davidson, B., Lam, S.K., Chen, D., 2018. A critique of the paper ‘Soil carbon 4 per mille’ by Minasny et al. (2017).’ *Geoderma* 309, 115–117.

<https://doi.org/10.1016/j.geoderma.2017.05.025>

- Wickham, H., 2016. *ggplot2: Elegant Graphics for Data Analysis*. Springer-Verlag, New York, NY.
- Wieder, W.R., Bonan, G.B., Allison, S.D., 2013. Global soil carbon projections are improved by modelling microbial processes. *Nat. Clim. Chang.* 3, 909–912.
<https://doi.org/10.1038/nclimate1951>
- Williamson, J.C., Menneer, J.C., Torrens, R.S., 1996. Impact of dicyandiamide on the internal nitrogen cycle of a volcanic, silt loam soil receiving effluent. *Appl. Soil Ecol.*
[https://doi.org/10.1016/0929-1393\(96\)00100-X](https://doi.org/10.1016/0929-1393(96)00100-X)
- Wolt, J.D., 2004. A meta-evaluation of nitrapyrin agronomic and environmental effectiveness with emphasis on corn production in the Midwestern USA. *Nutr. Cycl. Agroecosystems* 69, 23–41. <https://doi.org/10.1023/B:FRES.0000025287.52565.99>
- Wolt, J.D., 2000. Nitrapyrin Behavior in Soils and Environmental Considerations. *J. Environ. Qual.* <https://doi.org/10.2134/jeq2000.00472425002900020002x>
- Wrage, N., Velthof, G.L., Van Beusichem, M.L., Oenema, O., 2001. Role of nitrifier denitrification in the production of nitrous oxide. *Soil Biol. Biochem.* 33, 1723–1732.
[https://doi.org/10.1016/S0038-0717\(01\)00096-7](https://doi.org/10.1016/S0038-0717(01)00096-7)
- Wutzler, T., Reichstein, M., 2007. Soils apart from equilibrium - Consequences for soil carbon balance modelling. *Biogeosciences* 4, 125–136. <https://doi.org/10.5194/bg-4-125-2007>
- Xu, J.G., Heeraman, D.A., Wang, Y., 1993. Fertilizer and temperature effects on urea hydrolysis in undisturbed soil. *Biol. Fertil. Soils* 16, 63–65. <https://doi.org/10.1007/BF00336517>
- Xu, T., White, L., Hui, D., Luo, Y., 2006. Probabilistic inversion of a terrestrial ecosystem model: Analysis of uncertainty in parameter estimation and model prediction. *Global*

Biogeochem. Cycles 20. <https://doi.org/10.1029/2005GB002468>

Yeluripati, J.B., van Oijen, M., Wattenbach, M., Neftel, A., Ammann, A., Parton, W.J., Smith, P., 2009. Bayesian calibration as a tool for initialising the carbon pools of dynamic soil models. *Soil Biol. Biochem.* 41, 2579–2583. <https://doi.org/10.1016/j.soilbio.2009.08.021>

Zhang, W., Liang, Z., He, X., Wang, X., Shi, X., Zou, C., Chen, X., 2019. The effects of controlled release urea on maize productivity and reactive nitrogen losses: A meta-analysis. *Environ. Pollut.* 246, 559–565. <https://doi.org/10.1016/j.envpol.2018.12.059>

Zhang, Y., Gurung, R., Marx, E., Williams, S., Ogle, S.M., Paustian, K., 2020. DayCent Model Predictions of NPP and Grain Yields for Agricultural Lands in the Contiguous U.S. *J. Geophys. Res. Biogeosciences*. <https://doi.org/10.1029/2020JG005750>

Zhang, Y., Suyker, A., Paustian, K., 2018. Improved crop canopy and water balance dynamics for agroecosystem modeling using daycent. *Agron. J.* 110, 511–524. <https://doi.org/10.2134/agronj2017.06.0328>